Quarterly Progress Report
October 1 - December 31, 1950

BROOKHAVEN NATIONAL LABORATORY

Associated Universities, Inc.
Upton, New York

Printed at Upton, N.Y., for distribution to individuals and organizations associated with the national atomic energy program.

March, 1951 700 copies

DISCLAIMER

FOREWORD

This is the fourth of a series of Quarterly Progress Reports. With this issue of the Quarterly Progress Report, a system of designating the appropriate AEC budget activity numbers for the various research activities has been started. These numbers are given in parentheses, at the right hand side of the page, alongside the subject headings to which they pertain.

In the case of supporting activities, no budget activity number is indicated, since the cost is distributed proportionately throughout the Laboratory.

While most of the departments have summarized their work or used a form comparable to an abstract, the Chemistry Department has given both abstracts and complete reports on its work. The major part of the progress in the Reactor Science and Engineering Department is being presented simultaneously in a separate classified report.

CONTENTS

III

BNL-93

PHYSICS DEPARTMENT

As in previous quarterly reports, subjects are presented only when significant progress has been accomplished and the report is of definite scientific interest. In most instances, the material presented is an abstract or an abridged edition of a more complete coverage of the work which is either already submitted or is about to be submitted for publication in a scientific journal or for oral presentation before a scientific society. The items have been grouped under four general headings: 1) dynamic properties of nuclei, 2) stationary properties of nuclei, 3) high energy particle physics, and 4) theoretical topics.

Dynamic Properties of Nuclei

Measurement of Isomeric Transition Energies with a Scintillation Spectrometer (5212)*

An accurate measurement of isomeric transition energies is necessary for a comparison between theoretical and experimental gamma-ray lifetimes and therefore plays an important role in any systematic investigation of isomers. The gamma-ray scintillation spectrometer is particularly suited for the determination of isomeric transition energies whenever one or more of the following conditions is fulfilled: The isomeric transition is not too highly converted, the specific activity is low, or the lifetime is short. Under such circumstances the use of the scintillation counter may yield results that are superior to those of absorption measurements and may compare in accuracy with those attainable with a lens spectrometer. The scintillation counter shares with some other methods the disadvantage that the gamma ray observed does not necessarily correspond to the isomeric transition. It may follow the isomeric transition or appear in a beta or K branch. Therefore, in some cases, subsidiary experiments may be necessary.

This report is concerned with a series of measurements of isomeric transition energies which have been carried out with the help of a scintillation counter. NaI crystals activated with TlI were used. A comparatively small crystal (~2 cm in area and 1 cm high) was found most useful for a determination of low energy gamma rays. The crystal, covered with a layer of mineral oil, was fixed to a 5819 RCA phototube and backed by an aluminum foil reflector. The phototube was connected to a 204B Atomic Instrument Company linear amplifier and thence to a DuMont 248 oscilloscope for display of the self-triggered pulses (sweep time ~5 μsec). The pulse distribution was photographed with the help of a Polaroid camera. The linearity of the arrangement was checked with the following well-known gamma-ray lines: Co^{60m} (59 kev), Te^{123m} (159 kev), Te^{121m} (213 kev), Cr^{51} (320 kev), Cs^{137} (661 kev), and found to be satisfactory in this energy range. To obtain the metastable states that were investigated, suitable samples (metals or oxides) were exposed to slow neutrons in the Brookhaven reactor and then transferred rapidly to the scintillation counter. Table 1 summarizes the results. The apparent gamma-ray continuum previously found by Goldhaber, Muehlhause and Turkel (Phys. Rev. 71, 372 (1947)) for Ir^{192m} (1.5 min) in competition with the 57.4 kev internally converted transition found by Caldwell

*For explanation of these numbers, see Foreword.

Table 1

Isomeric Transition Energies

		Present Work	Previous Data		
Isomer	Half-Life Time	Energy of γ (kev)	Energy of e- (kev)	Energy of γ (kev)	Transition Energy (kev)*
Sc^{46m}	19.5 sec	135	165 (abs)	180 (abs)	180
Se^{77m}	17.5 sec	150		150 (abs)	150
Rh^{104m}	4.7 min	52	69.5 (spect)	50 (abs)	80;50
Sb^{122m}	3.5 min	68	110 (abs)		140
Hf^{m}	19 sec	215	86.1		150
			135.1 (spect)		
			190 (abs)		190
Ir^{192m}	1.5 min	Up to $\sim$57	44.1 L_I		57.4
			46.0 L_{III}		

*As given by K. Way et al., Nuclear Data, National Bureau of Standards, 499

(Phys. Rev. 78, 407 (1950)) yields a pulse distribution with an upper limit close to this energy but of very different appearance from that obtained for gamma rays of other isomers of similar excitation energy. This spectrum is being investigated further.

Antimony was used in isotopically enriched form (97.7% Sb^{121}). Present energy values are estimated to be accurate to 10%. The only serious discrepancy between these values and earlier ones appears in the case of Hf^{m} (19 sec) where Hole (Arkiv Mat. Astron. Fysik 36A, #9 (1948)) had found a transition energy of 150 kev with a beta-ray spectrograph, and where the present value is considerably higher (215 kev). The possibility of a two-step isomeric transition is being investigated.

C.E. Larson, Oak Ridge National Laboratory, supplied the hafnium metal and Dr. Keim's group supplied the isotopically enriched antimony sample. (E. der Mateosian, M. Goldhaber)

Gamma Rays in the Decay of Rh^{106} and Pr^{144} (5212)

Two isotopes, Ru^{106} and Ce^{144}, have been found capable of producing photoneutrons in Be and D. In both cases the isotope is derived as a fission product and is therefore obtainable in quantity; in addition, the lifetimes (1 year for Ru^{106} and 275 days for Ce^{144}) are long enough to make them useful as photoneutron sources. Photoneutrons are produced by gamma rays emitted with intensities of the order of 2% per beta ray in the decay of the daughters, 30-sec Rh^{106} and 17-min Pr^{144}.

Previous work on Rh^{106} by Peacock has indicated that the decay involves two excited states in Pd^{106} and that two cascades and a cross-over gamma ray occur. This isotope is also known to possess a strong gamma-gamma angular correlation. Theoretical attempts by Falkoff and others to explain this correlation on the basis of the

proposed level scheme have not been successful. Because of this aspect of Rh^{106}, the gamma-ray spectrum has been investigated by means of both a scintillation spectrometer and a magnetic lens spectrometer. With the scintillation spectrometer a 2.9-Mev gamma was found which is evidently the line responsible for the photoneutron yield.

Careful measurement with the lens spectrometer using both lead and uranium photoelectric converters, showed lines present with the following energies: 0.511, 0.621, 0.87, 1.045, 1.55, and 2.9 Mev. The first two are strong and of nearly equal intensity; they agree with internal conversion lines found by R.D. Hill (unpublished). No cross-over of 0.511 plus 0.621 Mev is observed. The 0.511- and 1.045-Mev lines are probably cascade gamma rays corresponding to the 1.55-Mev cross-over. These same lines have been observed by Mei, Huddleston, and Mitchell in the K-capture decay of Ag^{106}, also leading to the same product nucleus, Pd^{106}. It is probable that more than one pair of cascade gamma rays is present in the decay of Rh^{106}, and in such a case the analysis of the angular correlation would be more difficult than previously thought. Experiments are planned which may help to assign the various transitions by means of coincidence techniques.

The gamma-ray spectrum of Pr^{144} was also measured in the lens spectrometer and lines of 2.185 ± 0.015, 1.48, and 0.695 Mev were found. The first of these is responsible for the photoneutron production in Be, and its energy was determined by a direct comparison in the spectrometer with the 2.200-Mev line from radium. The sum of the other two lines is equal to the 2.185-Mev line within the experimental error, indicating a cascade process. The cross-over transition is the more intense. In addition, a low energy line was found which appears to be the L-conversion line of a 142-kev gamma ray. It is not possible at present to state the role of this line in the decay scheme. A very weak photoneutron yield in deuterium from Ce^{144} is also observed. Since the 2.185-Mev line is definitely below the D threshhold, an unobserved high energy line must also be present. (D. Alburger, E. der Mateosian, M. Goldhaber, S. Katcoff)

Radiations from Sn^{113} (5212)

An early study of radioactive tin by Barnes (Phys. Rev. 56, 414 (1939)) found evidence for a weak 85-kev gamma ray following the K-capture of Sn^{113} (105 days) and preceding the 1.74-hour metastable state of In^{113m} which decays by a converted 390-kev gamma ray. However, Nelson, Ketelle, and Boyd (ORNL 828) have reported an unsuccessful search for this gamma ray.

In the present work, stable Sn^{112} (enriched) was bombarded with slow neutrons and the radiation was studied with a 275-gauss photographic spectrograph and also with a scintillation counter. There was no evidence of the 85-kev gamma ray, either converted or unconverted. An upper limit for the percentage of 85-kev gamma rays compared to 390-kev gamma rays is 5%. An upper limit for conversion electrons from the 85-kev transition is 1%. K, $L_I + L_{III}$, and M conversion lines of the 390 ± 1.5 kev gamma ray were observed. (J.W. Mihelich)

Gamma Rays from Ti^{51} (5212)

The gamma rays of Ti^{51} (6 min), which decays by beta emission to V^{51}, were

studied with a scintillation counter and found to be identical with those of Cr^{51} (26 days) which decays by K-capture to V^{51}. Both isotopes emit 320-kev gamma rays. (E. der Mateosian, M. Goldhaber, J.W. Mihelich, A.W. Sunyar)

Cross-over Transition in Tc^{99m} (5212)

It has been shown by Medicus, Maeder and Schneider (Bull. Am. Phys. Soc. 25, #6, E1) that Tc^{99m} (6 hr) decays in two steps: A 1.8 ± 0.3 kev transition followed by a 141.2 ± 0.5 kev transition, the latter being 2^1 magnetic (conversion coefficient α_K = 0.095 ± 0.020). In a search for the expected cross-over transition, a molybdenum foil was bombarded in the Brookhaven reactor, thus forming Mo^{99} which decays to Tc^{99m}. The molybdenum foil was dissolved in a 60-ml distilling flask in 4 ml of H_2SO_4 and a minimum amount of HNO_3. The first fraction of the distillate containing the HNO_3 was collected and discarded. The remainder of the distillate (containing the technetium) was diluted to 4M, and the technetium activity was co-precipitated, as the sulfide, with 0.1 mg of Pt added as H_2PtCl_6. The sulfide was centrifuged, washed and mounted on a thin Al strip which was inserted in a high-resolution photographic 180° beta-spectrograph. The electron lines found are given in Table 2.

Table 2

Electron Energy	Relative Intensity	Interpretation
120.0	11.6	141.1 - K
122.1	1.6	143.2 - K
137.8	1.4	141.1 - L
140.0	1	143.2 - L and 141.1 - M, N

The difference between the two K lines is 2.1 ± 0.1 kev. The cross-over transition can be estimated to take place in 1-2% of all transitions. This permits a unique level assignment. It is of interest to note that the spin orbit coupling leads in this case to a remarkably small splitting of the g-levels. (J.W. Mihelich, M. Goldhaber; E. Wilson, Chemistry Department)

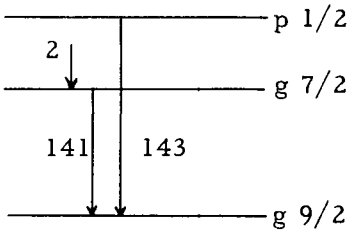

Study of Low Energy Gamma and Alpha Radiations Emitted From Pa^{231} and U^{234} (5212)

Macklin and Knight (Phys. Rev. 72, 435 (1947)) observed with a G-M counter a low energy gamma radiation from a thin source of U^{234}, an alpha emitter. By absorption of this radiation in Al they showed that its energy was comparable with that of the L radiation of Th. A further study of this radiation has now been carried out by Scharff-Goldhaber, der Mateosian, M. McKeown and Sunyar (Phys. Rev. 78, 325 (1950)) by means of argon-filled proportional counters. After passing through a preamplifier and linear amplifier with variable gain, the pulse from the proportional counter was analyzed by a single-channel pulse height discriminator and recorded by means of a scaler and mechanical counter.

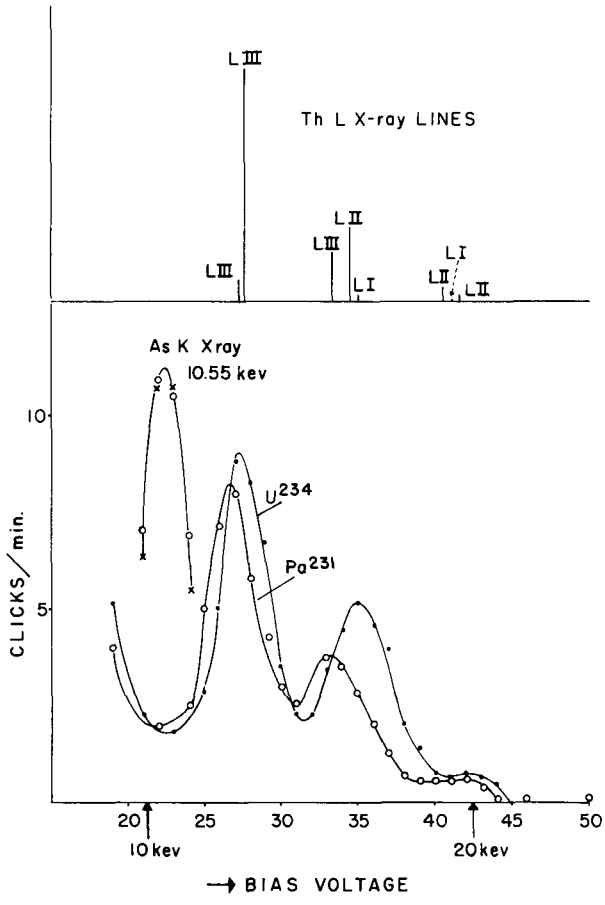

Figure 1. L X-ray spectrum of $U^{234} \rightarrow Th^{230}$ (2-90). For purposes of comparison, L X-ray spectrum of $Pa^{231} \rightarrow Ac^{227}$ (2-89) is shown. In the upper part, L lines from Th are shown.

A sample of about .4 mg of enriched U^{234} was placed above the beryllium window of the counter. The differential pulse height distribution is shown in Figure 1. An energy calibration was carried out with the As K X-ray emitted from Se^{75}, as K-capturer. In the upper part of the figure the intensities of L X-ray lines excited in Th with external X-rays (Compton and Allison, X-rays in Theory and Experiment, D. Van Nostrand, 1934), are plotted against the same energy scale. The agreement of the line groups with the measured peaks indicates that the radiations found by Macklin and Knight are indeed L X-rays. The energy resolution obtained is illustrated by the shift of the L X-ray spectrum due to element 89 which is produced by alpha decay of Pa^{231}.

Since at least one-quarter of the α-emissions of U^{234} were followed by L X-rays, it seemed reasonable to assume that they are produced by conversion of low energy gamma rays in the L shell. A search for these gamma rays is so far unsuccessful. J. Teillac (Compt. Rend. 239, 1056 (1950)) showed recently by means of a photographic plate technique that about every third alpha particle is accompanied by a conversion electron. The energies of these electrons fall into 3 groups of $\sim$36, 50, and 75 kev, the strongest one being at 36 kev. It therefore seems that in about 30% of the cases, the alpha decay of U^{234} is followed by strongly converted gamma rays of energies ranging between 50 and 90 kev.

A corresponding search for a nuclear gamma ray responsible for the L X-rays from Pa^{231} yielded a peak at $\sim$27 kev, as shown in Figure 2. The energy calibration was carried out by means of the K radiation from Te. Critical absorption of the nuclear gamma ray from Pa^{231} also showed that its energy lies between the absorption edges of Cd and In (26.7 and 27.9 kev). (Figure 3.) For this experiment Cd, In, and Sn absorbers were placed between the sample and the beryllium window and the discriminator voltage of the proportional counter was kept constant at the peak value for the gamma ray. By means of a Wilson chamber technique, J. Teillac (Compt. Rend. 229, 650 (1949)) had observed at least 3 conversion electron groups from this isotope. The most intense group was at 24 kev, which may be identified with the M-electrons from the 27-kev gamma ray.

M. Studier of Argonne National Laboratory and G. Harbottle of this laboratory prepared the Pa^{231} samples. (G. Scharff-Goldhaber, M. McKeown)

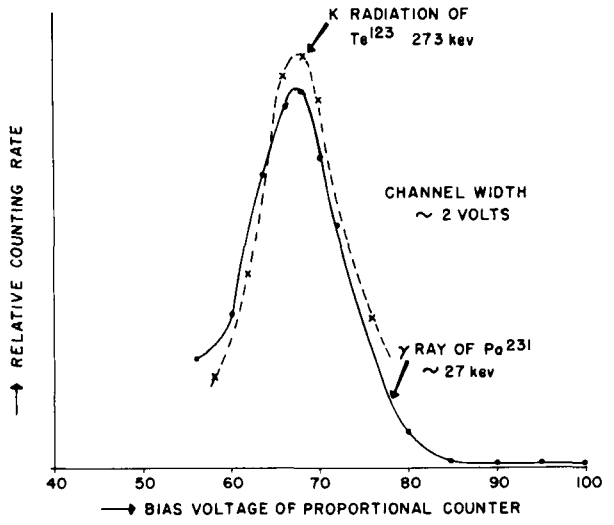

Figure 2 (Above). Differential pulse height distribution of 27 kev γ-ray from Pa^{231} with comparison of K-radiation of Te.

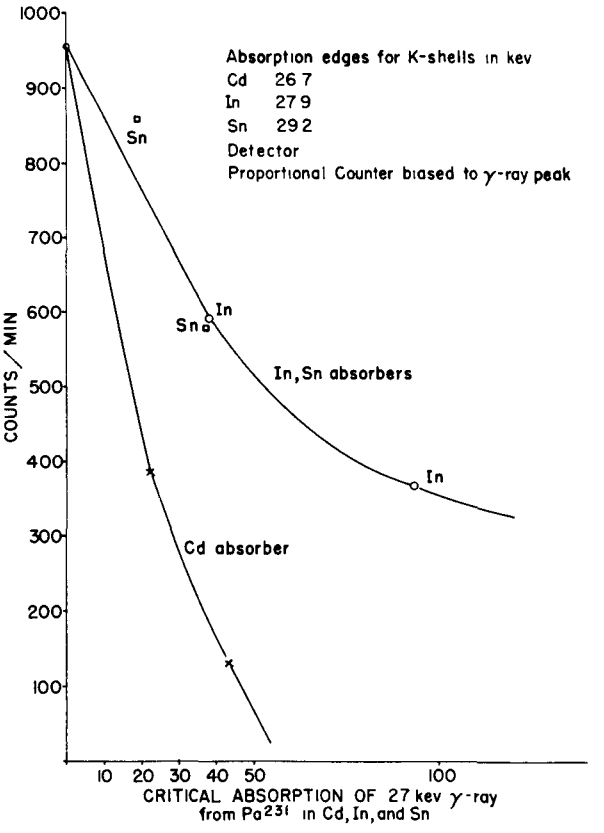

Figure 3 (Right). Counting rate of the 27 kev γ-ray from Pa^{231} as function of thickness (mg/cm^2) of Cd, In and Sn absorbers, showing critical absorption in Cd, and thus fixing the energy between 26.7 kev and 27.9 kev.

The Gamma-Gamma Correlation with Higher Multipoles (5212)

Recent experiments on gamma-gamma angular correlations by Brady and Deutsch, (Phys. Rev. 78, 558 (1950)) and the correlation in the long-lived isomer Pb^{204} observed by Sunyar, Alburger, Friedlander, Goldhaber, and G. Scharff-Goldhaber (Phys. Rev. 79, 181 (1950)) have emphasized the need to extend the angular correlation calculations to higher multipoles. Thus far the only published tables of gamma-gamma correlations are those of Hamilton (Phys. Rev. 58, 122 (1940)), but these are applicable only to successive nuclear transitions in which the gamma rays are either dipole or quadrupole. The extension of these tables using the method of Hamilton, although straightforward in principle, has thus far not been attempted because the amount of calculation required increases rapidly with the higher multipoles.

Several alternative methods of calculation are noted here which considerably simplify the problem of obtaining $W(\theta)$ for higher angular momenta. Specific results are given for some of the simpler cases of interest, and then a general method for obtaining more complete tabulations is indicated:

(i) Instead of calculating $W(\theta)$ for all possible transitions consistent with the angular momentum selection rules for fixed multipole orders of the gamma rays, as Hamilton has done, one can fix the multipole order of one of the gamma rays, say the second, and the spins of the intermediate and final states, and vary the multipole order and spin of the initial state. This method is particularly simple when the final state has spin zero. For example, for transitions of the type:

$$\text{IA:}\quad L+1 \xrightarrow{2^L} 1 \xrightarrow{2^1} 0$$

(here the multipole order of the gamma ray is indicated above the arrow), one obtains

$$W(\theta) = 1 + a_2 \cos^2\theta \text{ with}$$

$$a_2 = \frac{-(L^2 + L - 3)}{3L^2 + 7L + 3}$$

Since most of the nuclei in which gamma-gamma correlations have been measured are presumed to have spin-zero ground states, we have similarly calculated the coefficients a_{2i} in $W(\theta) = 1 + Z\, a_{2i} \cos^{2i}\theta$ as functions of L for correlations of type:

$$\text{IB:}\quad L \xrightarrow{2^L} 1 \xrightarrow{2^1} 0$$

$$\text{IIA:}\quad L+2 \xrightarrow{2^L} 2 \xrightarrow{2^2} 0$$

$$\text{IIB:}\quad L+1 \xrightarrow{2^L} 2 \xrightarrow{2^2} 0$$

$$\text{IIIA:}\quad L+3 \xrightarrow{2^L} 3 \xrightarrow{2^3} 0$$

$$\text{III B:}\quad L+2 \xrightarrow{2^L} 3 \xrightarrow{2^3} 0$$

The results are given in Tables 3-5. In all of the above cases the second multipole is the only one allowed by the angular momentum selection rule, while the first multipole is taken to be either the maximum allowed (IA, IIA, IIIA) or the next allowed (IB, IIB, IIIB), to cover the case when the former is forbidden by parity.

These tables confirm the expectation that $W(\theta)$ should become increasingly anisotropic with higher multipole gamma rays. It is noteworthy that none of these correlation functions can explain the "anomalous" correlation in Rh^{106} measured by Brady and Deutsch (loc. cit.). It should be remarked that excellent agreement can be had, of the correlation theory with the measurements on both directional correlation and direction-polarization correlation in Rh^{106} provided one assigns to the nuclear states the angular momenta 1, 2, 1, respectively, and takes both multipoles as electric quadrupole. However, this entails new difficulties in that an even-even nucleus is then assigned a non-zero spin, and some additional selection rule is then needed to account for the weakness of the expected cross-over gamma ray.

(ii) The most extensive tabulation of angular correlation functions which has appeared so far is that of J.W. Gardner (Proc. Phys. Soc. London 62, 763 (1949)) who treated $e^- - e^-$ correlations. Tables of equal completeness, i.e., applicable to transitions of any multipole orders provided these are restricted to the maximum, and next to maximum allowed angular momenta, can also be for the gamma-gamma correlation. Indeed, one can use the methods of G. Racah, (Phys. Rev. 62, 438 (1942)) which Gardner used to obtain directly the gamma-gamma correlation functions. However, this method, though elegant and more wieldy than Hamilton's, would involve an unnecessary duplication of effort. For it has been shown by Falkoff and Uhlenbeck (Phys. Rev. 79, 323 (1950)) that once correlation functions have been tabulated for any successive particle emissions, these same tables may be used to obtain $W(\theta)$ for other particles.

Table 3

a_2 in $W(\theta) = 1 + a_2\cos^2\theta$ for γ-γ Correlations of Types IA and IB

L	IA	IB
	a_2	a_2
1	+.076	-.333
2	-.103	+.429
3	-.176	.692
4	-.215	.810
5	-.239	.871
6	-.255	.907
7	-.266	.930
8	-.275	.945

Table 4

a_2 and a_4 in $W(\theta) = 1 + a_2\cos^2\theta + a_4\cos^4\theta$ for γ-γ Correlations of Types IIA and IIB

L	IIA		IIB	
	a_2	a_4	a_2	a_4
1	-.104	0	+.428	0
2	+.125	+.042	0	-.333
3	.313	-.021	-.455	+.121
4	.452	-.089	-.721	.433
5	.556	-.149	-.888	.640
6	.635	-.197	-1.000	.784
7	.698	-.237	-1.079	.889
8	.749	-.271	-1.138	.969

Table 5

a_2, a_4, a_6 in $W(\theta)$ for γ-γ Correlations of Types IIIA and IIIB

L	IIIA			IIIB		
	a_2	a_4	a_6	a_2	a_4	a_6
1	-.176	0	0	+.692	0	0
2	+.313	-.024	0	-.439	.156	0
3	.554	-.014	.018	-.441	.176	-.161
4	.676	+.045	.001	-.258	-.129	-.023
5	.742	.118	-.030	-.053	-.522	+.206
6	.779	.195	-.067	+.135	-.908	.447
7	.801	.264	-.102	.302	-1.260	.675

This theorem was applied in detail in the last reference cited where Hamilton's gamma-gamma tables were adapted to other correlation processes (such as β-γ, e^--γ, α-γ, etc.) which involved the same angular momenta. It thus appears that the most economical procedure for systematically obtaining $W(\theta)$ for higher angular momenta is to similarly apply the theorems of Falkoff-Uhlenbeck to the tables already worked out by Gardner. (D.L. Falkoff, Notre Dame University; T. Danielson)

Heat Production in Potassium (5212)

Recent determinations of gamma ray and beta ray energies of the decay constant, and the shape of the beta-ray spectrum of K^{40} now permit a more precise evaluation of the rate of heat production in potassium. Experiments of Sawyer and Wiedenbeck (Phys. Rev. 79, 490 (1950)) have shown that 28.3 $\pm$ 1.0 beta rays and 3.6 $\pm$ 0.3 gamma rays are emitted per gram K per sec. The gamma ray occurs in the K-capture branch and has an energy of 1.47 $\pm$ 0.01 Mev, an average value taken from the measurements of Bell and Cassidy (Phys. Rev. 79, 173 (1950)), Pringle, Standil, and Roulston (Phys. Rev. 77, 841 (1950)), and Hofstadter and McIntyre (Phys. Rev. 80, 631 (1950)).

The predominant heat energy occurs in the beta branch and estimates thus depend strongly on the characteristics of the beta ray spectrum. A calculation of the mean beta ray energy of K^{40} has been made based on the work of Bell, Weaver, and Cassidy (Phys. Rev. 77, 399 (1950)), Alburger (Phys. Rev. 78, 629 (1950)), and Feldman and Wu (Am. Phys. Soc. 25-5, 10 (1950)). Their values for the end-point energy have a weighted mean of 1.34 $\pm$ 0.02 Mev, and all three groups find that the shape of the spectrum above 500-700 kev agrees with the third forbidden correction factor. Since the deviations below 500 kev are attributed to source thickness effects, it is assumed here that the spectrum has the third forbidden shape over the entire range of energies.

The idealized momentum plot for a third forbidden type of beta emitter with end-point at 1.34 Mev was constructed using the non-relativistic function $f(Z,\eta)$ corrected for relativistic effects according to the table of Feister (Phys. Rev. 78, 375 (1950)). This was then converted to the energy distributions $N(W)WdW$ and $N(W)dW$ versus W and the areas under these curves were measured with a planimeter. The ratio of areas gives a mean energy for K^{40} beta rays of 0.605 $\pm$ 0.10 Mev, somewhat higher than the older value of 0.49 $\pm$ 0.06 Mev listed by Marinelli, Brinckerhoff, and Hine (Rev. Mod. Phys. 19, 25 (1947).

The total heat production using the revised beta- and gamma-ray energy values and Sawyer and Wiedenbeck's emission rates is readily computed to be (27 $\pm$ 1) x 10^{-6} cal/gK/yr. This may be compared with (22 $\pm$ 3) x 10^{-6} cal/gK/yr calculated by Gräf (Phys. Rev. 74, 831 (1948)) from earlier data. (D.E. Alburger)

Scintillation Spectrometry (5212)

A scintillation spectrometer is usually composed of a detecting head, a linear amplifier and some pulse height discriminating device. The detecting head consists of a scintillating crystal and a photomultiplier tube; the best combination of crystal and tube for gamma-ray spectroscopy appears to be a thalium-activated sodium iodide crystal and an RCA 5819 tube. NaI-Tl crystals, unfortunately, are hygroscopic and must be protected from atmospheric moisture. However, we have not found it necessary

to prepare these crystals in a dry box. A satisfactory procedure is to smooth the surfaces with fine sandpaper, place the crystal in a beaker of methyl alcohol, which is a good solvent for NaI, and after 10 or 15 sec, transfer the crystal to butyl alcohol, then to xylene, and finally to a beaker of Nujol. Any set of miscible solvents which range in solubility for NaI from very good to very poor should do as well as the three mentioned above.

Indirect and qualitative experimental observations make us strongly believe that the most important factor in mounting a crystal on a photomultiplier tube is the achievement of a geometric arrangement of crystal and light reflectors which will allow as much of the light as possible from one scintillation to pass through the photosensitive surface. With 1.5-cm cubes of NaI-Tl, best results were achieved by placing the crystal directly on the face of the photomultiplier tube and covering it with a cone-shaped aluminum reflector, adding enough oil to coat the crystal and tube face with a thin layer. Figure 4 illustrates this arrangement and shows a plot and a photograph of the output of a detector mounted in this fashion when irradiated by an uncollimated source of Cs^{137} which has one gamma ray of 660 kev.

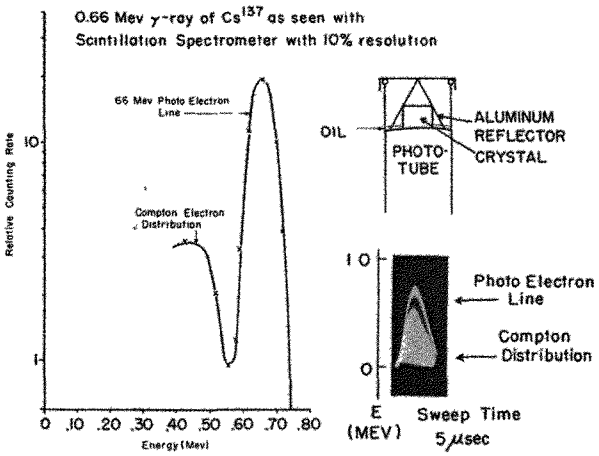

Figure 4.

The plotted data were taken with a single-channel pulse height discriminator built by the Electronics Division while the photograph was taken with a Polaroid camera and a Dumont 248 scope. In a few attempts to use larger crystals (3-cm cube), better resolution resulted when the crystal was mounted directly on the face of the tube. With still larger crystals, it may be advantageous, as Bell has found, to use a light pipe between the crystal and the photo surface. Measurements recently made by the Electronics Division indicate that in most photomultiplier tubes the sensitivity of the surface varies appreciably from point to point. It has been thought by some (e.g., Bell) that if crystals were mounted directly on the face of the tube, resolution would be lost, since scintillations occurring close to the photo tube would give up most of their light to the surface in their immediate vicinity. Scintillations of equal intensity occurring in different parts of the crystal would thus produce pulses of different size in the multiplier tube. More uniform pulses might result if a light pipe 3/4 in or more in length were used to distribute the light from each scintillation more uniformly over the photo-sensitive surface.

However, since we had not found that a light pipe increased our resolution, the following experiment was performed to check in a more direct manner the nature of the process by which light is transferred to the photo-sensitive surface from neighboring regions in a crystal. A "search crystal" was made by molding a NaI-Tl crystal (~.1 cu cm) into a small lucite button, which was mounted in a standard manner at different positions on the surface of an RCA 5819 tube. The tube had previously been tested by the Electronics Division for uniformity of sensitivity across its cathode.

Three positions were chosen on which to mount the crystal: (1) a region that was uniformly "good," (2) a region that varied from "good" to "bad," and (3) a region that was uniformly "bad." In positions (1) and (3) the crystal was adjacent to a region of constant sensitivity. After correcting for the statistical effect of large and small numbers of electrons leaving the photocathode, one would expect better resolution in regions (1) and (3) than in region (2), where areas of different sensitivity were exposed to the crystal. However, the best resolution was obtained in position (1), the second best in position (2) and the third in position (3). We conclude that the light from a given scintillation is thoroughly dispersed throughout the volume occupied by the crystal and its reflector and it is always well distributed over the photo-sensitive surface. Hence the average sensitivity, and not the uniformity, of the photocathode is important in determining the resolution one may expect with a given tube.

In designing reflectors for scintillating crystals an important factor is the loss of light in the crystal and its surrounding medium. A. Schardt called to our attention that resolution is reduced by filling the volume between the crystal and reflector with oil. This observation was confirmed by mounting a 1.5 cm cube of NaI-Tl in an aluminum reflector shaped like a cone, first with only a thin layer of mineral oil covering the face of the photo tube, then with the entire volume between the cone and crystal filled with oil. The line width was 12% in the first case and 18% in the second. The same results were obtained with silicone oil. However, the resolution has also been found to depend upon the shape of the reflector.

In another experiment all sides of a 3 cm cubical NaI-Tl crystal except that adjacent to the photocathode were covered with aluminum foil, pressed into close contact with the crystal. The output pulse size was then measured for a standard source. The experiment was repeated with all sides of the crystal covered by aluminum, and a small hole 1/4 in. in diameter cut in the face in contact with the photo-sensitive surface. The latter pulses were less than 1/20 the size of the former, indicating that appreciable light is lost in reflection from the aluminum and/or in traversing the crystal. Hence a reflector should be so shaped that the light is collected by the photocathode after a minimum number of reflections or traverses of the crystal.

The most common type of scintillation spectrometer is one that uses a single-channel, variable pulse height discriminator. Though slow, this method of recording is reliable and quantitative. Multi-channel devices reduce the time of taking data and allow one to study short-lived activities. Another convenient method of recording the data which is specially suited for preliminary survey work is to display the pulses on an oscilloscope and to photograph with a camera. Because of its short processing time the Polaroid camera is convenient. With visual observation, energy measurements can be made precisely and quickly by mixing the signal from the scintillator with that from an electronic pulser whose output can be varied in size. The pulser may be calibrated with standard sources and then used to match the pulses being studied.

A cathode-ray oscilloscope has been used effectively for determining the time coincidence of gamma rays. If one crystal is connected to the signal input and another to the input that triggers the sweep, the spectrum of gamma rays in prompt coincidence appears as a series of superposed pulse-shaped curves of different amplitudes, all starting from zero at the origin. The "resolving" time is the thickness of the trace, and, with fast scopes, this can be as short as 10^{-8} to 10^{-9} sec. Chance coincidences appear uniformly along the length of the sweep. Metastable states with lifetimes of the

order of the resolving time should appear as a smear starting with the sweep and fading exponentially in the direction of the sweep. When several groups of coincident gamma rays are present, but one group is not in coincidence with another group, one may select any one of the gamma rays by means of a pulse height selector in the trigger circuit and thus see which gamma rays are in each coincidence group. For studying beta-gamma coincidences the beta pulses in an anthracene crystal are used to trigger the sweep. (E. der Mateosian, W.F. Hornyak, M. McKeown)

Response of Scintillators to Recoils from 14-Mev Neutrons (5212)

From the $H^3(d,n)\,He^4$ reaction, 14-Mev neutrons were detected with a NaI (Tl) scintillation counter. A differential pulse height spectrum showed distinct "edges." This spectrum could be interpreted as indicating scintillations caused by recoil protons (and possibly recoil carbon ions) originating in the Nujol surrounding the NaI crystal and entering the crystal with various energies, and also scintillations caused by sodium and iodine recoils originating within the crystal itself.

A pulse height calibration based on secondary electrons produced by gamma rays combined with the observed location of the edges indicates that the scintillation pulse height produced by an ionizing particle is proportional in good approximation (for NaI) to the energy and is independent of the particle mass.

Equality of the observed integral pulse height spectrum with the calculated absolute recoil yield calculations corroborates the recoil identifications. The physical efficiency (ratio of recoils to neutron traverses) was of the order of 6% for a 1/2 in cube of NaI as measured by the sodium recoils. The physical efficiency for the recoil protons from the oil is approximately 30 times less at this neutron energy.

The differential pulse height spectrum of the scintillations produced by this same neutron source in a 5 g/liter solution of terphenyl in xylene (in a 2-in diameter and 1-in long cell) was also observed. This spectrum was flat between the maximum pulse height and approximately one-half that value. This observation is in agreement with the theoretically predicted spectrum based on S-wave single scattering in hydrogen. (W.F. Hornyak)

Activation of Scintillating Crystals (5212)

In a search for new scintillating crystals, single crystals of sodium iodide activated by various metals were grown by the Bridgman method as adapted by Hofstadter (Phys. Rev. 75, 796 (1949); Proc. I.R.E. 38, 726 (1950)). Reagent grade sodium iodide mixed with appropriate quantities (.05% - .5%) of salts of different metals were melted under fore-vacuum in Vycor crucibles. Indium and tin were introduced directly in metallic form. After sealing-off, the crucibles were lowered at a rate of .2 to .3 in/hr through combustion tube furnaces operated at a temperature about 50°C above the melting point of the host crystal.

A rough indication of the scintillation response of the crystal could be gained through a visual examination under ultraviolet illumination. None of the crystals that failed to luminesce under this type of excitation showed any scintillations. However, some of the crystals that fluoresce under ultraviolet excitation failed to scintillate.

These failures were attributed to long phosphorescent decay times. The following activators gave the indicated fluorescence under ultraviolet irradiation:

In - White, intense
Ag - Orange, weak
Sn - Yellow - green, intense
Ba - Yellow, intermediate
Zn - Green, intermediate
Ce - Blue, intense
La - Pale green, intermediate
Pb - Green, intermediate
Hg - Yellow, intermediate
Nd - Blue, intense

Metals that yielded no appreciable visible luminescence were Cd, Ni,Mn, Pt, Sb, Cu, Bi, Mg, and Ca. As well as the eye could detect, the luminescence ceased as soon as the excitation was removed in all activators except Hg; here the phosphorescence persisted for several seconds.

The scintillating properties of each crystal were determined using a standard crystal mounting on a 5819 photomultiplier tube connected through an Atomic Instrument Company 204-B linear amplifier to a Dumont 248 oscilloscope. Photographs of the pulse distributions from crystals that responded to gamma rays were taken with a Polaroid camera. Table 6 lists the pulse heights expressed as fractions of the height with thallium activation. The approximate concentration of the activator is given in parenthesis.

Table 6

Activator	In(.1%)	Ag(.05%)	Sn(.05%)	Ba(.5%)	Zn(.5%)
Pulse Height Compared to Tl	1/5	1/6	1/8	1/10	1/30

Not listed is the value for cadmium activation, since it was not possible to reproduce the results, although with one such crystal, pulses were obtained.

None of the activators tried gave pulses as high as those produced by thallium. Some improvement of relative pulse height could be induced by increasing the time constant of the input to the amplifier, but in all cases thallium activation resulted in the largest pulses.

Crystals of thallium-activated potassium iodide gave a pulse about 1/4 that of sodium iodide. The beta spectrum of K^{40} was plainly indicated in this crystal. Other activators for potassium iodide have not yet been tried. Pulses in sodium bromide (.1 % TlI) were 1/10 the height of those in NaI.

When two activators were used at the same time in a host crystal, the pulse height lay between those heights characteristic of each activator alone.

The quantity of activator which actually went into the host crystal in each case was not measured. The amounts indicated refer only to the quantity of material initially mixed in the crucible. It was noted that thallium activation gave the same pulse height whether .1% or .5% was used, and in both cases after the crystal had grown, excess TlI could be seen on top of the crystal. The responses of all the thallium-activated

crystals of this composition were the same as those supplied by Harshaw. When metallic tin was used to activate, the residual tin was recovered and weighed after the crystal was grown. The loss of weight amounted to .03%, indicating that relatively small amounts of this activator are required. The same procedure can be followed with indium and perhaps with other metals as well to determine the quantities of activator required.

Methods are being developed to introduce radioactive sources directly into scintillating crystals. By such procedures pulse height distributions may be obtained for weakly penetrating alpha and beta particles. The beta spectrum of In^{114} was observed in this way. Indium foil irradiated in the reactor was placed in a crucible containing sodium iodide with .1% TlI, and a crystal was grown. In this crystal the beta spectrum together with the 190-kev gamma line were clearly revealed. In a similar fashion, Sn^{119m} was introduced into a crystal and the total isomeric transition energy was observed. Several crystals have been grown which contain alpha emitters (Po, Pa, and Th). (G. W. Johnson, E. der Mateosian)

Differential Cross Sections in the Scattering of 14-Mev Neutrons by Protons (5212)

Because of its bearing on the theory of neutron-proton forces, work has been started for a precise measurement of the angular distribution of protons recoiling from 14-Mev neutrons. The neutrons are produced by deuteron bombardment of a tritium target in the Brookhaven electrostatic accelerator. Proportional coincidence counters were used to detect the protons recoiling from a thin polyethylene film. The relative differential cross sections, normalized to unity in the forward direction, are given in Table 7 for three angles of the recoil proton measured in the laboratory system. The angles of the scattered neutron in the center-of-mass (c.m.) system are also given. The table includes the results of the present work and the best previous values, obtained by Barschall and Taschek (Phys. Rev. 75, 1819 (1949)). It will be noted that within the improved accuracy of the present results there is still no evidence for any departure from spherical symmetry in neutron-proton scattering at this energy. (E. Wantuch)

Table 7

Angular Distribution in the Scattering of 14-Mev Neutrons by Protons

Proton angle in laboratory system	0°	15°	30°
Neutron angle in c.m. system	180°	150°	120°
Relative differential cross section:			
present work	1.00	$1.01 \pm .04$	$1.01 \pm .04$
Barschall and Taschek	1.00	$1.02 \pm .08$	$0.98 \pm .08$

n-D Scattering at 1.4 Mev (5212)

The angular distribution of neutrons scattered by deuterons has been measured in the past by a number of investigators for neutron energies from 2.5 to 14 Mev. This interaction is of considerable interest with respect to the nature of nuclear forces because it should make it possible to distinguish between ordinary and exchange forces

and because it is the simplest interaction that can be studied in which neutron-neutron forces are effective. Measurements at 1.4 Mev were undertaken in order to extend the energy range of the experimental data.

It was originally intended that the neutrons would be generated by the bombardment of lithium by protons, but the voltage obtainable by the Brookhaven electrostatic generator proved to be too low, so that deuteron bombardment of a carbon target was used instead. The deuteron beam produced a very strong neutron background since various oil-coated parts of the machine were exposed to it. The data obtained with this source are therefore to be considered preliminary. Work is now in progress on a thin target consisting of tritium absorbed in zirconium. Proton bombardment of this target should produce neutrons of the desired energy without background difficulties.

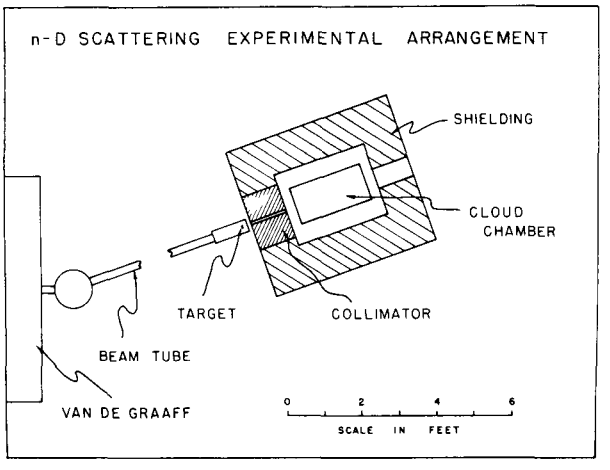

Figure 5.

A beam of neutrons was collimated by a slot in a 12 in block of paraffin, and made to pass down the center of a 24 in x 12 in x 8 in cloud chamber filled with deuterium at a pressure of about 65 cm Hg. The number of background neutrons arriving from unwanted directions was reduced by shielding the cloud chamber with 12 in of wood. The experimental arrangement is shown in Figure 5. Stereoscopic photographs were taken of the recoil tracks, and the angle in space and range of each track was calculated. About 1,000 tracks were measured for deuterium; a smaller number for hydrogen. Tracks that originated in parts of the cloud chamber out of the neutron beam were discarded as due to background, as were tracks occurring in the beam whose range and angle were not consistent with elastic scattering. About 370 acceptable tracks remained, and for them only a small background correction was necessary.

The control data taken with hydrogen cloud chamber fillings are shown in Figure 6. Within statistical uncertainties the results are consistent with the expected isotropic scattering. For neutron scattering angles less than about 75° the energy given to the recoil particle is too low to be measured, the minimum length counted being 6 mm.

The results for deuterium are given in Figure 7. Curves of Buckingham and Massey (Proc. Roy. Soc. A179, 123 (1941)) have been fitted to the data. The ordinary force curve gives a satisfactory fit, but the exchange force curve does not. The results are consistent with other experimental data at higher energies. Since the process is a three-body one, the theoretical calculations are difficult, and may not be accurate. As a result, one would hardly be justified in ruling out exchange forces on the basis of these data. (A. Thorndike, W. Wotring)

Coherent Neutron-Proton Scattering by Liquid Mirror Reflection (5212)

A measurement of the coherent neutron-proton scattering amplitude, utilizing total

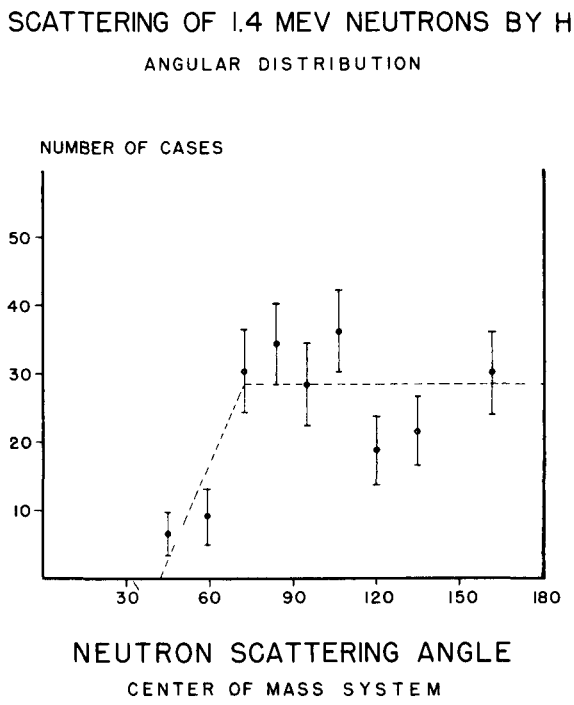

Figure 6.

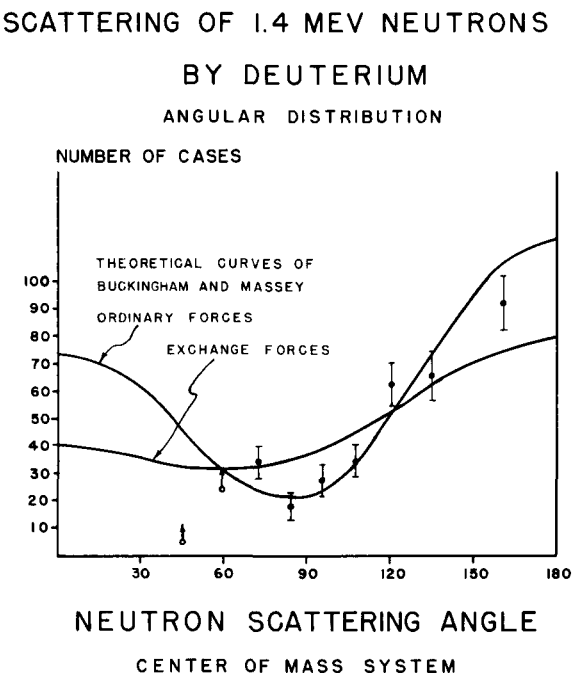

Figure 7.

reflection of slow neutrons from a liquid hydrocarbon, has been reported by Hughes, Burgy and Ringo (Phys. Rev. 77, 291 (1950)). As the result ($-3.75 \pm .03 \times 10^{-13}$ cm) was significantly different from existing values, the measurement was repeated with a series of carefully purified hydrocarbon liquids, by a method in which no measurement of neutron wave length was necessary. The ratio of the amplitude of hydrogen to that of carbon has been determined with a standard error of 0.3% and the final value of the hydrogen amplitude, including the error (0.5%) in the measurement of the carbon amplitude, made by Havens and Rainwater (Phys. Rev. 75, 1296 (1950)) is $-3.78 \pm .02 \times 10^{-13}$ cm (standard error). This value is the weighted average of the results obtained with purified liquids. (D.J. Hughes; G.R. Ringo, M.T. Burgy, Argonne National Laboratory)

Inelastic Scattering of Low Energy Neutrons in Graphite (5212, 5260)

In mirror experiments, graphite is very useful as a filter for passing long wave length neutrons. It is planned to use a graphite filter for some experiments involving reflection from a bismuth mirror and the possibility was investigated of improving the transparency of graphite at long wave lengths by cooling. The scattering by graphite at long wave lengths (> than 6.7 Å) is entirely inelastic as there is no spin dependent scattering. Isotopic incoherence and capture are also negligible. Since there have been several theoretical investigations of inelastic scattering but little experimental work, it was decided to check the theory by measurements at extremely long wave lengths. The thermal chopper described in Progress Reports BNL-AS-2 (1949) and BNL-S-4 (1948) is now in operation and has produced measurable intensities of 20 Å neutrons. It is therefore quite valuable for inelastic scattering measurements, and it was used for this work.

Theoretically, the inelastic scattering cross section for graphite is proportional to wave length and it varies rapidly with about the 5/2 power of the absolute temperature. The measurements made so far result in a cross section of 0.8 barns at 7 Å for graphite at room temperature. In the range 7 to 15 Å, the cross section is proportional to wave length. The variation with graphite temperature has been measured from 80° to 370° absolute. In this temperature range, the cross section changes with temperature less rapidly than predicted by theory. The possibility that adsorbed gas might be contributing to the cross section is being investigated by observing the neutron transmission of a graphite sample while it is held at a high temperature in a special furnace. (G.W. Johnson, H. Palevsky, D.J. Hughes)

Coherent Cross Section and Resonances in Tellurium (5212)

The incoherent scattering cross section of tellurium for slow neutrons has been measured by the method described in the last quarterly progress report and it is 0.6 ± 0.2 barns. The free cross section measures 4.6 barns. Separated isotopes are now being used to attempt to account for the incoherent scattering. Pomerance reports a thermal absorption cross section of 393 barns for Te^{123} and 68 barns for Te^{120}, with only small cross sections for all remaining isotopes. On the basis of his data the identification suggested in the previous quarterly report of the pronounced 2-ev resonance as due to Te^{124} is being re-examined. (I.W. Ruderman, C.S. Heindl, Columbia University; R.J. Weiss, Watertown Arsenal, Army Ordnance Department)

Coherent Neutron Scattering from Gases (5212)

Measurements on thermal neutron coherent scattering from O_2, N_2, He, and A were made at the Oak Ridge reactor and have been continued at Brookhaven. A well collimated beam was totally reflected at angles of 2 - 5 min from mirror surfaces of ethylene glycols, lucite and aluminum. Gas pressure in the surrounding chamber was varied from 0 to 150 atmospheres, thus varying the gas index of neutron refraction. Since reflected intensity depends on the square of the change of refractive index at the gas mirror interface, the refractive index of the gas, and hence the coherent scattering cross section, can be deduced from a pressure-intensity plot, according to the relations:

$$\left(\frac{I}{I_0}\right)^{1/2} = 1 - \frac{P}{P_0}$$

and

$$\delta/\delta_0 = n\sigma^{1/2}/n_0\sigma_0^{1/2}$$

where P = gas pressure
P_0 = pressure at which gas and mirror index are equal
δ = 1 - refractive index of the gas
δ_0 = 1 - refractive index of the mirror
n = atomic density of the gas
n_0 = atomic density of the mirror
σ = coherent cross section of gas
σ_0 = coherent cross section of mirror

Results for oxygen were in good enough agreement with the cross section of 4.2 barns obtained by Wollan and Shull from diffraction measurements to verify applicability

of the same equation for index of refraction in gases. The nitrogen cross section was about 2.5 times greater than that of oxygen, and disagrees with the value 4.6 barns from diffraction. More accurate measurements will be necessary to give quantitative values for He and A. (A.W. McReynolds)

Stationary Properties of Nuclei

Mass Values in the Region Al - S (5212)

Mass spectrograph data are now available for the Al^{27}, Si^{28}, Si^{29}, Si^{30} and S^{32} isotopes. Because of inaccuracies in the mass differences (Na^{23} - Na^{24}) and (S - Cl) data, the Al to S masses, like those of Ne and Na (reported in the last quarterly report), are isolated from other isotopes. However, it is not a straightforward calculation, as it is in the neon region, to fit the mass defects to agree with the more accurate mass difference data resulting in the latter region from the M.I.T. group's recent Q values (private communication). Because of this, a fit of these five mass defects in the silicon region has been made by the method of least squares. The observed and best-fit values are given in Table 8 and the reactions are illustrated in Figure 8. The observed values fit well into this scheme so that only small adjustments are necessary. However, a significantly decreased probable error results for the best-fit masses. The Al^{28}, P^{31} and P^{32} mass defects have been determined from an approximate fit of the observed mass differences with the results of the least-squares analysis. The best-fit values depend on the values of n,p,d and α. Variations in current values of α will cause a change in the best-fit values of about 0.02 milli-mass-units (mmu).

The value $S^{32} = -19.11 \pm .07$ mmu given by Okuda and Ogata has not been used because of its large discrepancy with other mass spectrograph data of Duckworth (private communication) Aston, and Smith (last quarterly report). The mass defects given

Table 8

Mass Defects in the Region Al - S

Quantity	Best-Fit Values (mmu)	Observed Value (mmu)
Al^{27}	$-10.17 \pm .06$	$-10.20 \pm .08$
Si^{28}	$-14.19 \pm .05$	$-14.19 \pm .08$
Si^{29}	$-14.29 \pm .05$	$-14.33 \pm .14$
Si^{30}	$-16.97 \pm .06$	$-17.10 \pm .15$
S^{32}	$-17.72 \pm .05$	$-17.63 \pm .09$
Si^{30} - Al^{27}	-6.79^9	$-6.79^9 \pm .01^5$
S^{32} - Si^{29}	-3.43^8	$-3.44^5 \pm .02^5$
Si^{30} - Si^{29}	-2.68	$-2.58 \pm .10$
Si^{29} - Si^{28}	-0.100	$-0.100 \pm .02$
Al^{28}	$-9.48 \pm .06$	
P^{31}	$-16.35 \pm .05$	
P^{32}	$-15.89 \pm .05$	

are consistent with the mass of A^{36} as given by Roberts and Nier (Bull. Amer. Phys. Soc. 24, 7 (1949)) and by reaction data. The agreement of these many independent measurements firmly substantiates the recent mass measurements of S^{32}. Fourteen other isotopes are linked to the Al - S chain by one or more reactions with errors of 0.1 to 0.3 mmu. A more complete list of mass defects and source data will be published for the range Z = 10 to Z = 20. (H. Motz)

Time-of-Flight Mass Spectrometer (5212)

The magnetic time-of-flight mass spectrometer, based on principles described previously, is now developed to the stage where measurements are being performed. The probable errors obtained to date are less than 2 mmu. Recent improvements in ion sources and vacuum conditions promise better precision in the near future.

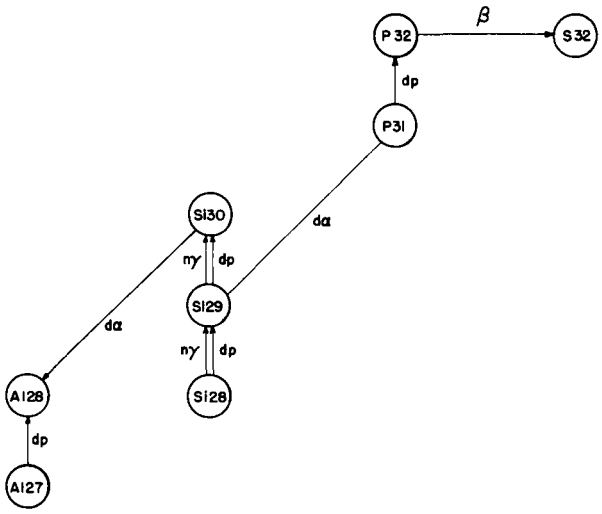

Figure 8. Reactions used for determining mass values of isotopes of Al to S.

The first new masses measured were those of Rb^{85} and Rb^{87}, namely, 84.9305 ± 0.0015 and 86.929 ± 0.0015. The mass of K^{41} was measured as 2.000 ± .002 larger than the known mass of K^{39}, which is 38.975.

In order to avoid systematic errors, the mass of Rb^{85} was referred to the mass of C_6H_{12} (84.1204 ± 0.0003) by measuring the ratio of their times of flight. A flight path of 6 revolutions was most suitable for observations, the time being about 900 μsec which could be measured with an error of about .01 μsec. For Rb alone, flight paths of 10 revolutions could be used with a flight time of 1400 μsec.

The precision measurements have revealed that systematic errors may be caused by electrical surface potentials. These affect the times of flight of different masses in a non-linear way and, moreover, their effect may change from day to day. By comparing the times of flight of two known masses, such as C_6H_{12} and C_6H_6, it was found that perturbing fields were usually less than 2 mv/cm and caused an error of less than 1 in 10^{+5} when masses one unit apart were being compared.

The time measurements are made by means of a pulse-matching system similar to that used in Loran navigation. It was constructed by the BNL Electronics Division. (E.E. Hays, P.I. Richards, S.A. Goudsmit)

Kramers' Theorem and Nuclear Effects in Paramagnetic Absorption (5212)

Shortly after the discovery of the hyperfine structure in solids by Penrose (Nature 163, 992 (1949)), Pryce (Nature 164, 116 (1949)) pointed out a relationship between ΔH, the separation of the hyperfine structure components of the cobalt ion, and θ, the angle

between the crystalline axis and the applied magnetic field. Later Ingram (Proc. Phys. Soc. A62, 664 (1949)) showed that this same relation applied to the copper ion. It seemed appropriate, therefore, to investigate the conditions under which Pryce's relation would be valid. His relation appears to be a consequence of Kramers' theorem (Proc. Akad. Amst. 35, 1272 (1932)), when the effect of the nuclear magnetic moment is taken into account to the first approximation.

Let ψ_1 and ψ_2 be the wave functions of a double degenerate electron ground state of a paramagnetic ion. In the presence of a magnetic field, the degeneracy will be removed and the wave functions of the two states becomes

$$f_{\frac{1}{2}} = \left[g_\perp \sin\theta\psi_1 + (g - g_\parallel \cos\theta)\psi_2\right] \Big/ \left[2g(g - g_\parallel \cos\theta)\right]^{\frac{1}{2}} \tag{1}$$

$$f_{-\frac{1}{2}} = \left[-(g - g_\parallel \cos\theta)\psi_1 + g_\perp \sin\theta\psi_2\right] \Big/ \left[2g\,(g - g_\parallel \cos\theta)\right]^{\frac{1}{2}} \tag{2}$$

corresponding to the magnetic energies $1/2\mu_B gH$ and $-1/2\mu_B gH$. Here g is given by $(g_\parallel^2 \cos^2\theta + g^2 \sin^2\theta)^{1/2}$. The quantities $g_\parallel$ and $g_\perp$ will depend, of course, upon the particular ion and the crystalline electric field, but the form of the wave functions as given above will be the same for any ion. The invariance requirement leads to the following expression for the nuclear interaction potential:

$$V = a_1 L\cdot I + a_2(3I\cdot r_s\cdot r/r^2 - I\cdot S) + a_3 I\cdot S \tag{3}$$

If J is a good quantum number, the above interaction potential can be expressed in the form $a_J I\cdot J$. In addition, there is the term representing the interaction of the nuclear magnetic moment with the external magnetic field. The diagonal elements of equation (3) can be written

$$(1,m|V|1,m) = -(2,m|V|2,m) = Am$$

where $m = I, I-1, \text{-----} L$. This follows from a relation pointed out by Kramers. The wave functions (1) and (2) then yield

$$(\pm\tfrac{1}{2},\ m|V|\pm\tfrac{1}{2},\ m) = \pm Amg_\perp \cos\theta/g$$

and, for the off-diagonal elements

$$(\pm\tfrac{1}{2},\ m+1|V|\pm\tfrac{1}{2},\ m) = \frac{\pm g_\perp \sin\theta}{2g} B\left[I(I+1) - m(m+1)\right]^{\frac{1}{2}}$$

The eigen values are

$$E(\tfrac{1}{2},m) = \tfrac{1}{2}g\mu_B H + \left[(\tfrac{1}{2}\Delta\nu_\parallel g_\parallel/g+\gamma H)^2\cos^2\theta + (\tfrac{1}{2}\Delta\nu_\perp g_\perp/g+\gamma H)^2\sin^2\theta\right]^{\frac{1}{2}}$$

$$E(-\tfrac{1}{2},m) = \tfrac{1}{2}g\mu_B H - \left[(-\tfrac{1}{2}\Delta\nu_\parallel g_\parallel/g+\gamma H)^2\cos^2\theta + (-\tfrac{1}{2}\Delta\nu_\perp g_\perp/g+\gamma H)\sin^2\theta\right]^{\frac{1}{2}}$$

In the above result, $1/2\Delta\nu_\parallel$ and $1/2\Delta\nu_\perp$ were substituted for A and B, since these quantities can be identified with one-half of the experimentally observed separation of the hyperfine structure components for parallel and perpendicular fields. For allowed transitions, $\Delta m = 0$, assuming γH is small compared to $\Delta\nu_\parallel$ and $\Delta\nu_\perp$, the energy separation for levels between which transitions are allowed is

$$E(\tfrac{1}{2},m) - E(-\tfrac{1}{2},m) = \mu_B g H_m + \frac{m}{g}\left[\Delta\nu_\parallel^2 g_\parallel^2\cos^2\theta + \Delta\nu_\perp^2 g_\perp^2\sin^2\theta\right]^{\frac{1}{2}}$$

Thus

$$\mu_B^2 g^4 (\Delta H)^2 = \Delta\nu_\perp^2 g_\perp^2 + \left[\Delta\nu_\parallel^2 g_\parallel^2 - \Delta\nu_\perp^2 g_\perp^2\right] \cos^2\theta$$

where ΔH is the separation between adjacent hyperfine structure components in magnetic field units. A similar relation, in a slightly different form, has been given by Pryce. (C. Kikuchi, Michigan State College)

High Energy Particle Physics

Nuclear Effects in Paramagnetic Absorption (5212)

The present study was undertaken to investigate theoretically the potentialities of the paramagnetic absorption technique for the measurement of certain nuclear constants, namely spins, magnetic moments, and electric quadrupole moments, and for the study of electric and magnetic interactions of nuclei in solids. For the pair of rare earth ions, Gd^{+++} and Nd^{+++}, it was concluded that the separation of hyperfine structure components for Gd^{+++} might be small, while that for Nd^{+++} might be large. This conclusion has in fact been confirmed in a recent experimental work by Bleaney and Scovil (Proc. Phys. Soc. 63A, 1369 (1950)). A phenomenological nuclear interaction potential was assumed in an attempt to correlate spectroscopic, paramagnetic, and nuclear specific heat measurements. It was found that the hyperfine structure coupling constants computed from the three measurements are in good agreement if it is assumed that the dipole-dipole term for crystalline ions is small in comparison with the electron-spin-nuclear-spin term. In the course of this investigation, a general relation for the angular dependence of the separation of hyperfine structure components was obtained:

$$g^4 (\Delta H)_\theta^2 = g_\parallel^4 (\Delta H)_\parallel^2 \cos^2\theta + g_\perp^4 (\Delta H)_\perp^2 \sin^2\theta$$

where $(\Delta H)_\theta$, $(\Delta H)_\parallel$, and $(\Delta H)_\perp$ respectively are the hyperfine structure component separations when the magnetic field makes the angles θ, 0, and 90° with respect to the crystalline axis. (C. Kikuchi, Michigan State College)

A Theory of Diffusion Cloud Chambers (5212)

The following phenomena must be explained by a quantitive description of diffusion chambers:

1. The depth of the chamber through which tracks are formed is usually not more than 3 in high. Greater depths up to perhaps 5 in have been observed, but seem to be only transient -- that is, may occur before complete temperature equilibrium has been reached.

2. Diffusion chambers work about equally well over a range of different temperature distributions.

3. Chambers filled with air or argon at pressures os several atmospheres give tracks only through a more restricted depth, while hydrogen and helium can be used only at higher pressures and are unstable at normal pressure if the vapor diffuses downwards.

4. If a diffusion chamber is irradiated continuously at a rate greater than 3 to 5 times that of cosmic radiation at sea level, the vapor supply is soon exhausted and no tracks can be seen. However, rather intense pulsed radiations can be tolerated if an electric sweeping field is applied between the pulses.

From (4) one concludes that the supply of vapor in a diffusion chamber is easily exhausted by dropwise condensation on ions. Therefore the theory must take condensation into account. Condensation on uncharged nuclei is a disturbing phenomenon which becomes more pronounced at high temperatures but may be neglected at lower temperatures where diffusion chambers generally operate better as regards quality of the tracks and stability of the gas in the chamber.

To formulate a theory, the following equations have been set up:

1. A diffusion equation takes account of the transport of vapor from regions at higher temperatures to those at lower temperatures, where supersaturation takes place. The vapor density is thus determined in part by the flux of vapor.

2. The gradient in vapor flux is determind by the amount of condensation taking place in the supersaturated region, while the amount of condensation on any drop is determined by the vapor density. Thus a diffusion equation for the vapor diffusing toward the drop is set up. As the drop grows its temperature increases, because of the release of latent heat. Therefore the vapor pressure of the drop increases, partially counteracting the diffusion process. Another equation describes the conduction of heat from the drop.

3. While a drop is growing it falls at an increasing speed determined by Stokes' equation. Thus the conditions around the drop change as it travels into regions of lower temperature and lower vapor density. This would complicate considerably the boundary conditions for the equations of diffusion and heat conduction around a drop, were it not that one can show that the drop falls so slowly that the resulting transients can be neglected. Therefore, semi-stationary solutions of the droplet problem may be used.

4. The gradient in vapor flux as affected by drop formation depends upon the ionization density in the gas.

5. The energy is balanced by heat supplied to the gas. The resultant heating is used to calculate the velocity the gas will assume when equilibrium is established with heat exchange to the walls of the chamber by convection.

A resulting integral equation has been solved for a number of cases, giving the temperature distribution necessary to obtain critical supersaturation through a given volume. The following general results have been obtained:

1. The temperature at the bottom, as well as the initial temperature gradient at the bottom of the chamber, must be arbitrarily chosen. The gradient necessary to sustain critical supersaturation through a given depth of the chamber is then a characteristic of the gas, the gas pressure, the vapor, and the ionization density. There is always a possible temperature distribution that is nearly linear, and this is the easiest one to obtain under controlled conditions. The linear gradient is calculated to be about $3.7^{\circ}C/cm$ for air at 1 atmosphere, and about $6.5^{\circ}C/cm$ for air at a pressure of 3 atmospheres. The calculations assume the use of methanol as a vapor in all cases because,

of the vapors usually used in cloud chambers, it has the lowest molecular weight, and the smallest amount of supersaturation is required for the growth of droplets. The temperature gradient required for operation at 3 atmospheres of air results in top temperatures so high that operation would be difficult, because of background fog and diffuseness of the tracks.

2. For operation at moderate temperatures, pressures have been calculated at which other gases will behave like air at a given pressure with its optimum temperature distribution. It is found that 1 atmosphere of air should operate as well as about 10 atmospheres of hydrogen, 5 atmospheres of helium, or 0.7 atmospheres of argon. Since operation with air would be unsuccessful at 3 atmospheres, one infers that a pressure limit for hydrogen is to be found near 30 atmospheres.

3. An increase in the amount of radiation from 3 to 5 times that of the cosmic radiation at sea level has the same effect as an increase of 2 to 4 times in pressure. Therefore elaborate shielding may be necessary for operation near accelerators. If stronger radiations are to be used it is necessary to give the vapor supply a chance to recover by pulsing the radiation. Cosmic radiation falling on a diffusion chamber at mountain altitudes may not overload it, but intensities at airplane altitudes are probably too high. (R.P. Shutt)

Operation of Diffusion Cloud Chambers at High Pressures (5212)

High pressure cloud chambers are well suited for the study of nuclear interactions in gases. Since high pressure expansion chambers cannot be cycled frequently enough for efficient utilization of accelerators, a continuously sensitive chamber for pressures up to 20 atmospheres has been constructed. It consists of a stainless steel cylinder 3/16 in thick, 13 in. in diameter, and 11 in high, with a 1 in thick steel bottom welded to it, and an O-ring-sealed lucite or glass window, 5-1/2 in x 3 in. A 2 in thick aluminum disk carrying a glass window 3 in. in diameter at the center is clamped to a flange welded to the top of the stainless steel cylinder. Heat is supplied electrically by means of resistance wire wound with asbestos cord and pushed through 1/4-in copper tubing, which is soldered around the steel cylinder. Heat can also be supplied to the top by means of similar units lying in grooves cut in the aluminum disk. A black Carrara glass plate forms the background at the bottom. Methanol vapor is evaporated from three concentric copper trays attached to the top disk. The unit stands in a circular tray filled with a mixture of alcohol and crushed dry ice. "Kimsul" is used for thermal insulation. Temperature distributions can be measured by means of thermocouples.

With air or argon at pressures above 2 atmospheres, it becomes increasingly difficult to obtain track formation through an acceptable depth of the chamber. With 1 atmosphere of air a nearly linear temperature gradient of 3.9°C/cm results in a track-sensitive depth of 2-1/2 in. At 3 atmospheres of air and with the optimum temperature gradient of 7°C/cm this depth is only 1-1/2 in and much background fog due to the formation of uncharged drops can be seen.

With the vapor diffusing downward, and helium or hydrogen as gases, the chamber becomes stable only at pressures of several atmospheres. With hydrogen at 12 atmospheres an average gradient of about 3.6°C/cm results in a track-sensitive layer 2-1/2 in deep. In all experiments the bottom temperature was kept at -60°C, while the temperature of the evaporating liquid was kept near 10°C, except for the experiment with

3 atmospheres of air, where a temperature of 30°C had to be used.

Moving pictures have been taken successfully at a rate of 8 and 16 frames per sec with air at 1 1/2 atmospheres and with hydrogen at 12 atmospheres. Light from a 1,000-w projector bulb beamed by means of a condensing lens was used as a source of illumination. With these pictures the amount of radiation that can be tolerated by a diffusion chamber and the effects of an electric sweeping field are being investigated. (D.H. Miller, E.C. Fowler, R.P. Shutt)

Effect of Proton Energy on Multiplicities in Stars From Large and Small Nuclei (5212)

By microscopic examination of photographic emulsions exposed to cosmic rays in high-flying balloons, it has been possible, as seen in previous BNL reports, to draw certain conclusions about meson production when high energy protons disintegrate the nuclei of the emulsion. To understand the results to be reported now, it is helpful to recall that among the earlier findings were the following:

(1) The "number of prongs" (tracks denser than shower tracks and caused mostly by emitted protons and heavier particles) identifies the size of the nucleus, and any star with 9 or more prongs represents the disruption of a heavy nucleus.

(2) The mean multiplicity of shower tracks (predominantly fast mesons) produced by 1-8 Bev (median energy 2 Bev) protons is about 1.4, the same whether from disintegrating light nuclei (C, N and O) or from heavy nuclei (Ag and Br).

(3) When the median energy of the protons is increased to about 14 Bev (all energies above 8 Bev), the mean multiplicity of shower tracks from light nuclei is again 1.4 but that from heavy nuclei is 4.2.

It was concluded from these facts that plural collisions within a nucleus are mainly responsible for the larger showers in the heavy nuclei.

In continuing the analysis, the large stars have been classified into two groups, one group with 9-15 prongs and the other group with 16 or more prongs, and attention has been focussed on the relativistic shower tracks due to fast mesons. The following table shows the mean multiplicities of shower particles of each group, as a function of the median energy of the incident protons (varied as before by flights at different latitudes). The multiplicity per collision is defined as the ratio of the number of shower tracks to the total number (including those without shower tracks) of proton-induced stars, while the multiplicity per shower is the ratio of the number of shower tracks to the number of proton-induced stars with at least one shower track.

The analysis also shows that, in both cases, the stars with 16 or more prongs are in about the same ratio to those with 9-15 prongs, i.e., the former are about three times more numerous than the latter. This result shows that the number of prongs in the stars is not systematically related to the energy of the incoming proton. One is left then with the conclusion that the number of heavy prongs, and, because of the correlation between prong number and multiplicity shown in the table, the multiplicity of the shower particles are determined by some statistical parameter of the collision.

Such a parameter is the radius of the impact, that is, the consideration of whether the impact is head-on or glancing.

Table 9

Mean Multiplicity of Shower Tracks in Stars Induced by Protons in Heavy Nuclei*

Shower Multiplicities	Median Energy of Incident Protons	
	2 Bev	14 Bev
Stars with 9-15 prongs		
per collision	0.8	3.2
per meson shower	2.0	4.0
Stars with 16 prongs		
per collision	2.3	3.2
per meson shower	5.1	5.7

*The standard errors are about 20%.

Such considerations may also throw some light upon the variation, shown in the table, of shower multiplicities with proton energy. Evidently the shower multiplicity in the stars of 9-15 prongs is more sensitive to the energy of the incoming proton than is that in the larger star.

This effect is most conspicuous in comparing the numbers of stars which have no shower tracks. In the 2-Bev group, these constitute half of the stars with 9-15 prongs but only one-fifth of those with more than 16 prongs, while in the 14-Bev group the fractions are one-fifth and one-tenth, respectively.

So far, no distinction has been made between prongs, but they may be subdivided into "black" prongs and "gray" prongs, according to their grain densities. Current views regard gray prongs as recoil protons of from 0.07 to 0.7 Bev energy, and black prongs as still less energetic protons or heavier particles evaporated from the disrupted nucleus. For the 14-Bev protons, we find the average multiplicity of gray tracks is 0.7 ± 0.2 in disintegrations of light nuclei and 5.0 ± 0.4 in disintegrations of heavy nuclei, a ratio of 1 to 7. Since the corresponding multiplicities of shower tracks is 1 to 3 (see item (3) of the first paragraph), it is seen that in going from a light to a heavy nucleus both mesons and fast recoil protons become more numerous, as one would expect if they are produced by plural collisions. The observation that the multiplicity of recoil protons increases with nuclear size more than that of the shower particles suggests that the latter may also produce recoil protons by collisions with nucleons as they leave the nucleus.

When the stars from heavy nuclei are divided into the two groups, 9-15 prongs and 16 or more prongs, it is found that the multiplicity of gray prongs is 3.4 ± 0.3 in the former group and 6.7 ± 0.5 in the latter. Evaporation, recoil and shower particles are

all more numerous in the large stars. The large stars therefore represent a greater transfer of energy but not necessarily a more energetic primary. (M. Blau, J. Hornbostel, E. Salant, J. Smith)

Nuclear Disruptions Under Graphite (5212)

The stars considered in the foregoing discussion were produced by relativistic ionizing particles in emulsions unprotected by absorbing material other than the 15 gsm/cm^2 of the atmosphere above them. On the same flight, the balloons also carried emulsions placed beneath a hemispherical shell of graphite, intended for studying the absorption of the primaries and the nuclear disruptions produced by secondary particles from the graphite. Carbon was chosen because of the extensive information already gained about nuclei of the size of C from studies of the stars from light nuclei in the emulsions. The thickness of the graphite was about a third of a collision mean free path for geometric cross section so that three-fourths of the particles incident upon the graphite were transmitted with only the ionization energy losses. The distribution in number of prongs of the stars produced by secondaries from the graphite has been deduced from the observed distribution of all stars under the graphite by subtracting three-fourths of the number in each class observed in an equal area of the unprotected emulsions.

Consider only those stars produced by relativistic ionizing particles, the so-called p-stars; the remainder, produced by the secondaries from the graphite, had a remarkably different distribution in prong number from similarly produced stars in the unprotected emulsions. Whereas large stars of 9 or more prongs constitute about half of the p-stars in the unprotected emulsions, few, if any, of those produced by the graphite secondaries had as many as 9 prongs and there were about equal numbers in the two groups of 1-5 prongs and of 6-8 prongs. (See Table 10.)

Table 10

Number of Stars of Various Prong Numbers per Day per gm of Emulsion

Exposure	Number of Prongs			
	1-5	6-8	9	Total
(A) Unprotected	121 (91)*	51 (39)	116 (87)	288 (217)
(B) Under graphite	140 (97)	80 (55)	69 (48)	289 (200)
(B) -3(A)/4	49 ± 16	42 ± 13	-18 ± 15	73 ± 28

*Figures in parentheses indicate actual numbers of stars measured in emulsions unprotected and under graphite.

If it is assumed that the secondary particles from the graphite are also protons, the smaller prong numbers of the secondary-produced stars as compared with those of

the primary-produced stars in the unprotected emulsions can only mean that the energies of the secondaries are lower. However, this conclusion conflicts with the fact that the tracks of the star-producing particles are relativistic, since the primary proton spectrum already extends down to 1 Bev at the latitude (57^{o}N) where the tracks begin to be more heavily ionized. It may therefore be concluded that the secondary star-producing particles are not protons, and must be mesons. A difference in character of these stars is also found in the fact that their shower multiplicity is only half that that characterizes the stars produced by primary protons.

A check on the rate at which the secondary particles from the graphite produce stars is obtained from a calculation of the number of mesons expected from the multiplicity of shower particles from stars in light nuclei observed in emulsions. One assumes again that one-quarter of the incident protons produce such stars in the graphite. In making this calculation it is assumed that the cross section for star production by mesons is also geometric. The number of stars so calculated agrees within statistical errors with the observed numbers.

The latitude of this flight was the same as that at which P.H. Fowler of Bristol determined the energy spectrum of mesons emitted from stars, and the mesons ejected from the graphite should have about the same energy distribution. Fowler's work placed the average kinetic energy of the mesons at about 200 Mev, and the average available energy, including the rest energy, at about 350 Mev.

It was recently reported from Columbia University that 350-Mev protons from the Nevis cyclotron produced no stars in emulsions with more than 8 prongs, and that the smaller stars predominated. A similar distribution characterizes our stars, produced by mesons of about the same total energy. Hence it appears that the character of disintegrations in this energy region depends on the total energy transferred and not on the character of the particle nor its momentum.

A flight with emulsions under a graphite absorber was made at latitude 31^{o} north where the median proton energy is 14 Bev. Here some of the secondary-produced p-stars had more than 9 prongs. This shows that the mesons from carbon nuclei are more energetic, on the average, when produced by 14-Bev primaries than when produced by 2-Bev primaries. This result is also to be expected from our older results on shower multiplicities in light elements. (J. Hornbostel, E. Salant, J. Smith)

The Nucleonic Component of Extensive Air Showers (5212)

A component of large air showers has been found by several authors which differs from both electrons and μ-mesons. It has been given the name "N-component" because of the similarity of its effects with those of the nucleonic component of the cosmic rays unassociated with air showers. However, the identity of the N-component of air showers with the unassociated nucleonic component cannot be considered definitely proven, and it presents some problems of remarkable interest. The intensity of these particles is about 1% of the electronic component, indicating that they are produced as a cascade. Their energy, of course, derives from the primary of the electronic shower which may be in the range 10^{13} to 10^{16} ev, but the mechanism by which the nucleonic cascades develops is still unknown.

In approaching this problem, the first question is the following: Do the N-cascades and the electronic cascades develop independently after being started by the same

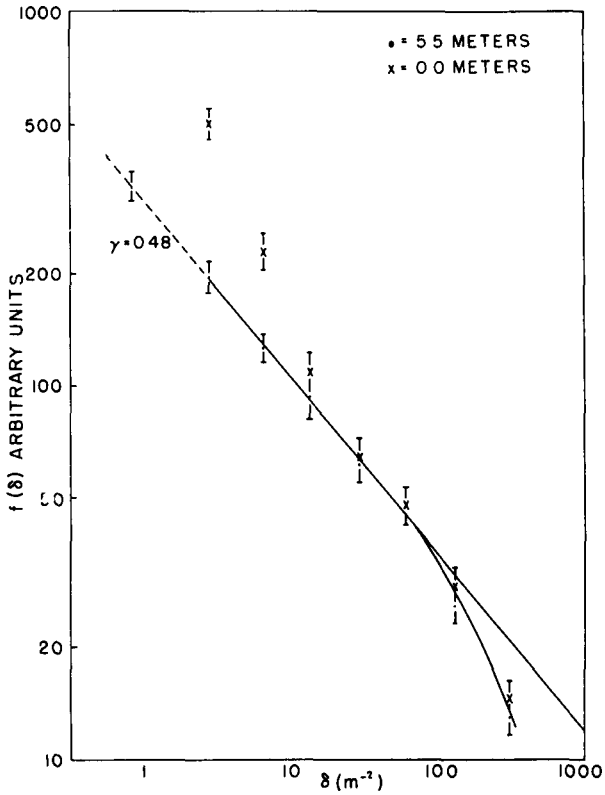

Figure 9. Frequency f(δ) of air showers which are coincident with a penetrating shower and whose density exceeds δ electrons per square meter. Points are shown for separations of 5.5 and 0 meters between the two detectors.

primary, or does one component continuously reproduce the other as it passes down through the atmosphere?

In studies carried on at the mountain station in Colorado, the intensity of the N-component is being observed by the use of a penetrating shower detector operated in coincidence with widely separated counters that detect extensive air showers. Measurements have been made at various elevations above sea level up to 14,000 ft, with an apparatus comprising two hodoscopes. One of these, containing 23 counters, measures the multiplicity of penetrating shower particles under a thick lead screen. Simultaneously, the other, which contains 80 counters and is located 5 meters away, measures the electron density.

The results are simply that the density of the N-component is proportional to the electron density for air showers whose densities differ by a factor of 100. The same proportionality factor holds at all elevations where measurements have been made, though the frequency of occurrence of air showers changes by a factor of 20.

Figure 9 shows a logarithmic plot of the frequency f(δ) of air showers that are coincident with a penetrating shower and whose density exceeds δ electrons per square meter. At the lower densities the probability for detecting a penetrating shower is proportional to the density of the N-component and the linearity represents the known power law spectrum of electron densities. From other observations this spectrum is known to follow a power law over the whole range of electron densities and the knee observed at about 100 particles per square meter is not a departure from this law but is to be accounted for by a saturation of the penetrating shower apparatus.

For electron densities above 100 per m^2 the density of the N-component becomes so great that the probability of response when a shower occurs in it approaches unity and is no longer proportional to the density. Comparison of the shower frequencies, observed with the penetrating shower detector in coincidence, with those observed with electron detectors alone shows that the penetrating shower detector responds with a probability of 10^{-3} when the electron density is 1 per m^2. From this datum the position of the knee may be correctly predicted. This prediction is based upon two assumptions that may therefore be regarded as established:

(a) The N-component is in the same ratio to the electron component in all air showers.

(b) Each penetrating shower is produced by a single particle of the N-component.

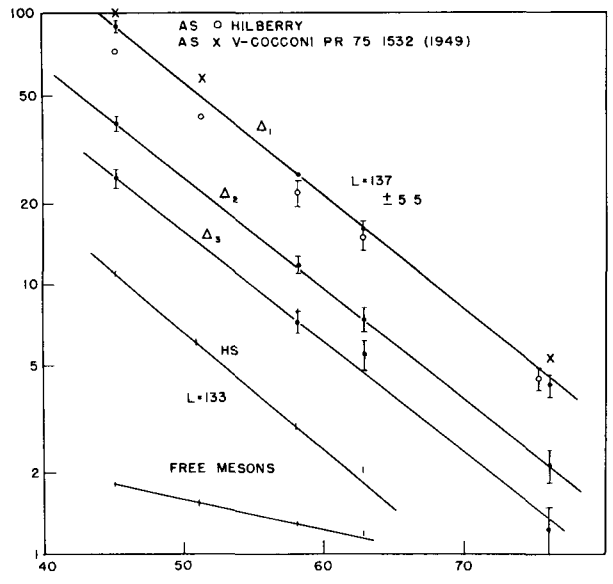

Figure 10. Frequency of air showers (plotted as ordinate) whose electronic density is in excess of Δ_1, Δ_2, and Δ_3 as function of atmospheric pressure in cm Hg. The open circles and crosses represent air shower intensities measured by Hilberry and Cocconi; the solid circles represent the present work. Data are also shown for penetrating showers (HS) and for free μ-mesons.

Figure 10 shows a semilog plot of the variation with atmospheric pressure of the frequency of air showers coincident with a penetrating shower, whose electronic density is greater than three different values, Δ_1, Δ_2 and Δ_3. Their linearity and slope indicate exponential absorption with a mean free path of 133 gm cm^{-2}, the same for all densities, and agreeing with the free paths for absorption measured by Coccini and Hilberry without the penetrating shower recorder. This agreement may be taken as evidence that the electronic and the N-cascades propagate interdependently, though, of course, the identity of their absorption coefficients might be a coincidence. However, the assumption that the N-component is produced in the case of the shower by high energy electrons and photons also permits an explanation of the concentration of N-particles within the shower. The limited experimental information now available on the angular spread of secondaries from nucleonic collisions indicates that an independently developed N-cascade should diverge much more than the electron cascades or the associated N-component observed in these experiments. Though the photogeneration hypothesis is satisfactory in these two respects there is some difficulty in accounting for the cross section needed to yield the observed intensities of the N-component. (O. Piccioni, R. Cool)

Theoretical Topics

Statistical Theory of Cascade Showers (5212)

The main results achieved so far in the electron-photon cascade shower theory are accurate calculations of the average energy spectrum, most recently those of Snyder and Bernstein of this Laboratory. However, the calculations needed for the interpretation of experiments should include information on the fluctuations from this average. Even further, information on the actual distribution in number of particles at a given depth is needed. For instance, it is not yet possible to calculate the chance that an electron of a few Mev will pass through a thin lead plate without the production of secondaries, thus giving the appearance of a non-radiating particle like a meson.

The present work starts from earlier results of Scott and Uhlenbeck, and, using a method recently proposed by Bhabha, along with some recent ideas of Jánossy and Friedman, develops a formalism for a general statistical theory of showers. This approach represents a fundamental improvement on the limited methods recently used by Arley. A simplified model is used in which electrons and photons are treated identically

but the generalization to the actual case is not difficult.

The main idea is the use of a set of master functions $P_N (E_0; E_1, E_2, .. E_N; t)$ $dE_1 .. dE_N$ which give the probability that at a depth t there are exactly N particles whose energies fall within dE_1 at E_1, dE_2 at E_2, etc. E_0 is the energy of the single particle initiating the shower at t = 0. Equations for P_N may be written down, with inclusion of the effects of ionization energy loss. Direct solution does not seem possible, but from the master equations, one may write equations for a set of functions K_n that give the average product of the numbers of particles with energies in $dE_1 .. dE_n$. Of this set, K_1 is the average energy spectrum, and the usual equation for it is obtained.

It is then proved that a solution for K_n can be obtained from K_{n-1} and further that the P_N may be obtained from all the K_n. Thus, in principle, the average energy spectrum contains all the information possible about a shower.

The problem of making calculations with this formalism is discussed, first with the adjoint theory introduced by Friedman. Differential-integral equations derived from physical considerations at the beginning of the shower turn out to have an adjoint relationship to those developed from the end of the shower. Janossy has written the equation for a generating function for the probability of there being at t, N particles of energy greater than E. The adjoint theory leads to some integral equations for this function, and establishes what appears to be the only proper and adequate basis for further work in this field.

The mathematical details are given in an article presented to the Physical Review for publication. (W.T. Scott, Smith College)

On Criteria for Multiple Scattering (5212)

Calculations have been made from the multiple scattering tables of Snyder and Scott on several types of mean value useful for experimental comparison. Use of the root-mean-square for experimental purposes depends on a general theorem concerning mean squares which is independent of any calculations. It is generally not useful because the larger angles, for which the statistics are poorest, are overweighted.

The mean absolute scattering angle (projected in a plane) is, however, a useful criterion in some cases. In others, the poor statistics for large angles can be better overcome by using the median angle. If background makes difficulties at large angles, they may be discarded altogether, and the half-width or 1/e width can be used. The latter utilizes somewhat more data than the former, and is very convenient to use in the Gaussian approximation. As a matter of fact, the accurate calculations fit a Gaussian expression quite well out to the 1/e width. A fifth method of comparison is to fit a normalized Gaussian to the central maximum of the scattered distribution. The Gaussian nature of the central part of the distribution is shown by the fact that the Gaussians calculated from the last three criteria are nearly the same. Indeed, Gaussians calculated from the recent theories of Molière and Butler give almost identical results.

Curves have been plotted for the five quantities as functions of the ratio of the path length t to the mean free path for scattering. All the curves may be fitted to within about 2% by simple logarithmic formulas.

Setting $Z = t/\lambda$ we have,

Mean: $\overline{\eta}^2 = Z\ (0.95 + 0.827 \log_{10} Z)$

Median: $\eta^2_{med} = Z\ (0.16 + 0.62 \log_{10} Z)$

1/2 width: $\eta^2_{1/2} = 1.80\ Z \log_{10} Z$

1/e width: $\eta^2_{1/e} = Z\ (0.50 + 2.50 \log_{10} Z)$

Initial value of normalized curve: $W^2(0) = \left[\pi\ Z\ (0.68 + 2.70 \log_{10} Z)\right]^{-1}$

These results have been reported to the New England section of the American Physical Society at Wesleyan University, November 4, 1950, and will be included in a more extended form in an article being prepared for the Physical Review. (W.T. Scott, Smith College)

A Phenomenological Treatment of Photo-Meson Production from Deuterons (5212)

A calculation which depends neither on meson theory nor on the strength of meson-nucleon coupling is made of the production of single photo-mesons from deuterons, relative to that from free nucleons. The most important approximation is based on the smallness of the meson Compton wave length compared to the radius of the deuteron. The deuteron cross section for this process turns out to be smaller than that of a free nucleon, partly because of binding effects and partly because of the exclusion principle. The former can be predicted, while the latter depends only on the probability of a spin change by the nucleon which emits the meson. As a consequence, an experimental comparison of the H_1 (γ,π^+n) and H_2 (γ,π^+n) reactions can yield this spin change probability.

The experimental information of Steinberger and Bishop (Phys. Rev. 78, 494 (1950)) about π-mesons produced by gamma rays incident on free protons has not thus far been satisfactorily interpreted, even though this is one of the simplest meson reactions. The difficulty lies in present meson theory which is incapable of making quantitative predictions. It seems necessary therefore to fall back temporarily to a phenomenological description of meson reactions and let the experiments show the way. One piece of experimental information which seems likely to be of value in suggesting or testing a future theory is the probability that the proton spin should flip in the photo-meson emission. The most naive picture of this emission process would liken it to the photoelectric effect, in which case the proton would serve merely as the binding center of a meson cloud and suffer no spin change. The already observed angular distribution of the emitted mesons shows that such a picture is inadequate, however, suggesting that the proton plays a more direct part. It is the purpose of this paper to show how the spin flip probability can be measured by comparing the number of mesons emitted when the target proton is bound in a deuteron to the number emitted when it is free.

Feshbach and Lax (Phys. Rev. 76, 134 (1949)) have already pointed out that unless the proton spin changes, the deuteron cross section for photo-meson production will be diminished relative to the free proton cross section. This is because the two neutrons will be left in a triplet spin state and due to the Pauli principle can have only odd orbital angular momentum. For gamma ray energies presently available from synchrotrons

and betatrons, the relative energy of the two neutrons is likely to be of the order of 15 Mev, or even less when the meson is emitted forward. The exclusion of S states can reduce the available phase space considerably. It is to be shown in an extensive paper for the Physical Review that the exclusion principle effect may be expressed in terms of the spin change probability without reference to meson theory. The conclusion reached, therefore, is that the ratio of deuteron to proton cross sections can be used to derive the spin flip probability no matter what theory of mesons and their coupling to nucleons turns out to be correct.

Formulas are also given which allow the experimentalist to calculate the relative probability of a nucleon spin change during π^+ emission, at a given angle relative to the incident photon direction, if he has measured the ratio of the cross sections at this angle for deuterons and protons. The calculation of these formulas is based on the assumption that the meson field surrounding the proton in a deuteron does not differ appreciably from that surrounding a free proton. Throughout the paper the π meson has been treated as though it had zero spin. Actually the final results do not depend on this point. (G.F. Chew, University of Illinois; H.W. Lewis, University of California)

Electronics Division

Pulse Height Analysis

In the last 3 months, three major improvements have been made: a new non-overload amplifier, a new expander amplifier and a new anti-coincidence circuit for use with discriminator circuits in the pulse analyzer proper. Full descriptions will be submitted for publication in the near future. The basic circuits are shown in this report and the following brief description will serve to indicate the methods used:

The non-overload amplifier (Figure 1) makes use of two duo-triodes. Because of the large cathode resistors, no grid current will be drawn for signals of less than 50 v amplitude. The maximum plate signals are about 25 v. Negative feedback is taken from the output plate circuit to the right-hand grid of the input tube. There is also a positive feedback loop in the circuit of the right-hand tube. The gain of the stage is 10, with a rise time less than 0.1 μsec. The balanced stages together with the feedback give greater gain stability than conventional pulse amplifier circuits. A complete amplifier with pulse shaper, inversion, attenuator and high-level output stage has been built and tested. (R.L. Chase)

The expander amplifier (Figure 2) consists of a balanced input stage using 6AH6s, a 6AN5 second amplifier and a 5687 cathode follower. The cathode follower assures low output impedance and also is used to "bootstrap" the plate resistor of the 6AN5. High and low frequency feedback are provided as shown. One of the diodes in the plate circuit of the 6AH6 sets the amplifier cut-off at the point where the current is evenly divided between the input tubes; the other eliminates capacity feedthrough of fast signals. This amplifier will accept 100-v positive pulses without drawing grid current; gain is 10; maximum output rise time is .05 μsec for 50 v into 100 μμfd. (R.L. Chase, W.A. Higinbotham)

In the anti-coincidence circuit (Figure 3), the 100 μμf capacitors are charged during the rise of the pulse and discharged during the recovery. If only the lower discriminator is triggered there will be an output signal from the pulse transformer. If both discriminators are triggered, both condensers will be discharged when the lower discriminator recovers and there will be no net signal across the transformer. The discriminators are conventional. The system responds to pulses as narrow as 0.1 μsec and will also work with slow pulses out to hundreds of μsec in width. It is suitable for single- and multiple-channel applications. (W.A. Higinbotham)

Several of the circuits described have been built and tested, together with the instruments described in the last quarterly progress report. The Atomic Instrument Co. has started production of 15 single-channel analyzers for AEC distribution under supervision of Brookhaven National Laboratory. Delivery is expected to start in April. Specifications are for 0 - 100 v input, expander gain of 10, channel width adjustable from 1/2 to 5 v at the input, stability of channel 1% of channel width, stability of position of channel better than 1/2% of input (1/2 v), output pulse 15 v negative.

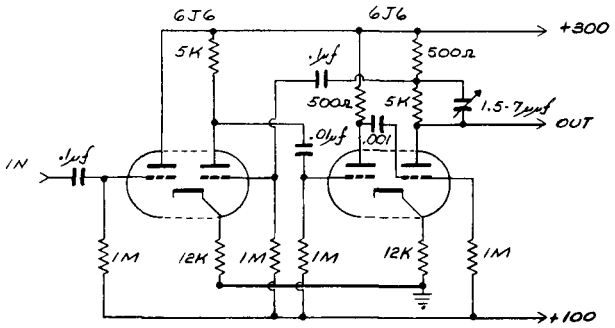

Figure 1. Non-overload amplifier.

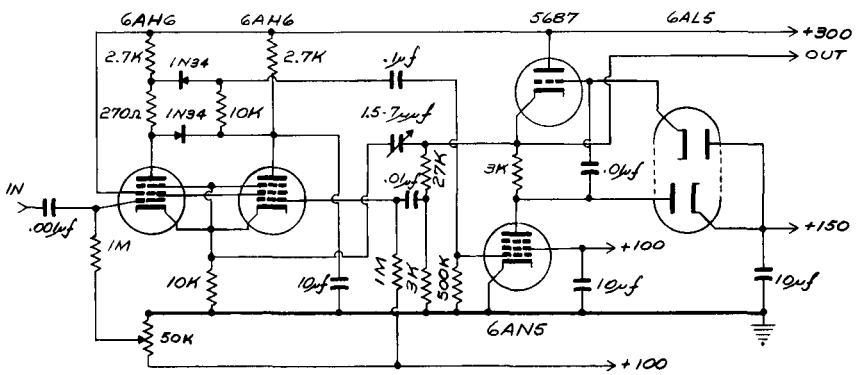

Figure 2. Expander amplifier.

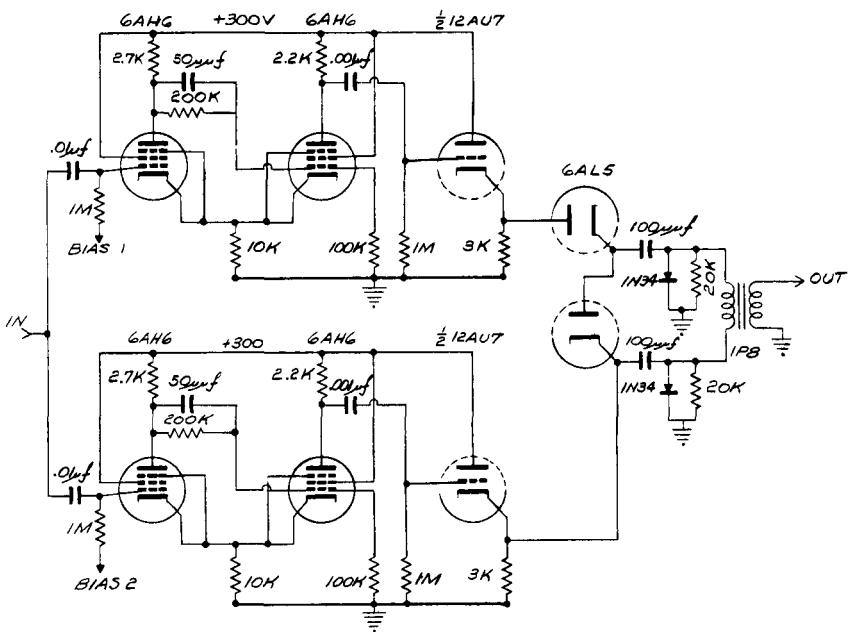

Figure 3. Anti-coincidence discriminator circuits.

A trapezoidal pulse generator was designed for testing the speed of operation of discriminators and pulse height analyzers. It generates a trapezoidal or triangular pulse with adjustable linear rise and fall. (W.A. Higinbotham)

A simplified 10-channel analyzer has been designed which uses only 22 tubes. However, it will only work on pulses several μsec in width. Versatile multiple-channel instruments have been so simplified that this development hardly seems to be worth pursuing. (S.J. Kramer)

Scintillation Spectrometers

An investigation is being made of the factors that influence the resolution of NaI (Tl activated) crystal spectrometers, and to determine how much of the spread in pulse height is caused by the statistical fluctuations in the process.

A wide variation in the resolution has been found which can be obtained with different photomultipliers, and several tests have been developed to determine the difference between tubes. The variation of sensitivity over the cathode surface of the 5819s and the relative quantum efficiencies of different cathodes have been measured for about 20 tubes. The results have been correlated with the resolution of internal conversion lines at different energies. The width of the peak in the pulse height distribution curve at half maximum, in percentages, is given in Table 1.

Table 1

Multiplier Tube	27 kev	670 kev
High sens. - non-uniform	30 - 40%	12 - 15 %
Low sens. - non-uniform	50 - 60%	14 - 17 %
Low sens. - uniform	50 - 60%	10 - 12 %
High sens. - uniform	30 - 35%	9 - 10%

At high energies non-uniformity is more important, whereas at low energies quantum efficiency is more important. All resolution measurements have been made with the same crystal (1/2-in cube) and optical system.

The plot of peak width vs. energy shows the expected statistical spread in the low energy region 8 - 50 kev. At higher energies the width is greater than predicted, indicating that the resolution is not dependent on the energy alone.

Optimum light collection occurs when the crystal is placed directly on the phototube with a film of "nujol" or silicone oil between the surfaces. A conical reflector is placed over all. No success has been achieved in improving the resolution with light pipes.

This system was also used for the comparison of several organic phosphors, using the Cs^{137} conversion line as the source and anthracene as the standard. (W. Bernstein, A.W. Schardt)

Radiation Measuring Instruments

A directional counter for detecting I^{131} was built for the Medical Department. A NaI crystal was used with two 1P21 photomultipliers and a coincidence circuit to reduce background counts. (P. Prentky)

An instrument is partially completed for recording the activity along a piece of copper wire which has been activated in the reactor. This will provide an easy way to record the distribution of neutrons in the pile. (W. Bernstein)

A large BF_3 counter and associated circuits were assembled for a neutron crystal spectrometer. (C.Z. Nawrocki)

Among the special counters produced in the review period were a BF_3 filling in a Victoreen "Thyrode" shell for monitoring a neutron beam, and a multiple wire proportional counter with 2-in diameter thin aluminum window for hard betas. (C.Z. Nawrocki)

The energy sensitivity of the scintillation type of civil defense monitor was measured, and suitable absorbers were determined to give a good approximation to the desired response.

Miscellaneous Circuitry

Orders have been placed for production of the precision high voltage supplies previously described, both 1500 and 5000 v models. The supplier is Burlingame Associates; the price is about $450 and $650, respectively.

Circuits have been designed for controlling a cloud chamber from coincidence of counts in two proportional counters operating in the cloud chamber volume. The circuits include amplifiers, coincidence circuit, timing circuits and means for removing the high voltage from the counters prior to expansion of the chamber. (A. Del Duca)

An expanded scale vacuum tube voltmeter has been designed for use with the generating voltmeter on the Physics Department's electrostatic generator. It consists of a stabilized A.C. amplifier, diode peak rectifier, and D.C. amplifier. The rectifier section may be biased in steps so that the meter will read any 10% interval of the maximum input voltage. (A. Del Duca)

A radio-frequency titrimeter was designed for the Chemistry Department and is now under test. (S.J. Kramer)

The timer for the time-of-flight mass spectrometer has been in operation for 3 months. A variable gain amplifier has been provided. The timing circuit presents the ion pulse of the first and n^{th} revolution of a given mass on the indicating scope. The variable gain amplifier permits independent adjustment of the gain of the amplifier for these two different times. The base lines of the two sweeps are separately controlled. (S. Rankowitz)

G.M. Tubes

Equipment has been set up for taking data on shelf life, life in use and time distribution of spurious counts in G.M. tubes. Considerable data have been collected and will be discussed in the future. (J.B.H. Kuper, C.Z. Nawrocki, F. Lacey, P. Prentky, J.J. Tuffley)

Health Physics Division

Building Survey

There has been a steadily increasing volume of survey work at the reactor as initial operations and early experiments have proceeded. A thorough film survey was made of the shielding to locate voids in the cement and leaks at experimental holes. X-ray films were used, 5 in x 7 in or 14 in x 17 in; several hundred were required to complete the job. In addition, a thorough study has been made of the gamma ray and neutron fluxes from the reactor from the point of view of radiation safety.

The extent of reactor monitoring can be judged from the following list of activities requiring the services of health physicists: air sampling for Argon-41 during an experiment with fans not operating, frequent removal and replacement of sections of the top of the reactor, testing of the pneumatic tubes, removal of contaminated graphite, loading and unloading of uranium slugs, evening and weekend maintenance and testing activities, protective arrangements for a neutron beam brought across a balcony, removal of isotopes from the reactor, survey of ionization chambers removed from the reactor, tests of activity of water in the canal, tests of activity of condensate from the heat exchanger, issuing Health Physics Instructions for maintenance jobs, contamination surveys in all parts of the area.

Survey activities in other laboratories have continued. A series of contamination control problems have developed in connection with the waste concentration experiments at the semi-works area of the Hot Laboratory. An extensive survey was made of the new X-ray installation at the Biology Department and suitable safeguards were set up. Plans for location of fences around the proposed 200-curie irradiation field have been made in cooperation with the Biology Department and a design of a remotely operated source-lifting mechanism is under way. The present irradiation source was assayed and repackaged. The effective strength of this source was found to be 16.4 curies. A 2-curie cobalt-60 source was set up in a field and dosage measured as a function of distance out to 50 ft. This setup was made in such a way as to approximate the Biology field situation. It was found that both pocket chambers and the shield readings of film badges followed an inverse square law closely. The implication is that scattering is not an important factor in this region. The presence of soft components was indicated by the fact that the ratio of densities for open window and shielded portions of the film badges varied with distance. Values of 1.33, 1.22 and 1.18 were obtained at distances of 4, 15 and 50 ft, respectively.

Problems of exposure control in connection with tune-up of the 60-in cyclotron and the 4-Mev electrostatic generator have been worked out. X-radiation has been

the principal hazard thus far. Excellent cooperation from the staff of the accelerator group and special arrangements for taking visual observations have combined to make possible really safe tune-up procedures for the cyclotron.

Area Survey

An internal report on the status of the background radiation monitoring program up to the time of the reactor startup, BNL-80 (I-12), has been written and distributed. This document covers the history of the program, the instrumentation, an analysis of costs, an evaluation of station efficiency and a summary of the results obtained in measuring background radiation. Average values for the chain of 16 area monitoring stations during the year ending June 30, 1950 are given in Table 2.

Table 2

Background Data for Year Ending June 30, 1950

Apparatus	Average Reading	Range of Readings
A	30 c/m	26 - 37 c/m
B	31 "	25 - 37 "
C	25 "	20 - 31 "
D	15 "	13 - 17 "
E	34 "	29 - 37 "
V	1.7 mr/wk	1.3 - 2.0 mr/wk
F - α	2.2 c/m	1.2 - 3.2 c/m
F - $\beta\gamma$	26 c/m	22 - 34 c/m

A - 35 mg/cm^2 glass-walled G.M. tube (Eck and Krebs type)
B - " " " " " " " " " " "
C - Same as A and B but with 83 mil brass shield
D - Same as A and B but with 1 1/2-in lead shield
E - Battery operated ratemeter using same type of tube
V - Ionization chamber and dynamic condenser electrometer
F-α - Continuous dust monitor and scintillation alpha counter
F-$\beta\gamma$ - " " " " mica end window G.M. tube

Numerous peaks of activity due to the radioargon in the cooling air from the reactor were noted during operation in the 1-5 megawatt region. An example of a peak of gamma radiation is shown in Table 3. The disturbances to background thus far have been too small and infrequent to permit a comparison between the dosage values predicated by the meteorologists and those measured by the area monitoring stations. This comparison will become possible with increased power and operation of the reactor over a longer period of time.

The over-all operating efficiency of area monitoring stations (fraction of possible data actually obtained) was determined to be 87% for the month of October. This is the highest value achieved thus far. Some of the loss of data comes from the necessity for servicing the equipment, and it is felt that an efficiency of 90% is about as high a value as can reasonably be expected.

Table 3

Type of Apparatus	Normal Level	Peak Level
$\beta\gamma$ counter (glass)	28 c/m	41.0 c/m
$\beta\gamma$ counter (glass)	28 c/m	39.5 c/m
$\beta\gamma$ counter (brass shield)	27 c/m	35.6 c/m
G.M. ratemeter	40 c/m	78 c/m
Ionization chamber	0.25 mr/day	0.33 mr/day

Personnel Monitoring

Personnel monitoring films and photographic facilities are used extensively for dosage measurements in connection with irradiation experiments conducted by the scientific departments. In this connection, calibration curves have been determined for both the sensitive and insensitive films contained in the personnel monitoring packets over a wide range of dosages. The sensitive film shows the expected reversal of density above about 150 r, but the variation of density with dosage is insufficient for practical use above 10-20 r. The insensitive film is useful up to 50 r, but above that level becomes too dense to be used. A special film known as "Adlux" has been calibrated for use in the high dosage region. The density of this film saturates at about 10,000 r, but is most useful over the nearly linear portion of its calibration curve which extends from 100 to 1500 r.

There has been a gradual increase in requirements for personnel monitoring services. In December, approximately 4000 film badges, 5500 pairs of pocket chambers and 700 neutron films were processed. There were no exposures over the weekly limit of 300 mr, although several individuals received more than 50 mr on individual days. Tests have indicated that wearing of the neutron film for several weeks is permissible without undue loss of tracks due to fading of the latent images. Other tests show that an exposure of neutron film to gamma radiation up to 1 r is tolerable before the resulting fog adversely affects the counting of proton tracks due to exposure.

Urinary Elimination of Strontium

During the preparation of a Sr^{90} source about a year ago, considerable activity was released into the air of the laboratory and inhaled by an experimenter. A study has been made of the urinary excretion of Sr^{90} by this individual since very little human data is available on this subject. It is of particular interest since there had been no previous ingestion of this material, the exposure was an acute one sharply localized in time, and all of the urine excreted immediately after the incident was collected. The amount of Sr^{90} permanently fixed in the body has proven to be only a small fraction of the tolerable amount.

Figure 4 shows the daily excretion of Sr^{90} activity. The rate of elimination per day dropped precipitously from 20,300 disintegrations/min on the first day to 130 disintegrations/min on the 27th day. Following this there is a period of about 3 months during which activity is eliminated with an effective half-life of 23 days,

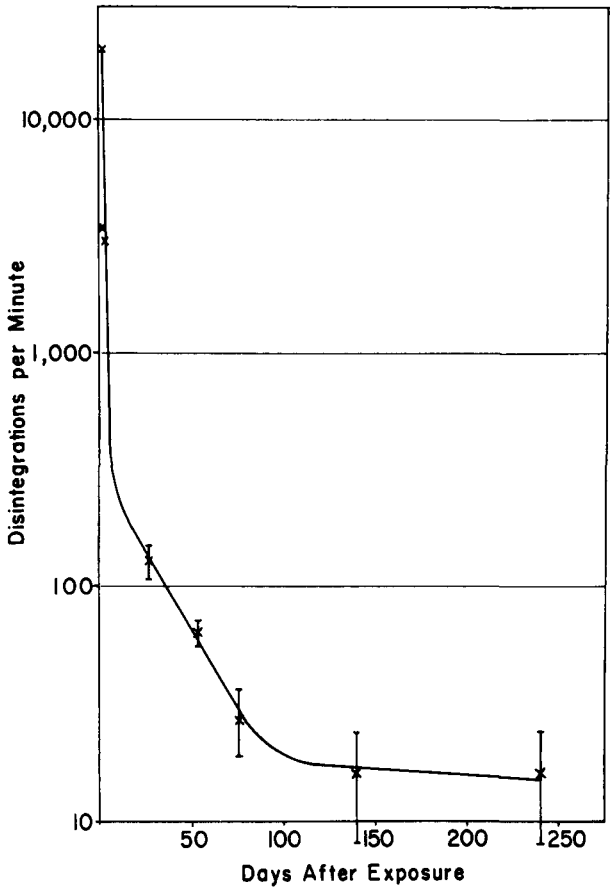

Figure 4.

presumably from material that is not tightly bound while deposited in the body. The elimination leveled off at 16 disintegrations/min, indicating a very small deposition in the bones. Data is insufficient to determine the effective half-life of elimination for this firmly fixed strontium.

Details of the handling of this case at the Laboratory clinic and of the chemical separation of the strontium, which was carried out at Oak Ridge National Laboratory, will be found in an article to be published in the American Journal of Roentgenology.

Miscellaneous

Arrangements have been made with a manufacturer of lantern slides to produce and offer for sale sets of slides of cuts appearing in the "Effects of Atomic Weapons." This was done as a sequel to the training course in defense against atomic attack that was given at Brookhaven National Laboratory last spring. While the Laboratory has no direct responsibility for civilian defense, except for the interim radiological monitoring team, individual members of the Health Physics Division have given numerous training lectures and public talks to groups interested in civilian defense problems.

A decontamination laundry has been set up and operation started by the Architectural Planning and Plant Maintenance Department. All protective clothing from radiation areas will henceforth be laundered by this facility.

There have been an average of one or two calls a week for the Health Physics emergency man.

The research and development program of the Health Physics Division has been established as a separate activity known as "Biophysics Research" effective January 1, 1951.

Publications

W.C. Herman, Beta calibration rack using uranium oxide, Nucleonics 7, 73-4, December (1950)

C.F. Stearns, Inexpensive drying cabinet for instrument storage, Nucleonics 7, 74-5, December (1950)

S. Block, A survey meter for measuring soft beta radiations in the atmosphere, Nucleonics (in press)

F.P. Cowan, L.B. Farabee, and R.A. Love, Health physics and medical aspects of a strontium-90 inhalation incident, American Journal of Roentgenology (in press)

M.M. Weiss and J.B.H. Kuper, Status report - background radiation monitoring program, BNL Report 80 (I-12), July 1, 1950 (for official use only)

J. Handloser and R.A. Love, Radiation doses from diagnostic X-ray studies, American Journal of Roentgenology (in press)

ACCELERATOR PROJECT

Cosmotron (5214)*

The past three months have seen the preliminary testing of the magnet power supply, one quadrant of the magnet, the low-power end of the radio-frequency system, and many parts of the vacuum system. A qualified fabricator for the vacuum chamber has finally been located, and a purchase order issued which, unhappily, does not specify the delivery of the complete chamber until September 1, 1951. This is some months later than the estimated completion date for all the remaining components. To make effective use of this interval, a program is being instigated for testing all completed components together in order to uncover the inevitable minor troubles before the vacuum chamber is installed. The year 1951 still seems a possible one for the completion of the accelerator.

Scheduling

In order that space, time, and manpower may be utilized to the fullest advantage, a rather detailed scheduling procedure has been organized for all work necessary to complete the fabrication of the Cosmotron. Time estimates of the particulars of jobs associated with each of the components of the machine have been studied in an effort to forecast a realistic completion date for each component and for the accelerator as a whole. These data have been analyzed to determine the design, fabrication, manpower, floor area, facilities, and maintenance requirements for the current calendar year. Frequent regular checks of the schedules will be made to determine the overall efficiency and status of operation. (W.H. Moore)

Injection

The injector Van de Graaff machine has been delivered by High Voltage Engineering Corp., Cambridge, Mass. and installation in the Cosmotron building is essentially complete. After searching, with little success, for a satisfactory solution to the electron loading problem with the 6-in aperture accelerating tube of higher pumping speed, the tapered aperture aluminum tube is now being reinstalled in the machine to permit the start of injection studies.

Revisions of the beam analyzer magnet and corona feedback circuits have been started to improve their stability. Improvements of the regulation of the focus, the probe and terminal accelerator power supplies, and the beam pulsing circuitry are underway.

All components of the injection ion optical system are complete except for some minor changes. Its control center is complete and installed and inter-wiring is in progress. (C.M. Turner, J.G. Cottingham)

---

*For explanation of these numbers, see Foreword.

Power

Testing of the motor-generator set that will supply power for the magnet coil of the Cosmotron has been continuing. The Ignitron tank sets have been degassed and the phases checked of the 12-phase A.C. generator output. The building power phasing was corrected to make power available for anticipated future needs. A three-phase line reactor has been installed in the 2400-v feeder to the radio-frequency power supply plate transformer and tests will start in January.

The 1200-kw motor-generator set, capable of supplying 7000 amps at 250 v, was connected to Quadrant I of the magnet for shakedown tests. (A. Wise, G.K. Green)

Magnet

A. Coil Fabrication: The entire magnet coil has been assembled and the last stage of final clamping is proceeding on the last quadrant. The northwest and northeast quadrants are complete except for final connection and adjustment of the water tubes. One-half of the entire group of windings has been leak-tested and work is proceeding on the remainder.

The northwest quadrant (Quadrant I) has been voltage-tested to 10,000 v D.C. from coil to ground for 30 sec; normal voltage is 3000 v D.C. Resistance, at this voltage, to ground is 2 megohms. Coil layer to coil layer resistance was found to be 8 megohms at 2500 v D.C. applied for 60 sec. Normal voltage is 750 v D.C.

The equipment for handling and purifying the water that will cool the magnet coil has been put into operation. The control circuits for this water-cooling system have been tested. (J.A. Kosh, L.D. Stoughton)

B. Resurvey of Magnet Blocks: Prior to the D.C. tests made on the magnet, a check was made upon the tightness and level of the magnet blocks to detect any changes that may have occurred during the six months since erection. Tightening was required because of the drying of the fishpaper insulation between the laminations. Surveying, carried out mainly by W.L. Homer, of the Architectural Planning and Plant Maintenance Division, revealed that the average azimuthal displacement of the front face of the upper magnet jaw with respect to the lower had not changed within the limit of measurement of ± 0.03 in; that the average of the radial level of the lower pole-face remained within ± 0.003 in. in 3 ft; and that the change in the tilt of the geometrical median plane of the entire magnet ring remained within the limit of measurement, ± 0.005 in. in 30 ft. (L.D. Stoughton, W.H. Moore)

C. D.C. Test on Magnet Quadrant: Quadrant I (the northwest quadrant) has been energized to full current, 7000 amps, by temporary connection to the 1200 kw generator, operating overloaded. The rise time in this test was quite long, of the order of 1/2 min. The behavior of the coil was quite satisfactory, but the necessity for some adjustment in the water-cooling system was revealed. Preliminary deflection measurements on the steel plates have been made and, as expected, show that the maximum deflections occur in the end blocks. The maximum deflection measurement, at 7000 amps, was 0.08 in. Strain gages were distributed throughout the quadrant on the coil clamps, tie bars, and spreader bars. The maximum stress on the coil clamps was about 6000 psi; thus, their design is quite satisfactory.

Further tests on this quadrant, including field measurements, will be concluded shortly. It is planned to power each quadrant individually in this way. (G.K. Green, J.M. Kelly, J.A. Kosh, W.H. Moore, L.W. Smith, L.D. Stoughton, A. Wise)

Pole-Face Windings

The pole-face windings, which will be inserted at the top and bottom of the magnet gap in order to correct the shape of the magnetic field, are in the first stage of fabrication. The copper bars for the windings are on hand, and a process for winding them with fiberglass has been established. The polyester resin in which they are to be imbedded is also on the site, and erection of the molds is now taking place. The first casting will be poured near the end of January.

Performance specifications for the generators for the pole-face windings have been forwarded to leading manufacturers of rotating machinery, and negotiations are in progress. (J.J. Mede, W.H. Moore)

Radio-Frequency System

The integrator, which provides the frequency computing system with a signal proportional to the magnetic field, has been finished and tested along with its cycling circuits. A dynamic test on the whole system of integrator, diode-network computer, and radio-frequency oscillator showed that the dynamic and static characteristics check within 0.05 %. Further testing of this system has been temporarily interrupted by the failure of the cycle-counter.

Control circuits for the high level power amplifier have been completed and partially tested. Final testing is awaiting removal to the Cosmotron floor. Work on the water system, air filters, and other auxiliary parts of the amplifier is under way. The automatic volume control and gating circuits for the power amplifier have been designed and laboratory-tested. Final construction is in process. (J.P. Blewett, J. Logue, M. Plotkin, L.C.L. Yuan)

Vacuum System

Assembly of the 20-in diffusion pump stations is now complete. All of the optically dense baffles have been installed. All of the stations have been leak-tested and all leaks repaired. Prior to final installation, all the diffusion pumps will be tested and conditioned with a charge of Octoil-S; experience with the prototype unit corroborates the opinion of outside consultants on the superiority of Octoil-S over Myvane 20 in the pumps.

The fabrication of the transition chambers, between the pumps and the vacuum chamber, is complete and the units have been received here in good condition. Many of the smaller components of the vacuum system, such as expansion joints, vacuum valves, pipe fittings and pipe for the fore-vac lines, have been ordered and received.

The contract for welding the straight section containing the radio-frequency core has been let to the Chicago Bridge and Iron Co., Greenville, Pa. Completion of the

weldments is scheduled for the end of January, and final machining at the Laboratory in March.

A 16-in diffusion pump station and fore-pump has been built for use in leak-testing the sections of the vacuum chamber and other large components of the final system. (C. Lasky)

Vacuum Chamber

The vacuum chamber has been redesigned and simplified to eliminate the "sky-hook" supports and the saw cut and spine structure outlined in previous reports. The new chamber now has a top and bottom structure consisting of a grid of steel bars, approximately 2 in wide, supported only at the ends, where there are hold-down strips for the airtight membrane that encloses the whole grid structure. A contract for the fabrication of the vacuum chamber has been let to the Wellman Engineering Co., Cleveland, Ohio, and work is to start immediately.

A 4-ft long prototype of the newly designed vacuum chamber has been built and evacuated. Mechanical deflections and vacuum tightness at the various gasketed joints were investigated and checked satisfactorily.

A new rubber, Myvaseal, of low vapor pressure, has been shown to be a suitable alternate to Kel-F for the airtight membrane of the vacuum chamber and to have considerable mechanical advantages (reported in "Special Investigations," below). Although to date no fabricator has been able to make satisfactory 36-in seals with 0.010-in Kel-F, the membrane material previously under consideration, satisfactory seals have been made in the laboratory and equipment is being designed to carry out a full-scale sealing job here, if required. This equipment will also be suitable for vulcanizing Myvaseal seams.

The equipment for handling and inserting the vacuum chamber in the magnet gap has been designed. A program for cleaning, assembling, leak-testing, etc., is in the planning stage. (D.D. Jacobus, I. Polk, L.W. Smith, L.D. Stoughton)

Control and Wiring

Fabrication of the master timing system, which provides time marker pulses, delayed pulses, etc., with respect to a starter pulse, is nearly complete. Delivery is anticipated before the end of January.

Equipment for the derivation of a timing pulser from the magnet coil current and the field is in the process of design and construction.

Schematics for the control wiring of all the major components of the Cosmotron are in final form, and wire schedules have been prepared from these schematics. Installation is proceeding on the control wiring on the main floor. The local control centers for the fore-vacuum system, the injector system, and the water-cooling system have been installed and wired. The communications center for the public address system, the private telephone system, and the intercom system has been wired. (E. Dexter, R.R. Kassner, J.M. Kelly, F.J. Seufert, J.L. Walsh)

Building

Several building modifications (doors, safety fences, platforms, auxiliary steam supply, etc.) have been made for extra safety and convenience. The gas-handling equipment for the injector Van de Graaff machine has been installed. (J.S. Medd, L.D. Stoughton)

Special Investigations

A. Electron Loading in Van de Graaff Tubes: The clean vacuum system and diode, mentioned in the last progress report, have been completed and a study of high field electron emission from contaminated surfaces is under way. This diode consists of a wire cathode and a coaxial cylinder anode; with its use, high fields can be applied to the wire without using high voltages. The effects observed in the parallel plane diode have been confirmed and extended. Heating of the wire produces a marked increase in emission. Bombardment in a gas discharge destroys the emission. A voltage threshold for initiation of emission has been noted, just as is observed for electron loading in Van de Graaff machines.

A study of the electron loading phenomenon in the injector Van de Graaff machine itself, using a large diameter vacuum tube, has not given any satisfactory solution of the problem and will be discontinued. (J.P. Blewett, S. Golian, C.M. Turner)

B. Eddy Current Analysis: A theoretical study has been made of the disturbances in the magnetic field of the Cosmotron gap to be expected from eddy currents in nearby components. Of particular importance are the eddy currents in the walls of the vacuum chamber. Extensive analysis of the eddy currents in the previous "saw cut" design for the top and bottom of the vacuum chamber showed that modifications needed for a mechanically sound structure would result in dangerous effects on the shape of the magnetic field. In the redesign of the vacuum chamber, further eddy current studies have set limits on the dimensions of its components.

The design of other structures in the Cosmotron is being monitored for items that would create possible eddy current or ferromagnetic disturbances in the magnetic field. (M.H. Blewett)

C. Particle Oscillations: An analysis has been made of the forced betatron oscillations in a synchrotron with straight sections. This treats of the modification, engendered by the insertion of the straight sections required in the Fourier analysis (in the case of a circular machine) of the azimuthal magnetic inhomogeneities and their effect on the betatron oscillations of the particles being accelerated. (N.M. Blachman)

D. Vacuum Testing: Tests on the vacuum properties of various plastic materials, as described in the last progress report, are continuing. Of considerable practical importance is the recent availability of a special form of rubber, Myvaseal. This rubber evolves gas at a rate considerably greater than Kel-F, but its mechanical properties, from the standpoint of joining and forming leak-tight seals at the gaskets, is so superior to Kel-F that it appears better suited to our needs. The gassing may be reduced

by finishing by grinding, or by greasing, the steel surfaces under the Myvaseal.

The following table gives the ultimate pressure in a test chamber, and the gassing rate (rise in pressure in 100 sec with the pumps blanked off) for various materials. The design of the test chamber and pumping system gives values approximately those of the final system.

Table 1

Material Forming Cover of Test Chamber	Ultimate Pressure after about 10 Days	Gas Evolution (Δp/100 sec)
Steel	0.8×10^{-6} mm Hg	4×10^{-6} mm Hg
Kel-F	1.0	--
Myvaseal on rough surface	4.0	80
Myvaseal on machined surface	2.0	75
Myvaseal with Apiezon N on machined surface	1.8	18

Use of liquid nitrogen reduces these values by a factor of about two. All data refer to T = 25°C.

In view of these results, plans now call for the use of a Myvaseal sheet over a vacuum chamber with a 32-microinch finish. It is not expected to be necessary to apply vacuum grease to the surfaces. (J.C. Street, G.B. Collins)

60-Inch Cyclotron (5214)

Following a relatively short period of operation at only minor beam currents, considerable radioactivity occurred within the vacuum tank and around the dees. From this it was apparent that after even a limited amount of running, it would be extremely difficult to make changes in the structure without subjecting personnel to the hazards of excess radiation. Accordingly, a very thorough test of the dee structure and deflector was undertaken without a beam present in order to uncover weak points in design while it was still relatively simple to correct them.

The radio-frequency shorting bar was moved to permit operation at a slightly (0.4 mc) higher frequency. First, a breakdown of the current finger connections, dee stem to shorting bar, occurred and was repaired. Then, the outside contact flat line fingers between the shorting bar and the obround (the outside oval-shaped container for the dee stems) burned up and were replaced with a new design, which failed after a running period of 12 days. A third version of the shorting bar-obround contacts resulted in 10% higher dee voltage, but after 11 days of test, the shorting bar - dee stem contacts failed. A redesigned contact arrangement was installed but failed the next day, this time between the shorting bar and obround. At present, a new clamped ribbon contact finger is on the drafting board. (W.W. Merkle)

G.E. Electrostatic Generator (5214)

The contract settlement with the General Electric Co. concerning this machine now allows the planning of a long-range program of modification and improvement, chiefly in the ion accelerating system, including the accelerating tube, the ion source and the vacuum system. In the meantime, research with this machine is continuing, with studies of gamma-ray spectra and particle emission from the light elements under proton and deuteron bombardment. (C.M. Turner)

CHEMISTRY DEPARTMENT

Eighteen individual reports, covering various phases of the Department's research, are given in the following sections. The detail in which the different reports are presented varies considerably, depending on the nature of the problem and the degree of completeness of the work.

Experiments on the low temperature absorption spectra of rare earth and heavy element compounds have been continued. The spectra of solid uranium tetrachloride and uranium trichloride are reported as well as the spectra of their solutions. Similar observations on gadolinium bromide and europium chloride are reported. The low temperature technique has also been employed to study the absorption spectra of chlorophyll; spectral evidence for a second component in chlorophyll b is found at low temperature.

The Department's 2-Mev electron Van de Graaff has been employed in service irradiations and in studies on the radiation decomposition of water, aqueous halide solutions, and aqueous peroxide solutions. Chemical methods for measuring the dosage due to the 2-Mev X-rays have been studied. The oxidation of ferrous sulfate solutions furnishes the most satisfactory method at present.

The electron transfer exchange reactions between ferrous and ferric iron, thallous and thallic thallium, and ferrocyanide and ferricyanide have been further investigated. The kinetics of the reaction in the first system are now well outlined. In the second, new information on the effect of chloride is reported. In the third, past work has been extended but no essentially new results have been obtained. The kinetics of the exchange reaction between nickelous ion and its complex with ethylenediaminetetra-acetate have been investigated. Earlier tracer measurements on the mechanism of the Willgerodt reaction have been extended, and it is proved that no skeletal rearrangements occur. In connection with this investigation, some questions of technique bearing on the validity of previous C^{14} work have been studied.

Interest in predicting the isotope effect on the mass spectral pattern of isotopic acetylenes has led to the calculation of the normal coordinates for the stretching modes of these molecules; the analysis of the stretching frequencies is reported. New data on the relative abundances of the neon isotopes have been obtained. An improved method for the mass spectrometric determination of deuterium in water has been developed. Based on the quantitative conversion of water to ethane, it minimizes many of the difficulties encountered in the conventional procedure of converting water to hydrogen and measuring the latter.

Some observations on the effectiveness of TTA-metal complexes in Szilard-Chalmers separations are described. A precise measurement of the half-life of I^{129} has been made, leading to a value of 1.72×10^7 yr. With certain assumptions, this is made the basis for an estimate of the time interval between the formation of the elements and the formation of the earth; the value calculated is 2.7×10^8 yr. The process of the ejection of electrons from an atom undergoing alpha decay has been studied through measurements on the characteristic lead X-rays emitted from Po^{210}; the results are compared with theory.

Absorption Spectra of UCl_4 and UCl_3 at 77°K in Solid and Solution (5311)*

S. Freed and K. Sancier

Abstract

Further work has been done on the ultraviolet irradiation of solutions of anhydrous UCl_4 in 10% n-propyl alcohol, 90% hydrocarbon (1:1 propane-propene) at 77°K. It is established that the UCl_4 is reduced photochemically to UCl_3 in solution. Anhydrous UCl_3 was prepared by reduction of UCl_4 with H_2; during this process an intermediate is obtained. The spectra of anhydrous UCl_4 and UCl_3 at 77°K as well as that of the intermediate are reported.

As reported in BNL 64 (S-6), p. 29, a solution of anhydrous UCl_4 in 10% n-propyl alcohol, 90% hydrocarbon (1:1 propane-propene), hereinafter called "proper" alcohol solution, is transformed from a green to a purple solution at 77°K by irradiation with a hydrogen discharge tube. Previously, it was found that a few hours' irradiation produced a purple coloration that disappeared upon warming from 77°K to 230°K. Successive cycles of irradiation and warming produced a condition in which no further purple coloration would form, although the solution appeared to the eye the same as the original green.

It may be mentioned that in the initial experiments of the preparation of "proper" solution of anhydrous UCl_4 some uranyl salt was formed; upon extended irradiation, its characteristic fluorescence disappeared, presumably because of photochemical reduction.

In order to obtain a high concentration of the purple solution, all of a small volume of UCl_4 solution was irradiated. This was done in a quartz cell 1 x 10 x 20 mm^3 containing 0.2 cc. The following procedure was used in preparing the "proper" solution of anhydrous UCl_4: In an extension of the quartz absorption cell, anhydrous UCl_4 (kindly supplied by N. Elliott) was dried at 150°C in an atmosphere of hydrogen chloride and sublimed into the absorption cell at about 500°C in vacuum. The extension was then sealed off. The sublimed UCl_4 formed a continuous thin film which was observed spectrally before dissolving. To obtain its "proper" solution, anhydrous n-propyl alcohol was condensed upon it, rapidly dissolving the UCl_4. Into this solution 1:1 mixture propane-propene was condensed, and finally mixed by agitation at 230°K (propane bp).

This solution was irradiated for 100 hr at 77°K and spectra were taken periodically. It was possible by use of a microscope to view the 1-mm cross section and thus have a 10-mm path length. With the hydrogen lamp irradiating the 10 x 20 mm side of the cell, the solution first became purple at the nearest quartz interface. This color slowly, over many hours, diffused throughout the solution. Prior to diffusion it was possible to take spectra of both the green and purple solutions concurrently. Figure 1 shows the spectral changes upon irradiation. In the near infrared (Figure 3), discrete

*For explanation of these numbers, see Foreword.

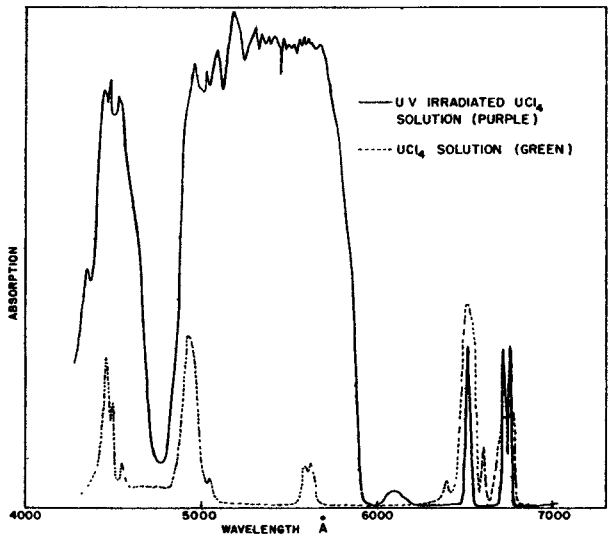

Figure 1. Spectra at 77°K of anhydrous UCl_4 in "proper" alcohol solution before and after ultraviolet irradiation.

structure appears; similar structure appears in the spectra of anhydrous UCl_3 crystals and of aqueous UCl_3 solutions but not in those of UCl_4. Further evidence that the purple solution is due to U^{+3} ions comes from the following facts: (1) Aqueous solutions of U^{+3} ions are purple; (2) after removal of the solvent, a chemical analysis of the ratio of chloride-to-uranium gave 3.2. The solution irradiated for 100 hr at 77°K remained purple at 300°K when the volatile hydrocarbon but not the alcohol was removed.

The visible spectrum of the irradiated UCl_4 solution at 77°K, corrected for the possible presence of UCl_4, cannot at present be brought into strict correspondence with the spectrum of the aqueous solution (M. Fred and C.J. Rodden, Analytical Chemistry of the Manhattan Project, Chapter VII, Photometric Methods) of UCl_3 at room temperature nor with the spectrum of anhydrous UCl_3 crystals at 77°K. The general absorption between 5000Å and 6000Å of the irradiated UCl_4 solution is somewhat unexpected, but it may possibly be accounted for by shifting and merging of the two intense bands of the aqueous UCl_3 at 5200Å and 6200Å; this is not typical of rare-earth-like ions. On the other hand, it may possibly arise from the "solvated" chlorine atom formed in the process of the reduction at the low temperature.

In order to check this behavior it was proposed to prepare chemically a solution of anhydrous UCl_3 and measure its spectrum at 77°K.

The spectrum of anhydrous UCl_4 at 77°K, prepared as described above, is shown in Figures 2 and 3. No discrete structure is observed in the near infrared (Figure 3). The ultraviolet spectrum exhibits general absorption below 4000Å. The absorption spectrum of anhydrous UCl_4 at 77°K recently reported by Freymann et al. (M. Freymann, R. Freymann, R. Rohmer, and P. Hamon, Compt. Rend., 1524-6, April, 1950) agrees in general with results found here, but differs in some particulars.

For the purpose of preparing the "proper" solution of anhydrous UCl_3, anhydrous UCl_4 was reduced in a quartz cell with hydrogen. In the initial experiment the UCl_4 was heated at about 500°C for 2 hr in slowly flowing hydrogen. The evacuated product was heated to 500°C to sublime off unreacted UCl_4. The product, having much the same light yellow-greenish color as UCl_4, was analyzed spectrally at 77°K (Figures 2 and 3). Its spectrum does not correspond to UCl_4, nor to UCl_3 (later to be described). That this reduction product is not UCl_3 seems clear from the absence of infrared absorption (Figure 3); it is not UCl_4 as evidenced from its spectra and its non-volatility. It may be a mixed valence salt, perhaps U_2Cl_7, as is suggested by analogy with U_2F_9.

Reduction of this product with hydrogen at 700°C produced olive green needle-like crystals of UCl_3 so small as to make impossible direct spectral examination of single

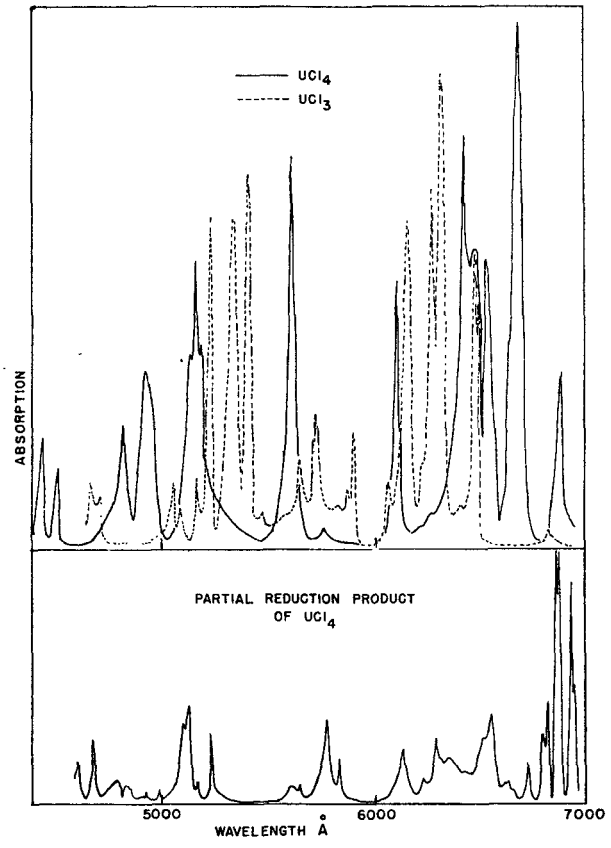

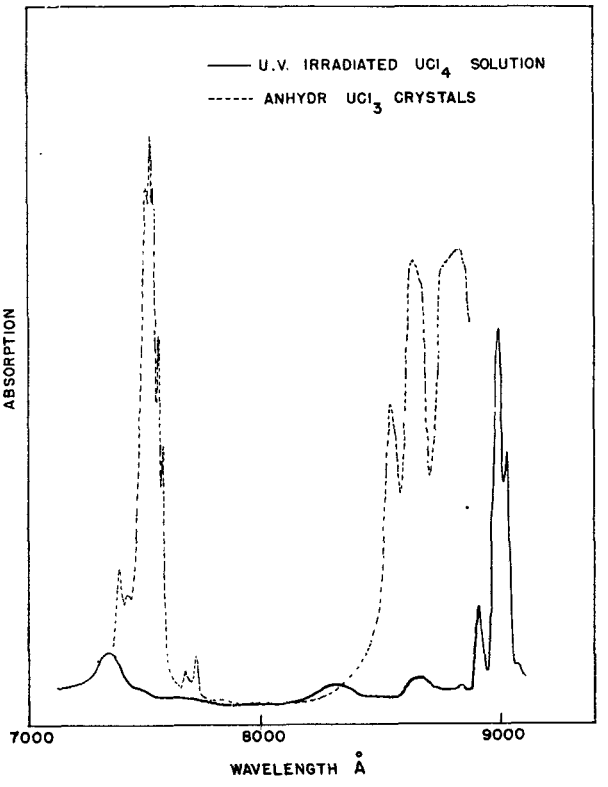

Figure 2 (Above left). Spectra at 77°K of anhydrous UCl_4 and UCl_3 crystals (above), and the partial reduction product of anhydrous UCl_4.

Figure 3 (Above right). Spectra at 77°K of anhydrous UCl_4 in "proper" alcohol solution after ultraviolet irradiation, and of anhydrous UCl_3 crystals. Anhydrous UCl_4 crystals and their "proper" alcohol solution do not absorb in this region.

crystals with our microscope. The crystals were birefrigent, a property that permitted their spectral examination: by placing the specimen at 77°K between the crossed nicols of a microscope, all light except that passing through the crystal was blocked.

The anhydrous UCl_3 spectrum shown in Figures 2 and 3 is sharper than the spectrum of UCl_4 and the lines are grouped in more rare-earth-like character.

Absorption Spectra of Gadolinium Bromide and Europium Chloride (5311)

S. Freed and K. Sancier

$GdBr_3 \cdot 6H_2O$

The absorption spectrum of gadolinium bromide hexahydrate was examined in 10% "proper" alcohol solution at 77°K using a 65 cm solution path. It was possible to

examine the 2700Å and the 3000Å groups in the first and second order of the grating, but it was not possible to examine the 2500Å group, probably because of excessive light scattering.

The absorption lines of gadolinium in the "proper" solutions are almost as sharp as those found for the crystal. Furthermore, the wave lengths of this Gd^{+3} in solution and in the crystal (S. Freed and F.H. Spedding, J. Am. Chem. Soc. 52, 3747 (1930)) are nearly coincident with only slight shifts up to 5Å.

$EuCl_3$

The absorption spectrum of anhydrous europium trichloride at 77°K was studied using the crossed nicol technique to permit observation of light that passed through crystals, and no other. The spectral region from 3600Å to 9000Å was examined in the first, second, and third order of the grating, and with an effective crystal thickness of about 1 mm.

A sample of $EuCl_3 \cdot 6H_2O$ was dehydrated by passing HCl over the salt at about 190°C. This spectrum exhibits fewer lines that that reported for EuF_3 (S. Freed and S.I. Weissman, J. Chem. Phys. 8, 878-9 (1940)).

Further dehydration in an HCl atmosphere at 250°C reduced the number of lines in the spectrum enormously, especially in the 4000Å group. In addition, the 5798Å and 5835Å lines disappeared, and the 5362Å line and others in the near infrared appeared.

When heated from 190°C to 250°C, some of the light amber $EuCl_3$ crystals became coated with a dark layer sufficiently thick to make a few crystals opaque. The spectra of the individual crystals revealed no difference between the dark and light varieties.

The Absorption Spectra at Low Temperatures of Solutions of Chlorophyll a and of Chlorophyll b (5311)

S. Freed and K. Sancier

Abstract

The visible and ultraviolet absorption spectra of chlorophylls a and b were measured in solutions of 10% propyl ether and 90% 1:1 propane-propene at 230°K and 77°K. Variations in the spectrum of chlorophyll b at 77°K for two different samples suggests the presence of a second component in chlorophyll b.

The absorption spectra of solutions of chlorophyll a and of chlorophyll b at 230°K and 77°K were obtained to observe refinements in the spectra which are to be expected from a reduction in temperature. The solvent was a fluid consisting of 10% by volume di-n-propyl ether and 90% hydrocarbon, equally divided between propane and propene.

The chlorophylls had been prepared and purified at the University of Minnesota by R. Livingston and his associates who also generously sent the absorption spectra of their solutions in anhydrous ethyl ether. These spectra resembled rather closely those obtained by Zscheile and his collaborators (e.g., F.P. Zscheile and G. Comar, Bot. Gaz. 102, 463 (1941)).

The first stage in the preparation of the solution, that of dissolving chlorophyll in di-n-propyl ether, followed a suggestion of Professor Livingston: The di-ethyl ether was displaced after successive additions of di-n-propyl ether and subsequent partial evaporations of the resulting solvent almost to dryness at 273°K with immediate addition of more propyl ether. This procedure led to a solution having an estimated content of less than 0.01% di-ethyl ether. The solutions of the chlorophylls in di-n-propyl ether were brought to the temperature of dry ice, and then propane and propene (Research Grade, Phillips Petroleum Co.) were condensed in, thus homogeneously diluting the ethereal solution. At 230°K, the boiling point of propane, the solutions were highly mobile; at 77°K, the viscosity appeared to be about that of glycerine at room temperature. The final chlorophyll concentration was about 2×10^{-4} M.

The absorption spectra were taken by means of a Cary double beam spectrometer through a path length of about 1 mm. The fused quartz absorption cells were thoroughly washed with distilled water to remove traces of any acid, then flamed under high vacuum. The quartz in the two beams was made almost optically equivalent and complete compensation for quartz, solvent and coolant at the two temperatures was achieved by obtaining balances with the multipot over the ranges studied.

Table 1

Maxima of Absorption for Chlorophyll a

230°K		77°K	
Wave Length λ (Angstroms)	Intensity I (Density Units)	Wave Length λ (Angstroms)	Intensity I (Density Units)
2500	.25	2600	.15
2800	.01	----	
2960	.06	3020	.35
3100	.01	3330	.02
3280	.2	3410	.5
----		3620*	.04
3810	.7	3900	1.2
4150	3.0	4200	> 3.0
4250	4.0	4400	> 4.0
5000	.02	5150	.02
5350	.04	5400	.03
5800	.10	5850	.02
6200	.3	6200*	.06
		6350	.30
6650	1.3	6700	1.4

*New band.

Table 2

Maxima of Absorption for Chlorophyll b

230°K		77°K	
Wave Length λ (Angstroms)	Intensity I (Density Units)	Wave Length λ (Angstroms)	Intensity I (Density Units)
2530	.2	2530*	.02
2580	.02	2550	.4
		2590*	.02
2880	.02	2900	.02
----		3030	.01
3050	.1	3140	.4
		3400*	.02
3330	.1	3440	.4
3600	.02	3680	.04
3800	.02	3890	.06
4300	.4	4500	.6
4700	1.5	4800	1.75
----		4815*	.1
----		5200*	.01
5550	.01	5600	.04
----		5850*	.01
5950	.07	6050	.15
----		6300*	.2
6500	.5	6600	.5

*New band.

In general, reduction in temperature as can be seen from the spectra brings about a sharpening of the bands and a shift of the corresponding peaks toward longer wave lengths, similar to that observed in the spectra of carotene (S. Freed and C. J. Hochanadel, Science 110, 298 (1949)). Reduction in temperature from 230°K to 77°K enhances the intensity of most bands. However, in Figures 1-4, intensities of the spectra at the two temperatures are not to be compared because of differences in concentration caused by precipitation of a small fraction of the chlorophylls upon lowering the temperature of these solutions. Changes in structure of the spectra brought about by reduced temperature are the primary consideration.

In Tables 1 and 2 are tabulated in angstroms the wave lengths, λ, of the maxima of the absorption bands appearing at 230°K and 77°K for chlorophylls a and b, respectively. The estimated relative intensity within a spectrum of each band in density units, read from the Cary instrument, is also given to help correlate the band movements.

In the spectrum of chlorophyll a shown in Figures 1 and 2, all bands are shifted to the red upon lowering the temperature. The 6200Å and 6350Å bands at 77°K seem to arise from the 6200Å band at 230°K. But the 3620Å band at 77°K seems to have no counterpart at 230°K.

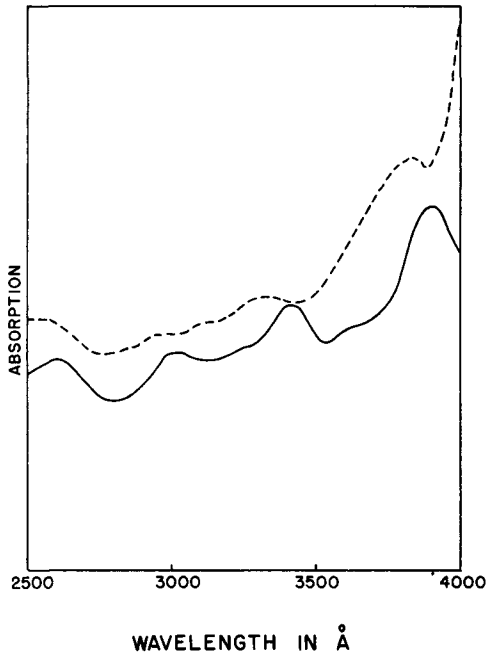

Figure 1. Changes with temperature of ultraviolet absorption spectrum of solutions of chlorophyll a.
230°K, - - - - -; 77°K, _____ .
(Curves taken at different concentrations.)

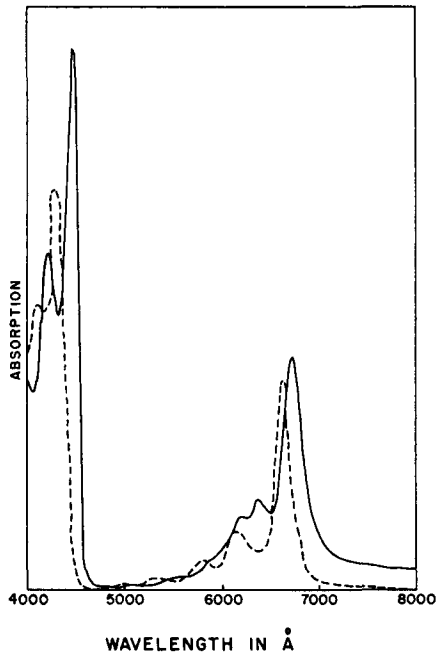

Figure 2. Changes with temperature of visible absorption spectrum of solutions of chlorophyll a.
230°K, - - - - -, 77°K, _____ .
(Curves taken at different concentrations.)

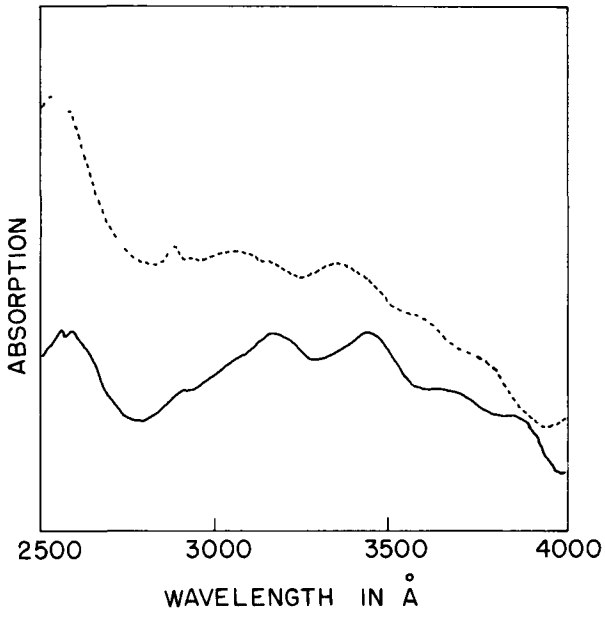

Figure 3. Changes with temperature of ultraviolet absorption spectrum of solutions of chlorophyll b.
230°K, - - - - -; 77°K, _____ .
(Curves taken at different concentrations.)

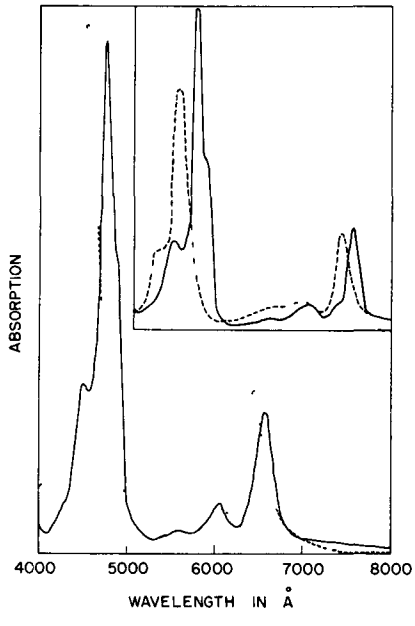

Figure 4. Changes with temperature of visible absorption spectrum of solutions of chlorophyll b.
230°K, - - - - -; 77°K, _____ .
(Curves taken at different concentrations.)

In the spectrum of chlorophyll b shown in Figures 3 and 4, structure appears at 77°K which was obscure at 230°K. At present the correlation of absorption maxima is in some doubt for intensities equal to or less than .02 (see Table 2). The 4800Å and 6300Å bands at 77°K are new, and in two different samples their intensities vary together relative to the rest of the spectrum (see the two sets of curves in Figure 4). The 4300Å (230°K) or 4500Å (77°K) band also shows intensity variations according to sample, and at low temperature its intensity parallels the intensity behavior of the new bands; this band at 300°K is indistinguishable from reported spectra. On the possibility that solvation of the chlorophyll with residual ethyl ether in the solvent might be responsible for the new bands, about 30% ethyl ether was added to the propyl ether. However, no change was observed in the spectra at 77°K. The behavior of these three bands suggests the presence of a component closely related to chlorophyll b, detectable at low temperature because finer discrimination is possible there and because the relative shift of wave length of the two substances as a function of temperature may be favorable.

After the chlorophyll solutions had been at 77°K, the 230°K spectrum was retaken with the chlorophyll completely dissolved and was found to be unchanged. The room temperature spectra (chlorophylls in ethyl ether) were finally taken and found to agree in all respects with previous work.

Radiation Chemistry

A.O. Allen

Operation of Generator

The Department's 2-Mev electrostatic generator operated very satisfactorily throughout the quarter. It was used intensively for the researches in radiation chemistry described in the following sections. In addition, the following service irradiations were made for other groups:

For G. Friedlander and E. Wilson (Chemistry Department), tests on coloration by X-rays of various types of glass for windows in radiation shields.

For A. Edelmann and G. Mateyko (Biology Department), cathode-ray irradiation of the pituitary gland in living rats.

For H.A. Scheraga and L.F. Nims (Biology Department), irradiation by X-rays of fibrinogen solutions.

An integrating current meter, developed by the Electronics Division was placed in service. This gives a reading of the total dose of radiation delivered by the machine, and also allows accurate reading of cathode-ray currents over a very wide range of current.

Experiments on the decomposition of water and aqueous solutions and on dosimetry measurements are described in the following sections.

Decomposition of Water and Dilute Halide Solutions with 2-Mev X-Rays (5311)

E.R. Johnson and A.O. Allen

It is shown that dilute potassium iodide or bromide solutions decompose in a reproducible manner to hydrogen and oxygen. At high dosages with 2-Mev X-rays a material balance between these products is not obtained, indicating the presence of other products.

Some comparison between the decomposition of halide solutions and water is given.

It is a well-established fact that during X-ray bombardment of pure water little decomposition occurs, but in the presence of dilute salts such as KBr or KI measurable decomposition does occur. This research is concerned with the mechanism by which these salts increase the decomposition yield of water. A thorough understanding of this problem should provide necessary information for the understanding of more complex solutions. Theories regarding the mechanism of this process have been presented in the literature (A.O. Allen, J. Phys. Colloid Chem. 52, 479 (1948); Dainton, ibid., 490).

Experimental

The water used in these experiments is redistilled from permanganate, then dichromate followed by hydroxide, and collected in a quartz receiver. Figure 1 shows the general arrangement for filling the sample bulbs. The bulbs are blown from 2-mm pyrex capillary tubing which is first heated to softening under a constant stream of oxygen to remove any absorbed organic material. During the actual blowing, the breath is filtered through cotton and glass wool. The sample bulbs (about 10-cc volume) are first

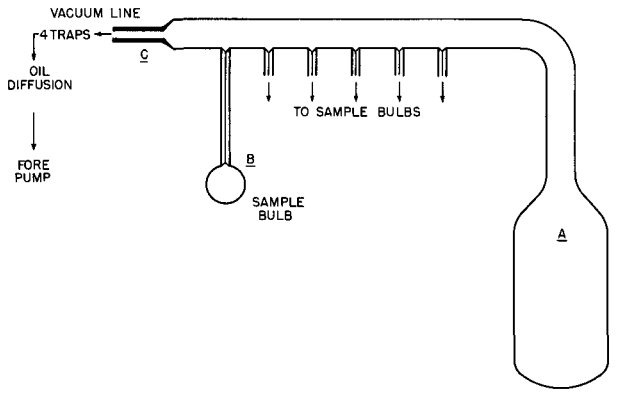

Figure 1 (Above). Filling line.

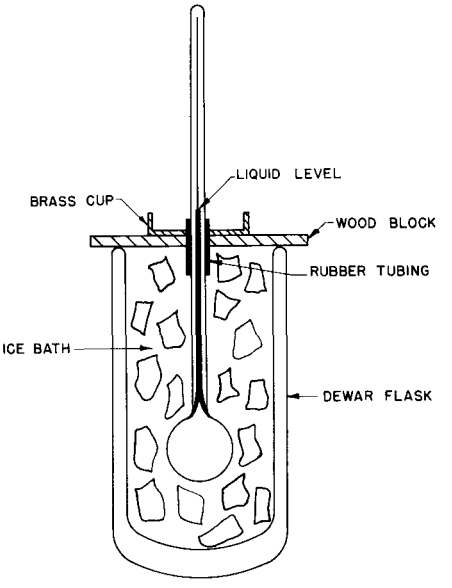

Figure 2 (Right). Seal-off arrangement.

filled with pure water and then allowed to soak for 24 hr, after which time they are emptied and sealed to the line (protected from organic vapors from the breath with a dry ice trap). The solution bulb (A, Figure 1) is treated in a fashion similar to the reaction bulbs.

The procedure for filling the bulbs is as follows: The solution to be irradiated is placed in bulb (A) and frozen with liquid N_2 while the entire system is being pumped down. When the pressure is less than $1x10^{-5}$ mm (as measured by an ion gauge), the liquid N_2 trap is removed from the solution bulb and the solution boiled (about 40-50°C) and refrozen. When the pressure is again less than $1x10^{-5}$ mm, that part of the line containing the solution and reaction bulb is sealed off from the remaining portion by means of the heavy walled tubing (C). The solution is then brought to room temperature and the reaction bulbs filled by simply pouring in the solution. The bulbs are sealed off in such a fashion that when the solution is at room temperature only the liquid phase is present. This is accomplished by arranging the bulb as shown in Figure 2. The metal cup is kept filled with liquid N_2 and the capillary sealed off about 8-9 mm above the frozen liquid level.

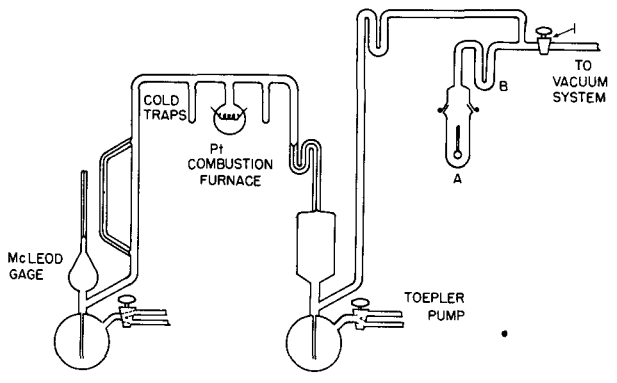

Figure 3. Analysis line.

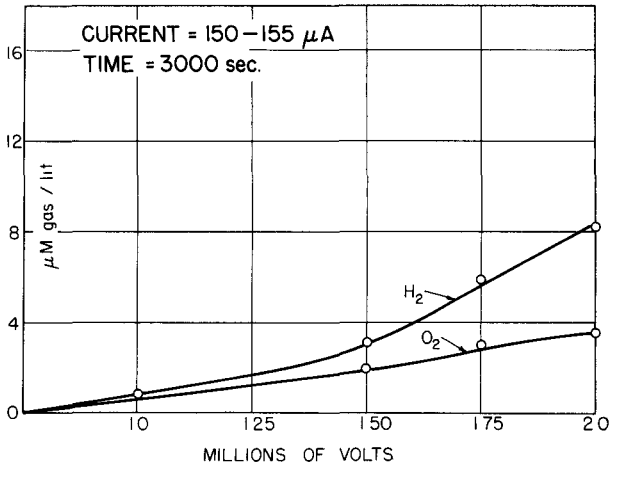

Figure 4. Yields of hydrogen and oxygen from pure water.

The irradiated samples are analyzed in a simple vacuum system shown in Figure 3. The sample is placed in trap (A), and when a vacuum of less than $1x10^{-6}$ mm is obtained, stopcock 1 is closed and an n-butyl bromide bath (-118°) is placed on trap (B). After a few moments a dry ice and acetone bath is placed under trap (A); this freezing mixture causes the bulb to break in about 1/2 hr. After the bulb has broken, the sample is degassed by pumping, boiling the liquid, freezing with dry ice and acetone, pumping again, until the solution is gas-free. The n-butyl bromide trap removes the water vapor only and does not trap out any CO_2 that may be present. The gases are held in the McLeod section of the system during the pumping by the mercury capillary trap on top of the Toepler pump. When the sample has been thoroughly degassed (the only gases known to be present are H_2, O_2, and CO_2, plus some H_2O vapor), it is removed from the line and analyzed for H_2O_2. The gases are analyzed in the conventional manner.

Table 1

Observed and Calculated Values for Degassing and Combustion Procedures

Values	Degassing (cc N.T.P.)	Combustion (Gas Remaining) (μM)
observed	0.260	389
calculated	0.261	392
observed	0.322	511
calculated	0.333	508
observed	0.507	905
calculated	0.518	926
observed	4.40	567
calculated	4.94	578

Both the methods of degassing and analysis of the products were checked with known samples and found to be reproducible within about 2 % for the pressure range studied. Table 1 lists the observed and calculated values obtained for both the degassing and combustion procedures. Combustion procedures are reported in terms of residual gas after combustion.

Results

All irradiations unless otherwise noted were carried out 15 cm from the target and at a current of 155 μamp. The dose-rate was about .16 r/μamp/sec as determined by Victoreen chambers. (Work in this laboratory on dosimetry indicates that the Victoreen chamber readings are high. Until more definite information can be obtained, the present values must stand.) Dosage is reported here as a simple function of current x time which appears to be more convenient at this writing. Multiplication of the current x time readings by the factor 1600 will give dosages in roentgens.

Little work on the decomposition of pure water has been done in this laboratory. The information obtained so far, in general, supports the work of others, which indicates that the decomposition, even after high dosages, does not exceed 8-10 μM/l of hydrogen plus some oxygen.

The data that have been obtained on the decomposition of pure water are shown in Figure 4. This is a plot of micro-moles of gas liberated in a given time as a function of accelerating voltage. The dosages are 16,000, 45,000, 80,000 and 100,000 r respectively at the points shown in the figure. At a dosage of 300,000 r, one would not anticipate any more decomposition than that found at the 2-Mev point in Figure 4 (8 μM/l of H_2). It may be added that the results with water are often erratic. Several ideas have been advanced to explain this; the one receiving the most support is that this is due to traces of organic impurities.

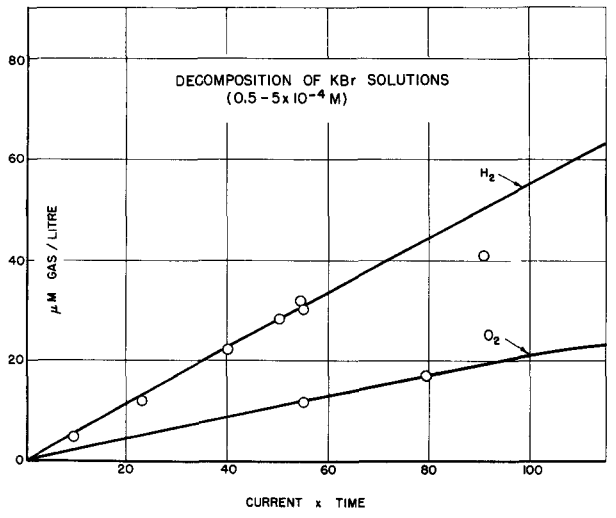

Figure 5. Yields of hydrogen and oxygen from potassium bromide solutions.

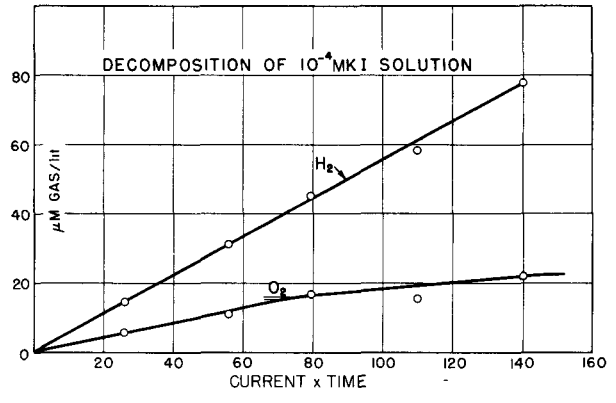

Figure 6. Yields of hydrogen and oxygen from potassium iodide solutions.

In contrast to water, a dilute neutral solution of KBr or KI shows considerably more decomposition and the results are more reproducible. Figures 5 and 6 show the results obtained for KBr and KI solutions, respectively. In the range of KBr concentrations employed, 0.5 to 5×10^{-4} M/l, the yield was independent of concentration. In neither case (Figures 5 or 6) was the reaction carried out to a steady state condition, which would presumably be reached at some high dosage. The highest dosage given to any of these samples (not shown here) was about 350,000 r. At this point the steady state condition had not been attained. The slopes of the hydrogen yield for both the KI and KBr solutions are identical as are those of the oxygen curves; the effect of the halide ions appears to be the same.

It has not been possible to effect a material balance in these studies (KBr and KI solutions) except at low dosages. At higher dosages, corresponding to 120 on the current x time ordinate, the material balance is off by 40%. This is far beyond the experimental error and can only mean that some other product is present. There are indications that some oxidized form of the halogen is present, and also that there is some free halogen. This, of course, is a very critical point and it is hoped that definite evidence will be found shortly to support the above indications.

At high dosages the oxygen yield (Figures 5 and 6) appears to level off. This leveling-off is paralled by the appearance of an equivalent amount of hydrogen peroxide. Discussion of this interesting fact will be postponed to a later time when more information will be available.

Studies on the Decomposition of Hydrogen Peroxide Solutions with 2-Mev X-Rays (5311)

E.R. Johnson

It is generally assumed that, in the decomposition of neutral or alkaline solutions of KI or KBr, hydrogen peroxide is a primary product which rapidly decomposes to yield oxygen. In acid solutions of these halide salts, hydrogen peroxide is indeed found (H. Fricke and E. Hart, J. Chem. Phys. 3, 364 (1935)). Consequently it is of interest to

obtain some information about the rate of decomposition of hydrogen peroxide in pure water, dilute halide solutions and in the presence of the products formed during the decomposition of halide solutions (hydrogen and oxygen). No information on the latter has been obtained at this writing.

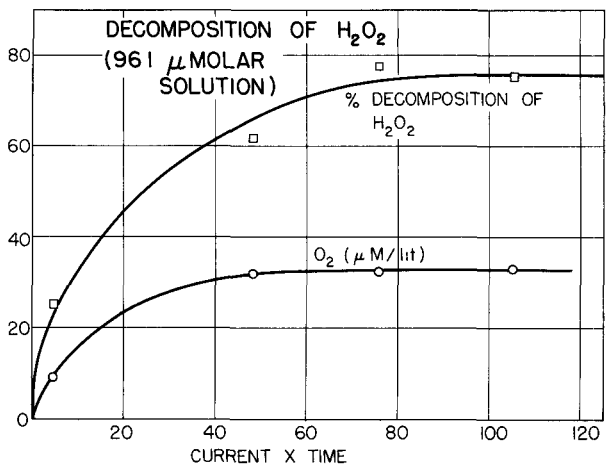

Figure 1. Radiation decomposition of hydrogen peroxide solutions.

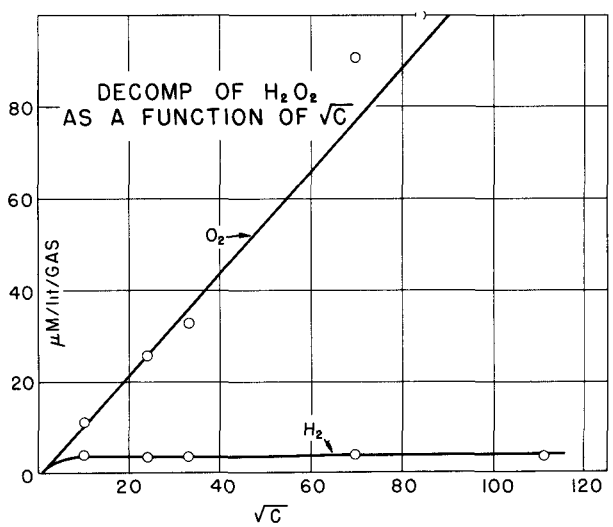

Figure 2. Decomposition of hydrogen peroxide solutions at various concentrations.

In Figure 1 are plotted data on the decomposition of a 96.1 μM solution of hydrogen peroxide in pure water. The rate of decomposition is not very rapid and a steady state condition is attained after a total dosage of less than 80,000 r. The material balance found (after taking account of the hydrogen formed) is within the experimental error. Other data have been collected on more concentrated solutions (4,000 μM/l) but are not sufficiently complete to present here.

The rate of evolution of oxygen as a function of hydrogen peroxide concentration has been studied at low dosages (8,000 r). In agreement with the results of other workers, it was found to be proportional to the square root of the concentration (Figure 2) at concentrations of about 5,000 μM/l or less. Above this, the decomposition becomes slightly greater.

During the decomposition of H_2O_2, hydrogen is liberated; a fact not reported by other workers. At low dosages the hydrogen liberated is independent of concentration (Figure 2) but at higher dosages there is some concentration dependence. A plot of hydrogen formation as a function of dosage is shown in Figure 3. Curve A represents the hydrogen formed from solutions varying in concentration from 1200-3000 μM/l, while curve B represents the hydrogen from a 96.1 μM solution. The effect of initial peroxide concentration on hydrogen production is not very large. For a twenty-fold increase in initial concentration, there is only a two-fold increase in the steady state concentration of hydrogen. It is interesting to note the initial slope of Curve A, Figure 3, is the same as that for the hydrogen curves of Figures 5 and 6 of the previous paper. In addition to intensity measurements, further experiments on hydrogen production as a function of initial peroxide concentration at high dosages are being carried out.

In the presence of iodide ion, the rate of decomposition of hydrogen peroxide is accelerated to about 2.5 times as fast as in the absence of iodide ion. In Figure 4 is shown a plot of the decomposition of 45.4 μM solution of hydrogen peroxide in the

presence of 10^{-4} M KI. After an exposure of only 8000 r the solution is about 75% decomposed. Sufficient data are not yet available to show the concentration dependence (with respect to the iodide ion and the initial peroxide) of the rates of decomposition of

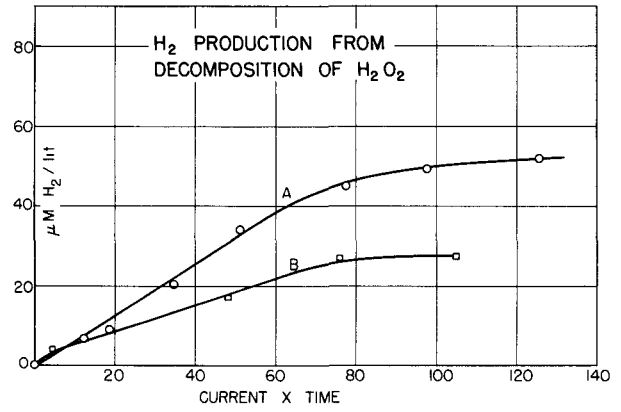

Figure 3. Hydrogen from hydrogen peroxide solutions as a function of dosage.

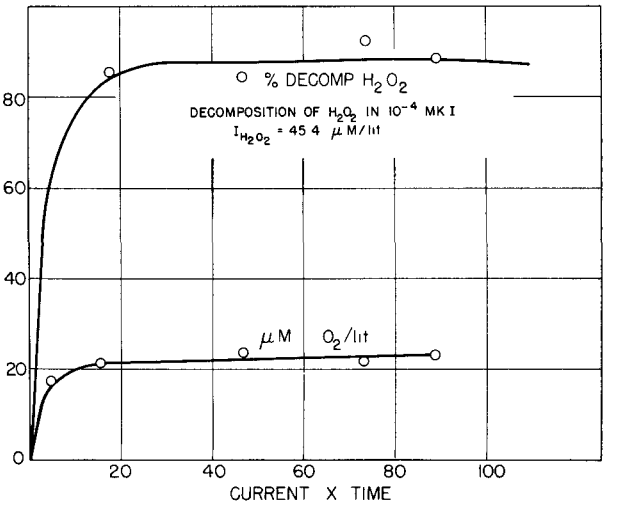

Figure 4. Radiation decomposition of hydrogen peroxide solutions containing iodide.

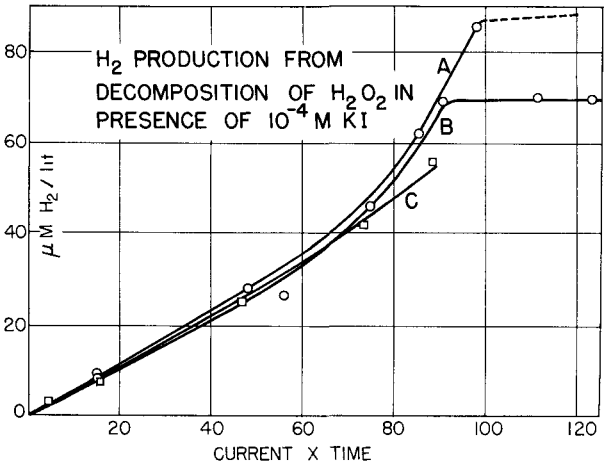

Figure 5. Hydrogen yield from hydrogen peroxide-iodide solutions.

peroxide in these systems, but indications are that the kinetics will be complex.

Hydrogen production during the decomposition of hydrogen peroxide in the presence of iodide ion gives some indication of the complexity of the system. Figure 5 shows the rate of hydrogen production as a function of dosage for three initial H_2O_2 concentrations: A = 4500 μM/l, B = 2200 μM/l and C = 45.4 μM/l. The differences in initial slopes are negligible and the breaks in the slopes are real. The data for curves A and C are not complete, but if curve B is a measure of the situation, one can say that the only essential difference is in the steady state concentration of hydrogen.

In curve C more than 90% of the hydrogen peroxide has been decomposed before the break in the curve appears. It seems unlikely that the small residual peroxide (3-4 μM) present is directly related to this accelerated decomposition of the water, but rather some other component or components of the system. Further support for this view is found in the system plotted in Figure 6 of the preceding paper. Here, at high dosages (where the O_2 curve levels off) there is present about 5-6 μM/l of hydrogen peroxide, and there is no break in the hydrogen curve. However, in this system the mol ratio of hydrogen to oxygen (at the high dosages) is slightly greater than 2 while in the former system (curve C, Figure 5) the ratio is less than 2. The effect of hydrogen and oxygen in these systems is being investigated further.

Dosimetry of 2-Mev X-Rays (5311)

A. Levy and A.O. Allen

No accurate standard exists for dose measurements on high energy, high intensity X-rays of the type produced by the Department's electrostatic generator. The problem of developing methods of dose measurement falls into two parts: the accurate determination of relative doses, and the determination of absolute dose in terms of energy input to the irradiated materials. The first of these questions is now being studied; the second problem will be attacked by calorimetric methods in the near future.

X-ray doses can be determined by measuring the ionization produced in air in a chamber, or by determining the amount of a chemical reaction produced by the rays. The ionization chamber method is preferred by roentgenologists, who usually operate with lower energy X-rays at lower dose-rates than we have to deal with. Extensive experiments with standard calibrated Victoreen thimble chambers have been performed here. It was found necessary to surround the chambers with 1/4 in of plastic to obtain equilibrium with Compton electrons; without the plastic, readings were much too high, the meters apparently being affected by electrons generated by X-rays in the surrounding lead shielding. Even with this precaution, however, the performance of these meters has been very unsatisfactory. They frequently give aberrant readings for no obvious reason, and there is some suspicion that they may read low at high radiation intensities because of incomplete collection of ions.

A chemical dosimeter in principle is preferable in our case, where the radiation is to be used for producing chemical reactions, and the doses given are consequently in the range conveniently measured by chemical means. Many reactions have been reported in the literature as having been tried for this purpose. The ideal reaction should be readily measured, should not occur in the absence of X-rays, and its extent should be proportional to the quantity of energy input, and independent of the wave length of the X-rays and their intensity.

From the above criteria, the best known reaction and most frequently used is the oxidation of dilute air-saturated solutions of ferrous sulfate in normal sulfuric acid. This reaction, determining colorimetrically by a thiocyanate method the amount of ferric ion formed by the radiation, has been studied. Small glass vessels, surrounded by 1/4 in of lucite and containing 3 ml portions of the solution, are irradiated in fixed positions near the X-ray target, with various currents in the machine for various lengths of time.

Results are reproducible to about $\pm 2\%$. At a given position and current, the iron oxidized is exactly proportional to the time of irradiation. At a low current, however, the amount oxidized is slightly greater than that produced by the same energy input at higher currents. The yield of the reaction -- that is, the amount of reaction per given energy input -- thus appears to drop at high radiation intensities. Other researchers working at lower intensities have reported that the yield is independent of intensity. Either this independence fails to hold at higher intensities, or else the X-ray intensity produced by our machine is not strictly proportional to the current. This point is being further investigated.

In the hope of correlating radiation experiments with the kinetics of thermal reactions involving free radicals, irradiations were made of ferrous sulfate in acid solutions containing alcohol. The results are complicated, and much further work would be required to obtain a complete picture. Results were sought which could be compared with A.I. Medalia's work on the reaction between ferrous ion and hydrogen peroxide in the presence of alcohol and oxygen. The radiation results suggest that the yield of oxidized iron increases with oxygen concentration and decreases with ferric ion concentration, as would be expected from the thermal reaction; this at least is not in disagreement with the idea that similar mechanisms are operating in the two cases. Consideration of the expected free radical mechanisms shows that simpler and more easily interpretable results may be found if ferrous sulfate is irradiated under hydrogen. Such experiments will be tried, and, if the results are favorable, will be compared with experiments on the thermal reaction of ferrous sulfate with hydrogen peroxide under hydrogen.

Large yields of hydrogen peroxide were obtained when aerated aqueous alcohol was irradiated. This reaction did not appear promising for further study because of the difficulty of determining all the possible organic reaction products.

Ferrocyanide solutions, irradiated in the presence of air, were oxidized, but the yield decreased with increasing dosage, and the reaction is obviously less suitable for dosimetry than the ferrous sulfate oxidation.

Temperature and Chloride Effects on the Rate of the Ferrous-Ferric Exchange Reaction (5311)

J. Silverman and R.W. Dodson

Abstract

The rate of the ferrous-ferric electron transfer exchange reaction has been investigated as a function of acid concentration, chloride concentration and temperature. In 0.55 f perchloric acid, the acid independent term in the rate expression has an activation energy of about 9 k cal/mole. Chloride catalyzes the reaction in a way that suggests the participation of $FeCl^{++}$ in the exchange.

In the preceding progress reports (BNL 64 (S-6), p. 31, and BNL 82 (S-7), p. 54) it has been shown that the rate of the ferrous-ferric electron transfer exchange reaction in perchloric acid solutions is proportional to the product of the total ferrous and total ferric concentrations and increases linearly with the reciprocal of the acid concentration. The acid effect has now been studied over a wider range of acidity, and at different temperatures. In addition the effect of chloride ion has been studied at different temperatures. The reaction is accelerated by chloride. In the presence of chloride, it retains its second order character with respect to the iron concentrations.

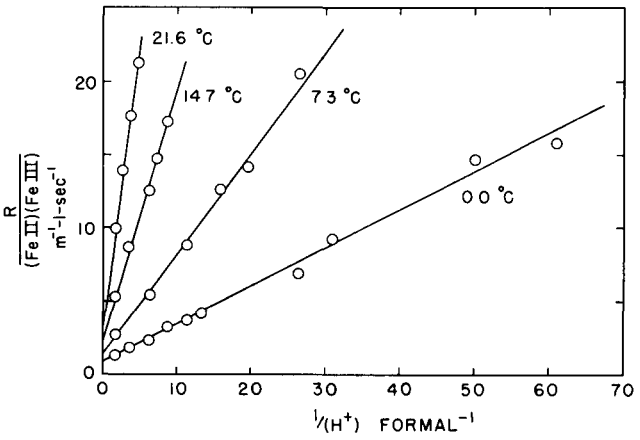

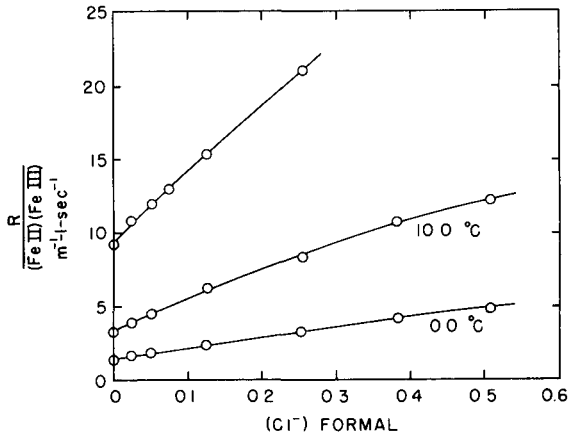

Figure 1 (Above left). Reaction rate vs reciprocal acid concentration in perchloric acid - sodium perchlorate solutions. μ = 0.55 formal.

Figure 2 (Above right). Reaction rate vs chloride concentration in HCl-$HClO_4$ solutions. (H^+) = 0.55 formal.

The experimental methods have been described previously. All experiments were carried out at a volume formal ionic strength of 0.55. In the experiments on the acid effect $NaClO_4$ was substituted for $HClO_4$ in various proportions. The experiments with chloride were carried out at constant acid concentration, (H^+) = 0.55 formal, HCl being substituted for $HClO_4$ in various proportions.

Acid Effect

Figure 1 shows the effect of acidity on rate in perchlorate solutions at four temperatures ranging from 0.0°C to 21.6°C. The data are seen to follow the rate law previously reported,

$$R = (FeII)(FeIII)\left\{k_1 + \frac{k_2}{H^+}\right\}.$$

In the interpretation given in BNL 82 (S-7), k_1 is the specific rate constant for the reaction between the unhydrolyzed species Fe^{++} and Fe^{+++}, while k_2 is a combination of the specific rate constants and hydrolysis constants. The constant k_1 is given by the intercepts of the curves in Figure 1, although the extrapolation cannot be considered accurate at the higher temperatures. The values so obtained lead to an activation energy of about 9 k cal/mole for the exchange reaction between unhydrolyzed ions.

Effect of Chloride

In the corresponding electron transfer reaction between thallous and thallic thallium, chloride exerts a profound effect on the reaction rate, inhibiting or accelerating it depending on the concentration of chloride (G. Harbottle and R.W. Dodson, J. Am.

Chem. Soc., in press; L. Eimer and R.W. Dodson, see report which follows). The data given in Figure 2 show that chloride accelerates the ferrous-ferric exchange reaction over the range of chloride concentration 0 - 0.55 formal. The nearly linear dependence of rate on (Cl^-) suggests that a complex ion involving a single chloride (e.g., $FeCl^{++}$) participates in the reaction at a greater rate than the uncomplexed species. The data have not as yet been quantitatively analyzed to the point where they can be interpreted in terms of the known equilibrium constants of the chloride complexes of iron.

It is of interest that, in contrast to the thallium system, the catalytic effect of chloride is relatively weak, and that no region of inhibition by chloride is observed. It is also to be noted that catalysis by traces of chloride is completely negligible.

The order with respect to iron was checked for the chloride catalyzed reaction by independently varying the ferrous and ferric concentrations. The results are given in Table 1.

Table 1

Check of Reaction Order in Presence of Chloride

(0.0^oC, (H^+) = 0.55 f, (Cl^-) = 0.51 f)

FeII (formal x 10^4)	FeIII (formal x 10^4)	Half-Time (sec)	Second Order Rate Constant = R/(FeII)(FeIII) ($mole^{-1}$-liter-sec^{-1})
1.03	1.05	691	4.82
2.05	1.07	477	4.65
4.10	1.11	279	4.77
4.10	2.15	224	4.95
4.10	3.18	196	4.86
			mean 4.81 ± 0.08

It is seen that chloride does not change the reaction order with respect to iron.

Effect of Chloride on the Thallous-Thallic Exchange Reaction (5311)

L. Eimer and R.W. Dodson

It has been reported (G. Harbottle and R.W. Dodson, BNL Conference Report BNL-C-8, p. 226, and J. Am. Chem. Soc., in press) that chloride has a marked effect on the rate of the thallous-thallic electron transfer exchange reaction, causing a great increase in rate at chloride concentrations of the order of a tenth formal and higher, but a decrease (compared to the rate in the absence of chloride) at lower concentrations. A detailed study of this effect is being carried out. Data have now been obtained at ionic strength 0.5 and 30^oC which map out the complete course of the chloride effect

Table 1

Chloride Catalyzed Thallous-Thallic Exchange

((H^+) = 0.5 formal, (ClO_4^-) + (Cl^-) = 0.5 formal)

Thallic Concentration (formal x 10^3)	Thallous Concentration (formal x 10^3)	Chloride Concentration (formal)	(Cl^-) (Tl III)	$t_{1/2}$ (min)	Rate Constant ($formal^{-1} min^{-1}$)
1.18	4.64	0	0	11,100	.0107
3.94	9.3	.000101	.03	5,200	.0101
3.94	9.3	.000500	.13	4,900	.0107
3.94	9.3	.00131	.33	9,900	.0053
3.94	9.3	.00200	.5	11,600	.0045
3.94	9.3	.00400	1.0	56,000	.00094
3.94	9.3	.00500	1.27	130,000	.00040
3.94	9.3	.00600	1.52	134,000	.00039
3.94	9.3	.00700	1.78	100,000	.00052
3.94	9.3	.00800	2.01	82,000	.00064
3.9	9.2	.0100	2.5	67,500	.00079
3.94	9.3	.0130	3.3	34,500	.0015
3.94	9.3	.0180	4.6	11,400	.0046
3.9	9.35	.0300	7.58	7,200*	.0073*
3.9	.998	.0390	10.	4,900*	.029*
4.02	.519	.0595	15.	2,040	.075
3.9	.998	.1200	31.	490	.289
3.9	.998	.265	67.9	100	1.4

*Extrapolated value.

through the region of decreased rate and into that of strongly accelerated rate. These data are summarized in Table 1 and plotted in Figure 1. The figure, in which the second order rate constant is plotted on a log-log basis against the ratio between the number of moles of chloride and the number of moles of thallic thallium, exhibits the striking minimum in rate which occurs at chloride concentrations of the same order of magnitude as the concentration of the thallic species.

The measurements are somewhat tedious, since the half-time of runs near the minimum is about 3 months. Each run was continued until exchange was about 90% complete, except where the half-life is indicated as "extrapolated value" in the table. In spite of the long time elapsed, the data were reproducible and followed the proper "first order" exchange law.

The minimum in the rate (Figure 1) occurs where the chloride concentration is about 1.5 times the thallic concentration. It has been reported (G. Harbottle and R.W. Dodson, preceding reference; P. Benoit, Bull. Soc. Chim. de France 5-6, 518 (1949)) that thallic thallium forms stable chloride complexes of the type $TlCl^{++}$, $TlCl_2^+$, $TlCl_3$, and $TlCl_4^-$. The present data show that the lower complexes $TlCl^{++}$ and $TlCl_2^+$ react only very slowly with thallous ion, much slower than does uncomplexed thallic ion.

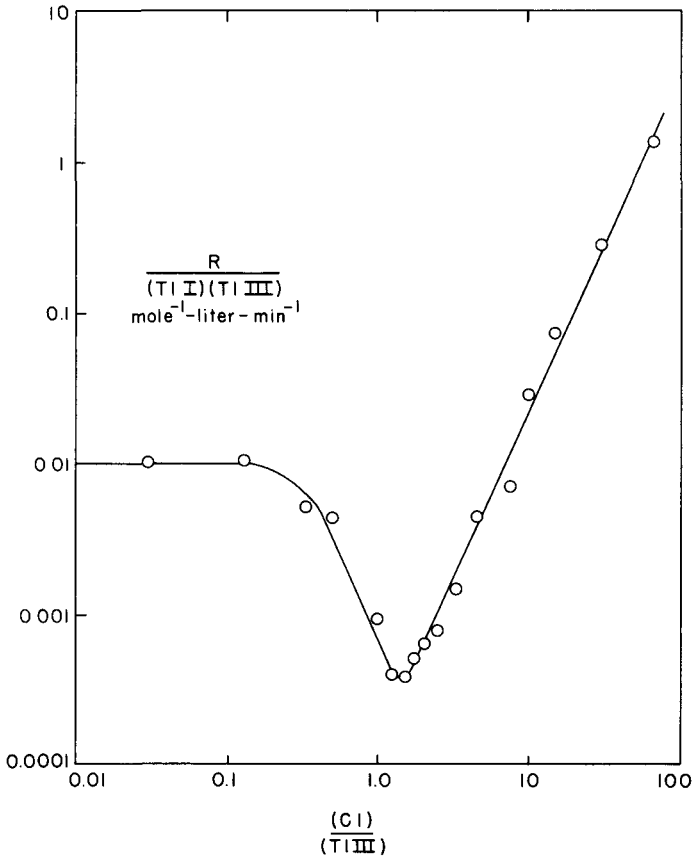

Figure 1. Effect of chloride on rate of thallous-thallic exchange reaction. Ionic strength, 0.5; temperature, 30.0°C.

Ferrocyanide-Ferricyanide Exchange Reaction (5311)

L. Eimer and R.W. Dodson

The ferrocyanide-ferricyanide electron transfer exchange reaction is of particular interest not only because the ions involved are large, symmetrical and highly charged negative ones, but also because there exists in the literature many conflicting reports as to whether it is a rapid or extremely slow exchange. Seaborg et al. (unpublished work mentioned by G.T. Seaborg, Chem. Revs. 27, 199 (1948)) failed to observe any exchange. Heanny (University of Lausanne, Switzerland, Private communication mentioned by W.B. Lewis (below)) found a half-life of exchange of at least several days. W.B. Lewis (Tech. Report #19, ONR Task Contract N5-ori-07806, Isotopic Exchange by Electron Transfer Between Complex Ions, MIT, Jan., 1949) duplicated the procedure of Seaborg by using the ferric ion to separate the species and he found complete exchange in 30 sec. He also separated the ferrocyanide as argentous and plumbous salts and found complete and rapid exchange in both cases. R.C. Thompson (J. Am. Chem. Soc. 70, 1045 (1948)) reported complete exchange within 1 min. He employed a chemical separation of the ferrocyanide, by precipitation of $KCeFe(CN)_6$. Cobble and Adamson (J. Am. Chem. Soc. 72, 2276 (1950)) avoided chemical precipitation methods of

separating the two chemical species, since such procedures may induce exchange. Using a diffusion separation technique that required from 4 to 17 hr they found 100% exchange. Electrophoretic separation, taking 5 hr, showed 100% exchange, as did an ion exchange resin separation that took 4 min.

On the hypothesis that the reports of complete exchange may mean that the reaction is actually extremely rapid rather than catalyzed to completion by the various separation methods, experiments were run in which both concentration and temperature were reduced as much as feasible in order to slow down the rate. Complete exchange was found in the shortest times employed (10 sec to 1 min).

The tracer used was Fe^{55}, obtained from Oak Ridge. A stock of $K_4Fe(CN)_6$ containing active Fe^{55} was synthesized by the addition of ammonia and solid potassium cyanide to a solution of ferric chloride, followed by evaporation to dryness. The residue was leached with hot water and the product purified twice by recrystallization from water-ethanol mixtures. The experiments were carried out by mixing a solution of the active ferrocyanide with a solution of ordinary potassium ferricyanide and separating the two species as quickly as possible.

In one set of experiments the separation was accomplished by precipitation of ferrocyanide as the thallous calcium double salt. After this precipitate was filtered off, the ferricyanide was precipitated as its cadmium salt. In separate experiments the chemical separation was shown to be complete and quantitative. Both precipitates were counted. Typical results are tabulated in Table 1.

Table 1

$K_4Fe(CN)_6$ (formal)	$K_3Fe(CN)_6$ (formal)	Temperature (°C)	Contact Time (min)	Exchange (%)
.001	.001	29 ± 2	1.2	103
.0005	.0005	27 ± 2	0.8	101
.0005	.0005	0	0.8	102

Extraction techniques were investigated in hope of finding a rapid method applicable to low concentrations. An attempted separation by extracting the ferrocyanide from 4N HCl solutions with tributyl phosphate was unsuccessful due to irreproducibility and back extraction difficulties. It was found however that essentially all the ferrocyanide was extracted from a solution approximately 3×10^{-3} f in each species and that only about 50% of the ferricyanide was extracted.

A chloroform extraction of ferricyanide from solutions containing a large excess of tetraphenyl arsonium chloride was more promising. In solutions 1.8×10^{-3} f in each reactant, the ferrocyanide was not extracted and about 96% of the ferricyanide was extracted. A crude run at a concentration of 1.3×10^{-3} f in reactants and at room temperature gave essentially 100% exchange within the time required for the separation (about 10 sec). This method will be studied further, at lower concentrations.

Kinetics of the Exchange of Nickel Ion with Nickel Ethylenediaminetetra-Acetate Ion (5311)

C.M. Cook, Jr. and F.A. Long*

Abstract

The exchange reaction between nickelous ion and its complex with ethylenediaminetetra-acetate has been measured with tracer nickel. The reaction is found to proceed in three paths differing in their dependence on the acid concentration. The kinetics are discussed.

Introduction

Ethylenediaminetetra-acetic acid, which will be abbreviated as H_4Edt, is known to form stable complexes with di- and trivalent ions of many metals. The nickelous complex, $NiEdt^{=}$, is sufficiently stable not to react with sodium hydroxide, dimethylglyoxime, or ammonium sulphide solutions. The blue color of this complex ion and the observation by Klemm and Raddatz (Z. anorg. allg. chem. 250, 204 (1942)) that this ion has nearly the same magnetic susceptibility as nickelous ion indicate that the $Edt^{=}$ group does not form a square complex with the nickelous ions. The ethylenediaminetetra-acetate ion contains 6 possible coordinating groups; since the acid H_2NiEdt is strong in both protons, it is likely that all 6 groups are coordinated and that the complex is octahedral.

The stability of this complex is such that exchange between nickel in the complex and free nickelous ions is slow. The data reported here show that the kinetics of this exchange are quite complex in that at least three separate paths are involved.

Preparation of Reagents

Nickel metal powder containing Ni^{63} (half-life, 85 years; maximum β^- energy, 63 kev) was obtained from Oak Ridge National Laboratory. The metal was dissolved in nitric acid and then purified from active Co and Fe contaminants by addition of cobaltous and ferric ion carriers to the solution followed by precipitation of nickel dimethylglyoxime. After several repetitions of this procedure, foreign activity had been reduced to a negligible level.

Ethylenediaminetetra-acetic acid was recrystallized several times from hot water until the water showed no test for the sodium sulfate contaminant normally present. The acid was then oven-dried at 105°C. Labeled nickel hydroxide in slight excess was dissolved in a solution of the acid, and sufficient sodium hydroxide was added to raise the final pH of the solution to 10. The excess nickel hydroxide precipitated at this pH

*Cornell University, Ithaca, New York.

and was filtered from the solution. The concentration of $NiEdt^{=}$ was determined by analysis of the solution for nickel.

Experimental Methods

The exchange between nickelous and $NiEdt^{=}$ ions was initiated by pipetting quickly a known portion of nickel chloride solution into a solution containing the labelled complex ion and buffer in known concentrations. During the course of the exchange aliquots were removed from the solution and the nickelous ion was separated from the complex by addition of excess sodium hydroxide and filtration of the resulting nickel hydroxide. The nickel was subsequently plated upon copper disks and its activity determined in a windowless proportional counter. In all cases the plated samples were effectively "infinitely thick" and had identical counting geometry.

The ratio of the specific activity of the separated nickel to that at isotopic equilibrium gives the fractional exchange, x/x_∞, between the nickelous ion and the complex ion. The data were plotted on a graph of $\log(1 - x/x_\infty)$ vs reaction time, the best straight line was drawn through the resulting points, and the rate of exchange was calculated from the slope of this line and the concentrations of the reactants. (E.g., see G. Friedlander and J. Kennedy, Introduction to Radiochemistry, John Wiley and Sons, 1949, p. 287.) In nearly all runs this rate could be determined to within ±5%. For all rate constants, concentrations are in moles per liter and time is in minutes.

Rate Law for the Exchange

The kinetic data for the exchange show that it goes by three competing mechanisms, so that the over-all rate expression is

$$R = R_0 + R_1 + R_2 = k_0(Ni^{++})(NiEdt^{=}) + k_1(H^+)(Ni^{++})(NiEdt^{=}) + k_2(H^+)^2(NiEdt^{=}).$$

At pH values of from 1 to 2, R_2 is the dominant term; at pH values of from 3 to 4, R_1 is dominant. R_0, the straight bimolecular term, is dominant at pH values of 4.5 and higher.

The R_0 and R_1 terms in this rate expression were determined from the results of runs made in the pH region 3.5 to 5. The nickelous and complex ion concentrations were varied by a factor of 2 and the hydrogen ion concentration was varied by a factor of 30 for these runs. These runs can be divided into three series, with nickelous and complex ion concentrations held constant and hydrogen ion concentration varying within any one series. Plots of R vs $\log 1/(H^+)$ are shown in Figure 1, with smooth curves drawn through the experimental points corresponding to the three series. The values of k_0 and k_1 derived from the data of Figure 1 are shown in Table 1.

The data show definitely that in this pH region the rate is first order in both nickelous and complex ion concentrations and that for the R_1 term the rate also depends on hydrogen ion to the first power. The value of k_1 is given with fair precision by the data; it is seen to decrease with increasing ionic strength. The listed value of k_0 is less well known.

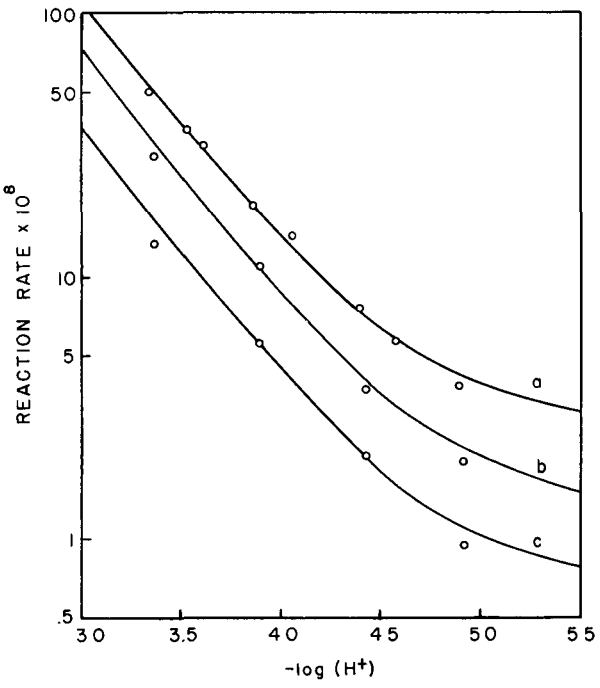

Figure 1. Rate of exchange plotted against negative logarithm of the hydrogen ion concentration (p_cH) for three series of runs:
(a) $(Ni^{++}) = 0.00361$, $(NiV^{=}) = 0.00185$, $\mu = 0.029$
(b) $(Ni^{++}) = 0.00180$, $(NiV^{=}) = 0.00185$, $\mu = 0.017$
(c) $(Ni^{++}) = 0.00180$, $(NiV^{=}) = 0.00093$, $\mu = 0.014$

The data shown in Figure 1 were obtained in solutions in which the p_cH was regulated by acetate buffers. When phthalate buffering was used, in an attempt to extend the p_cH range beyond 5, the orders of the kinetic terms in the rate expression were unaltered, but k_0 and k_1 were lowered to about half of their previous values. These data are shown in Table 2. A similar effect was noticed in the region of $p_cH = 3$ when an attempt was made to shift from acetate to chloroacetate buffering. This effect is being investigated further; presumably, it is due to a small amount of complex formation between the free nickelous ion and the buffer ion.

The R_2 term in the over-all rate expression was investigated in the region p_cH 1 to 2. The values of R_0 and R_1 in this region were computed from the previously determined values of k_0 and k_1 and then subtracted from the over-all rate to yield R_2. The data listed in Tables 3 and 4 show that R_2 is second order in hydrogen ion, first order in $NiEdt^{=}$ ion, and zero order in nickelous ion; k_2, averaged over 20 runs, is $6.4 \pm 2.5 \times 10^{-6}$ $l^2 M^{-2}$ min^{-1}. The study of the exchange is complicated in this low p_cH region by the acid-induced dissociation of the complex ion, which results in large "immediate" exchange. This effect has been used to study the dissociation constant of the $NiEdt^{=}$ ion; results of this study will be reported separately.

Table 1

Determination of k_0 and k_1 in the p_cH Range 3.3 to 5.0 with Acetate Buffer

Series	Ionic Strength	(Ni^{++})	$(NiEdt^{=})$	k_0	k_1
a	0.029	0.00361	0.00185	0.004	170
b	0.017	0.00180	0.00185	0.004	210
c	0.014	0.00180	0.00093	0.004	220

Only superficial studies of ionic strength effects have so far been made. Present data do not give k_0 with sufficient accuracy to detect ionic strength effects. The value of k_1 appears to follow the expression $\log k_1 = \log k_1^0 - 3\sqrt{\mu}$ over the range of ionic strengths from $\mu = 0.01$ to 0.03. The sign and magnitude of this effect are about as expected for a reaction between ions with the given charges. The value of k_2 appears, rather unexpectedly, to be independent of ionic strength in the region $\mu = 0.05$ to 0.20;

Table 2

Determination of k_0 and k_1 in the pH Range 4.8 to 5.8 with Phthalate Buffer

Series	Ionic Strength	(Ni^{++})	$(NiEdt^{=})$	k_0	k_1
d	0.031	0.00392	0.00201	0.002	120
e	0.031	0.00196	0.00201		
f	0.028	0.00181	0.00093		

Table 3

Effect on k_2 of Change in Acid Concentration

$\left((Ni^{++}) = .0017\ \underline{M},\ (NiEdt^{=}) = .00085\ \underline{M},\ \text{Ionic Strength} = .10\right)$

(H^+)	Observed Rate $(x10^6)$	Calculated R_2 $(x10^6)$	$\frac{R_2}{(H^+)^2\ (NiEdt^{=})} = k_2$
.0207	5.55	2.77	7.3
.0397	14.63	9.27	6.6
.0988	71.8	68.5	8.9

Table 4

Effect on k_2 of Change in Ni^{++} and $NiEdt^{=}$ Concentrations at Constant Acidity

$((H^+) = 0.06\ \underline{M},\ \text{Ionic Strength} = .07)$

(Ni^{++})	$(NiEdt^{=})$	$\frac{(Ni^{++})}{(NiEdt^{=})}$	Observed Rate $(x10^6)$	Calculated R_2 $(x10^6)$	k_2
.00093	.00089	1.05	27.9	22.7	7.2
.00182	.00179	1.02	57.4	37.4	5.9
.00180	.00089	2.02	30.4	20.3	6.4
.00181	.00090	2.01	34.3	24.0	7.4

this point is still being studied.

Various mechanisms can be devised to account for the observed kinetic terms. The bimolecular term which gives k_0 without doubt results from a simple collisional process,

$$Ni^{++} + \overset{*}{N}iEdt^{=} + \overset{*}{N}i^{++} + NiEdt^{=} \qquad \text{(Slow)}$$

The term which gives k_1 can be explained by a mechanism of the type

$$H^+ + \overset{*}{N}iEdt^= = H\overset{*}{N}iEdt^- \qquad \text{(Equil.)}$$

$$Ni^{++} + H\overset{*}{N}iEdt^- = HNiEdt^- \qquad \text{(Slow)}$$

The third term which gives k_2 is independent of the nickelous concentration. Therefore, the rate-determining step must be dissociation of the complex. One possibility is

$$H^+ + \overset{*}{N}iEdt = H\overset{*}{N}iEdt^- \qquad \text{(Equil.)}$$

$$H^+ + H\overset{*}{N}iEdt^- = \overset{*}{N}i^{++} + H_2Edt^= \qquad \text{(Slow)}$$

Work is continuing on the reaction at high pH and on the effect of changes in ionic strength.

Studies on the Mechanism of the Willgerodt Reaction I. The Over-All Mechanism (5311)

E.V. Brown*, E. Cerwonka** and R.C. Anderson

Abstract

Whether there is a single mechanism of the Willgerodt reaction with non-rearrangement of the carbon skeleton or whether there are two paths, one involving rearrangement, are questions that have been studied recently by tracer methods. The over-all course of the Willgerodt reaction on acetophenone has been reinvestigated using C^{14}. By employing the Hofmann degradation in the study of the reaction products phenylacetic acid and phenylacetamide, it is shown that no skeletal rearrangements occur. Data are also presented indicating that thermal decarboxylation procedures may be the source of unreliable information concerning mechanism studies.

The mechanism of the Willgerodt reaction has been of interest to many investigators since Willgerodt published (J. prakt. Chem. (2) 80, 192 (1909); and Ber. 21, 534 (1888)) the result of his original experiment with acetophenone.

$$C_6H_5COCH_3 \xrightarrow[H_2O]{(NH_4)_2SS_X} C_6H_5CH_2CONH_2 + C_6H_5CH_2COONH_4$$

The ketone was heated with ammonium polysulfide in a sealed tube for 5 hr at 200-220°. Phenylacetamide was the main product, while small amounts of ammonium phenylacetate and phenylacetic acid were also isolated.

---

*Fordham University, New York.
**AEC Pre-Doctoral Fellow.

Later the scope of the reaction was seen to include olefins, acetylenes, aldehydes, alcohols and mercaptans in addition to the original aryl alkyl ketones. (For a review of this work, see Carmack and Spielman, Organic Reactions, John Wiley and Sons, New York, Vol. III, Chapter 3.) Concurrently there developed fresh interest in the mechanism, and the ideas of both Willgerodt and Kindler were reviewed. The former had visualized the migration of a functional group along the chain, and hence no carbon skeleton rearrangement. Kindler (Ann. 431, 193, 222 (1923), and Kindler and Li, Ber. 74B, 321 (1941)), however, postulated a rearrangement of the chain which involved the migration of a phenyl group.

In the case of aryl alkyl ketones, the question could be decided by discovering whether isovalerophenone yields α-methyl-γ-phenylbutyramide (A) or β-methyl-γ-phenylbutyramide (B).

$$C_6H_5COCH_2CH(CH_3)CH_3 \longrightarrow C_6H_5CH_2CH_2CH(CH_3)CONH_2 \qquad (A)$$

$$\text{or} \quad C_6H_5CH_2CH(CH_3)CH_3CONH_2 \qquad (B)$$

The α-methyl isomer (A) is the actual product, according to Willgerodt. The β-methyl compound (B) would result from migration of the phenyl group. Moreover, the issue appeared to be conclusively settled by the work of Carmack and DeTar (J. Am. Chem. Soc. 68, 2029 (1946)) and McMillan and King (J. Am. Chem. Soc. 68, 632 (1946)). Both groups repeated the experiment and both agreed that the product is α-methyl-γ-phenylbutyramide (A).

Carbon isotopes have been employed by two groups of workers who have investigated the Willgerodt reaction mechanism. The Kindler modification of the original Willgerodt reaction was studied by Shantz and Rittenberg (J. Am. Chem. Soc. 68, 2109 (1946)) who employed acetophenone-(carbonyl)-C^{13}. They reported that the phenylacetic acid, obtained by hydrolysis of the thiomorpholide, was not rearranged.

Dauben, Reid, Yankwich and Calvin (J. Am. Chem. Soc. 68, 2117 (1946)) studied another modification of the original Willgerodt reaction in which the ketone is treated with sulfur, ammonia and pyridine in a sealed tube. They first reported that acetophenone-(carbonyl)-C^{14} yields phenylacetamide-α-C^{14} and phenylacetic acid-(carboxyl)-C^{14}. The amide was said, therefore, to be formed by migration of a functional group along the carbon chain, while the acid was pictured as resulting from a different mechanism involving rearrangement of the carbon chain.

In a second publication Dauben and co-workers (J. Am. Chem. Soc. 72, 121 (1950)) have modified their original contention and feel that the rearrangement takes place only to a minor extent.

Interest in the problem was aroused here by the first publication of Dauben's group, since it appeared unlikely to us that two mechanisms would operate, one yielding amide, the other acid. The conclusions of the second paper modified the original hypothesis of these workers. However, independent study of the matter using both acetophenone-α-C^{14} and acetophenone-(carbonyl)-C^{14} has since been completed at the Laboratory. Willgerodt reactions were carried out on each and the products studied. The ketones were prepared by the following sequences of reaction, the yield for each step being indicated in parenthesis to the right of the equation.

$$C^{14}H_3I + NaCN \longrightarrow C^{14}H_3CN + NaI \quad (70\%)$$

$$C^{14}H_3CN + C_6H_5MgBr \xrightarrow{H^+} C_6H_5COC^{14}H_3 \quad (70\%)$$

and

$$(CH_3)_2SO_4 + NaC^{14}N \longrightarrow CH_3C^{14}N + NaCH_3SO_4 \quad (90\%)$$

$$CH_3C^{14}N + C_6H_5MgBr \xrightarrow{H^+} C_6H_5C^{14}OCH_3 \quad (70\%)$$

The synthesis of acetonitrile-2-C^{14} followed the method of Auger (Compt. rend. Acad. 145, 1287 (1907)), modified by conducting the reaction in a sealed tube at room temperature (Kilmer and duVigneaud, J. Biol. Chem. 154, 247 (1944)). A fraction, bp 76-100° C, was distilled from the mixture and the desired nitrile was extracted from the water by means of benzene in a closed liquid-liquid extractor of the type described by Collins (J. Am. Chem. Soc. 70, 2418 (1948)). In adding the dry benzene solution of the nitrile to the Grignard reagent, a ratio of 1 M of nitrile to 4 of arylmagnesium salt was employed. This is in accordance with the suggestion of Shriner and Turner (J. Am. Chem. Soc. 52, 1267 (1930)) whose procedure was followed in its entirety. Walden's original instructions (Berichte chem. Ges. 40, 3214 (1907)) were followed for the preparation of acetonitrile-1-C^{14}. Although Kilmer and duVigneaud declared this method to be unsatisfactory (using C^{13}) no difficulty was experienced here. Pure dimethyl sulfate was added in small portions to an aqueous solution of the radioactive sodium cyanide. The product was distilled and the rest of the procedure was that followed with acetonitrile-2-C^{14}.

The Willgerodt reactions were accomplished by treating each of the labeled acetophenones with sulfur, ammonia and pyridine in a sealed tube for 5 hr at 165°C. The products, phenylacetamide and phenylacetic acid, were separated and purified.

To determine the relative amounts of activity in each compound, the ketones, amides and acids were combusted by a modified Van Slyke-Folch reagent. The evolved carbon dioxide was trapped first in sodium hydroxide-hydrazine sulfate solution, then in a barium hydroxide-barium chloride reagent. The dried barium carbonate precipitate from each combustion was counted in a Nucleometer and the specific activity in each case (as listed in Tables 1 and 2) represents counts per minute, above background, per square centimeter of a barium carbonate layer of infinite thickness. The method of assay and carbon analysis will be published shortly. It follows in a general way the method described by R. Steele and T. Sfortunato in "Techniques in the Use of C^{14}" (BNL-T-6).

Each purified amide was subjected to a Hofmann degradation with barium hypobromite (Hoogewerf and von Dorp, Rec. trav. chim. 5, 251 (1886)). The evolved carbon dioxide was obtained directly as barium carbonate and the amine was distilled from the alkaline filtrate. It was subsequently combusted as the crystalline hydrochloride. The free acid obtained in each Willgerodt reaction was converted to amide by way of the acid chloride. The amide so obtained was also degraded with barium hypobromite.

Diagrams 1 and 2 summarizes the reactions with acetophenone-α-C^{14} and acetophenone-(carbonyl)-C^{14}, respectively. The "percentage specific activity" figures were computed from the data of Tables 1 and 2, to which the "standard error" ($\pm$ 1.5%) was

Table 1

Compound	Specific Activity
(A) $C_6H_5COC^{14}H_3$	600 (8x75)
(B) $C_6H_5CH_2C^{14}ONH_2$	600 (8x75)
(C) $C^{14}O$	600
(D) $C_6H_5CH_2NH_2$	0
(E) $C_6H_5CH_2C^{14}OOH$	592 (8x74)
(F) $C_6H_5CH_2C^{14}ONH_2$	608 (8x76)
(G) $C^{14}O_2$	612
(H) $C_6H_5CH_2NH_2$	0

Table 2

Compound	Specific Activity
(A) $C_6H_5C^{14}OCH_3$	640 (8x80)
(B) $C_6H_5C^{14}H_2CONH_2$	632 (8x79)
(C) CO_2	0
(D) $C_6H_5C^{14}H_2NH_2$	630 (7x90)
(E) $C_6H_5C^{14}H_2COOH$	640 (8x80)
(F) $C_6H_5C^{14}H_2CONH_2$	624 (8x78)
(G) CO_2	0
(H) $C_6H_5C^{14}H_2NH_2$	637 (7x91)

applied. When the carbon dioxide is evolved from the isotopic carbon atom exclusively, as for example in the Hofmann degradation of $C_6H_5CH_2C^{14}ONH_2$, the specific activity is equal to the number of counts above background directly indicated. When, however, the carbon dioxide is evolved from the other carbon atoms (as well as in the combustion of the same amide) the number of counts indicated is multiplied by 8 in order to correct for dilution by the 7 non-radioactive carbon atoms in the molecule.

On the basis of the above results no rearrangement of the carbon skeleton is indicated in the formation of either the phenylacetamide or the phenylacetic acid obtained in the Willgerodt reaction using acetophenone.

Decarboxylation of Phenylacetic Acid

A number of experiments have been carried out in which labeled phenylacetic acid was decarboxylated in the presence of a metallic catalyst. The results obtained were not nearly so unequivocal as those found by means of the Hofmann degradation. This observation has also been made by Dauben.

Decarboxylation of organic acids with metallic oxides was studied comprehensively

Diagram 1

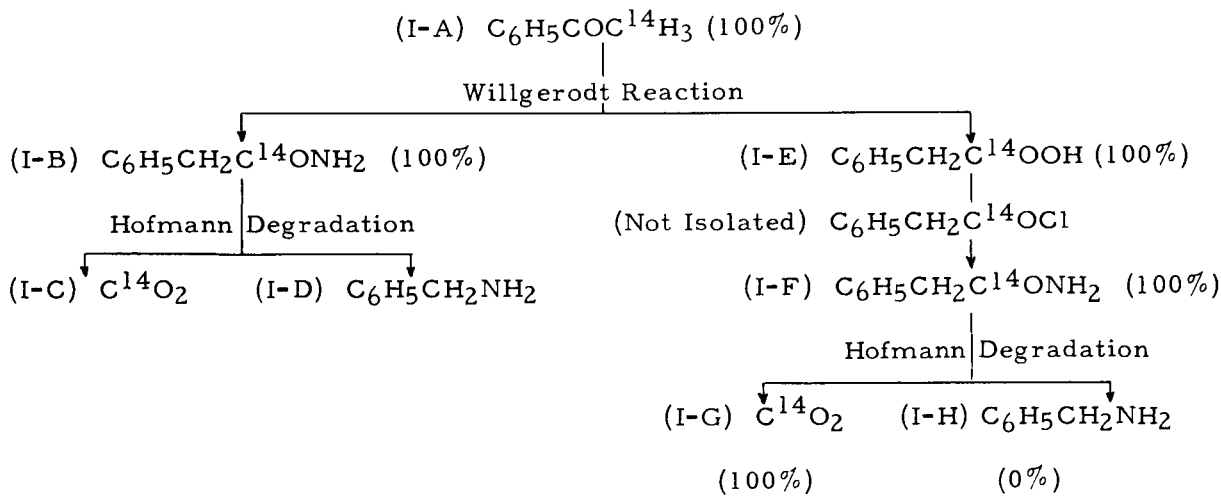

Diagram 2

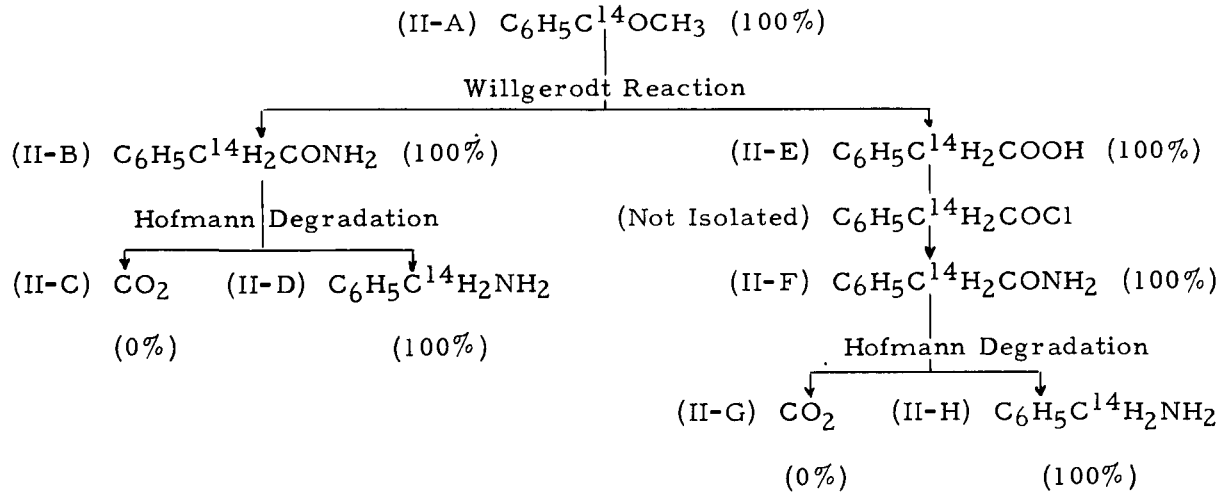

by Sabatier, Senderens and others (Catalysis in Organic Chemistry. Translated by E. Emmet Reid, D. Van Nostrand and Co., N.Y., 1922, paragraphs 831-9). Shepard, Windlow and Johnson (J. Am. Chem. Soc. 52, 2083) in 1930 introduced the use of quinoline in the decarboxylation of halogenated furoic acids. The function of the quinoline was to combine with the liberated halogen acid, thus preventing resinification of the halogenated furan products. The catalysts used by Johnson were "reduced nickel" and "copper bronze." In the literature (Fieser, Experiments in Organic Chemistry. John Wiley and Sons, 2nd Ed., p. 201; Dauben and Coad, J. Am. Chem. Soc. 71, 2928 (1949)) the copper bronze catalyst is erroneously referred to as copper powder.

Thus far, there has been no study reported in the literature of the products resulting from the decarboxylation of phenylacetic acid with copper bronze or copper powder.

Shantz and Rittenberg assumed the product to be mostly dibenzyl ketone in their decarboxylation of phenylacetic acid-α-C^{13} with iron filings. However, they did not isolate this product but oxidized the residue to benzoic acid. Decarboxylation of this benzoic acid accounted for only 80% of the expected C^{13}. Although this discrepancy does not necessarily invalidate the result of their experiment, it points up the fact that the true reaction equation is unknown.

Dauben and Coad, on the other hand, assumed the reaction product to be toluene. Partial oxidation of this product is presented as the explanation for the appearance of traces of C^{14} in the carbon dioxide obtained by decarboxylation of phenylacetic acid-α-C^{14}.

In accordance with a suggestion given by Dauben and Coad, an attempt was made at first to decarboxylate phenylacetic acid with copper powder and quinoline. Pure copper metal (Mallinckrodt) was heated with the acid and quinoline in the presence of "prepurified" nitrogen. No decarboxylation was observed up to a temperature of 260°C. Copper chromite catalyst was then successfully employed under the same conditions. This catalyst had been made by the method of Harman (J. Am. Chem. Soc. 64, 2293 (1942)) for the synthesis of methyl iodide-C^{14} (Melville, Rachele and Keller, J. Biol. Chem. 169, 419 (1947)). The catalyst was used in its unreduced form. Decarboxylation was observed to start at about 170°C (sand bath) and to proceed smoothly at an optimum temperature of 230°C. Yields of CO_2 varied in different experiments from 40 to 80%.

Four labeled phenylacetic acids were then decarboxylated by this method. They were (1) phenylacetic acid-α-C^{14} obtained directly from the Willgerodt reaction, (2) phenylacetic acid-(carboxyl)-C^{14} obtained in the same manner, (3) phenylacetic acid-α-C^{14} prepared by saponification of phenylacetamide-α-C^{14}, (4) phenylacetic acid-(carboxyl)-C^{14} prepared by saponification of phenylacetamide-(carbonyl)-C^{14}. Table 3 summarizes the results.

Table 3

Compound	Percentage of Specific Activity	Yield CO_2
(2) $C_6H_5CH_2C^{14}OOH$ (I-E)	83%	80%
(1) $C_6H_5C^{14}H_2COOH$ (II-E)	9%	70%
(4) $C_6H_5CH_2C^{14}OOH$	95, 99% (Two runs)	40-50%
(3) $C_6H_5C^{14}H_2COOH$	5, 0, 3, 0% (Four runs)	40-50%

The discrepancies in these results have not yet been explained. It is noteworthy, however, that if the reaction proceeds according to the equation

$$(A)\quad 2\ C_6H_5CH_2COOH \longrightarrow C_6H_5CH_2COCH_2C_6H_5 + CO_2 + H_2O$$

the expected yield of carbon dioxide based on phenylacetic acid is 50% as compared with a yield of 100% from

$$(B)\quad C_6H_5CH_2COOH \longrightarrow C_6H_5CH_3 + CO_2$$

Moreover, with the production of toluene there exists the possibility of its oxidation, in part, by an unknown mechanism. The production of toluene as well as its oxidation products would result in a higher yield of carbon dioxide, as was the case with compounds (1) and (2). The consequence of such oxidation might be to introduce in the case of (1) some non-radioactive carbon dioxide and in the case of (2) radioactive carbon dioxide. The ambiguous nature of the decarboxylation data suggests the desirability of knowing the reaction mechanism involved, so that attempts could be made to isolate and assay both fragments of the degraded molecule.

Experimental

The copper chromite catalyst used in the preparation of methyl iodide-C^{14} and in the decarboxylation of phenylacetic acid was prepared by the method of Harman. Methyl iodide-C^{14} was synthesized by the method of Melville.

Preparation of Acetophenone-α-C^{14}

Methyl iodide-C^{14} (7.75 gm, .055 M) was shaken for 24 hr in a sealed tube with sodium cyanide solution containing 3 gm (.061 M) of the salt in 6 ml of water. The solution was slowly distilled in a microdistillation apparatus fitted with an indented fractionating column. A fraction, bp 76-100°C, amounting to 4.0 ml was collected as crude acetonitrile-2-C^{14}. The fraction was then extracted 10 times with benzene in a liquid-liquid extractor that had been especially constructed for work with radioactive liquids. The acetonitrile-benzene was dried with a little anhydrous sodium sulfate before being added to a 0.16 M solution of phenylmagnesium bromide. The method of addition as well as the separation and hydrolysis of the resulting ketimine were performed according to the procedure of Shriner and Turner. The acetophenone resulting from hydrolysis of the ketimine hydrochloride was distilled in a short path still under reduced pressure. There was obtained 3.5 gm of liquid, bp 83-85°C/12 mm, representing 53% of the theoretical yield based on methyl iodide-C^{14}.

Preparation of Acetophenone-(carbonyl)-C^{14}

To a solution of 4.9 gm (0.1 M) of radioactive sodium cyanide in 10 ml of water there was added in small portions 12.6 gm (0.1 M) of freshly distilled methyl sulfate. Each addition was followed by shaking, which initiated the exothermic reaction, whereupon the solution was cooled in an ice bath. The preparation should be carried out in the hood and, if properly performed, there should be no loss of acetonitrile by volatilization as a result of the exothermic character of the reaction. After addition of all the methyl sulfate, the solution was distilled in the same manner as noted in the preparation of acetonitrile-2-C^{14}, yielding 8.6 ml of a fraction which boiled at 76-100°C.

Acetonitrile-1-C^{14} was extracted from aqueous solution by the use of benzene, the benzene solution of nitrile was added to the Grignard reagent and the resulting complex was hydrolyzed in the same manner as described in the preparation of acetophenone-α-C^{14}. The product, acetophenone-(carbonyl)-C^{14}, was collected and distilled under reduced pressure in a short path still. There was obtained 7.5 gm of liquid, boiling at 83-85°C/12 mm. This represented a yield of 63% based on the weight of sodium cyanide-C^{14}.

The Willgerodt Reaction

In a Carius tube were sealed 3.75 gm sulfur, 2.5 gm acetophenone, 3.0 ml pyridine and 5.0 ml of 15 M aqueous ammonia. Five such tubes were charged with acetophenone-α-C^{14} and five others with acetophenone-(carbonyl)-C^{14}. The tubes were heated for 4 hr in a calibrated electric furnace at 165°C. After cooling, the tubes were opened and the reaction products from the run with acetophenone-α-C^{14} were washed into a single beaker with concentrated ammonia solution. The products of the reaction with acetophenone-(carbonyl)-C^{14} were treated in the same way. The respective reaction products and washings were evaporated to dryness on the water bath. Each dry residue was ground in a mortar, then extracted with 200 ml of boiling water in several portions. Upon cooling, the first crop (10 gm) of crude phenylacetamide crystallized, and was removed by filtration. A second crop of about 1.2 gm was obtained by evaporation of the filtrate to half its volume, followed by cooling. At this time the filtrate was acid (pH = 5), which was no doubt due to decomposition, at least in part, of ammonium phenylacetate to phenylacetic acid during the process of evaporating the reaction mixture to dryness.

In order to remove the residual amide before extracting the free acid, it was necessary to make the filtrate alkaline with sodium carbonate. By extracting five times with ether the remaining amide (0.5 to 1.0 gm) was completely removed, since no residue remained after allowing a drop of the final extract to evaporate on a watch glass. The filtrate was now made acid with hydrochloric acid and the phenylacetic acid product of the Willgerodt reaction was removed by extraction with ether. Five such extractions were performed. Evaporation of this ether yielded 0.5 gm crude phenylacetic acid in the form of an oil. This oil was dissolved in a little aqueous sodium carbonate solution, from which crystalline phenylacetic acid was obtained by slow addition of hydrochloric acid. The phenylacetamide was recrystallized from hot water and melted at 156.5-157.5°C. There was obtained 80% of the theoretical amount. The phenylacetic acid was recrystallized from petrol ether and melted at 76.5-77.5°C, the yield amounting to 2% of theoretical.

Conversion of Phenylacetic Acid from Willgerodt Reaction to Phenylacetamide

Phenylacetic acid (100 mg) was refluxed with 1 ml of thionyl chloride in a microdistillation flask fitted with a reflux condenser. After 10 min the mixture was cooled and the excess thionyl chloride, with some hydrogen chloride, was taken off under vacuum. The crude acid chloride was dissolved in 1 ml of absolute ether and added dropwise to 5 ml of cold concentrated ammonia. Evaporation of this ether gave crystalline phenylacetamide. To obtain the best possible yield, the ammoniacal solution was evaporated to dryness and the crude amide recrystallized from hot water. Phenylacetamide obtained in this way melted at 156.7-157.5°C. (The yield was 75% based on phenylacetic acid.)

Hofmann Degradation of Phenylacetamide

Pure phenylacetamide (45 mg, .33 mM) was suspended in 6.0 ml of 0.18 M barium hydroxide and bromine (.67 mM) was added to the flask by means of a lambda pipette. The receiver flask was then attached to an apparatus that contained a three-way stopcock permitting evacuation and sealing of the receiving flask. Before evacuation,

however, the contents were frozen with liquid nitrogen to prevent loss of bromine.

After the evacuation and sealing, the flask was allowed to warm to room temperature and was shaken until all the amide dissolved in the barium hypobromite. The degradation reaction started at 70°C (hot water bath) as shown by precipitation of barium carbonate and was complete in 3 or 4 min. Coagulation of the precipitate was effected by immersing the flask in boiling water for an additional minute. After cooling the flask, the vacuum was released by means of the stopcock. The precipitate was separated on a suction funnel and washed with two or three portions of water to remove as much benzylamine as possible.

The barium carbonate still contained traces of amine and cyanide and was reprecipitated before counting. The precipitate was therefore dissolved with concentrated sulfuric acid in an assay apparatus and the evolved carbon dioxide was collected in barium hydroxide solution.

The alkaline filtrate, barium carbonate-free with washings, was then slowly distilled in a microdistillation apparatus with an indented column. The oily benzylamine distilled with the first few milliliters of water. Addition of two drops of concentrated hydrochloric acid to the distillate converted the amine to its hydrochloride. To obtain the dry salt the solution was evaporated to dryness in vacuo. Before the benzylamine hydrochloride was combusted it was recrystallized from butanol and melted at 256°C. The yield of barium carbonate was quantitative based on phenylacetamide, while the yield of amine was 70-80% of the theoretical amount.

Decarboxylation of Phenylacetic Acid

Phenylacetic acid (50 mg) and 50 mg of copper chromite catalyst were placed in a small flask fitted with a reflux condenser and a gas inlet tube. Purified quinoline (5 ml) was added and the mixture was flushed for 20 min with "prepurified" nitrogen. The mixture was then heated in a sand bath at 230°C for 30 min with nitrogen being passed in continuously and the evolved carbon dioxide was passed with the nitrogen stream through the top of the condenser into a barium hydroxide bubbler. The reaction mixture was allowed to cool while the apparatus was flushed with nitrogen for an additional 10 min. In order to remove traces of quinoline, the barium carbonate was dissolved in concentrated sulfuric acid and the evolved carbon dioxide reprecipitated from barium hydroxide solution, as in the treatment of the barium carbonate resulting from the Hofmann degradation of phenylacetamide. Yields of barium carbonate were 40-80% based on phenylacetic acid.

Dr. R.B. Loftfield gave valuable suggestions in the work, and H.C. Prosser prepared the methyl iodide-C^{14}.

Normal Coordinates for the Isotopic Acetylene Molecules HCCH, HCCD, and DCCD

(5311)

O.A. Schaeffer

Abstract

The stretching frequencies for the acetylene molecules, HCCH, HCCD and DCCD have been fitted to a single set of valence type force constants. For this potential, the normal coordinates for the stretching modes have been calculated.

In order to predict the isotope effect on the mass spectral pattern of a molecule by the method recently presented (O.A. Schaeffer, J. Chem. Phys. 18, 1501 (1950)), it is necessary to have the normal coordinates for the stretching modes of the molecules in question. For this reason the necessary calculations were made for several isotopic acetylene molecules. As the normal coordinates are of particular interest, they are presented at this time.

The Secular Equations

The linear symmetrical molecules HCCH and DCCD have the point symmetry $D_{\infty h}$. The usual group theory arguments show that of the three stretching modes of vibration, two will be of species Σ^+g and the other one of species Σ^+u. In symmetry coordinates, the secular equation will factor into a linear and a quadratic equation.

Let R_1, R_2, R_3 be the internal coordinates. R_1 and R_3 represent the displacements from equilibrium of the internuclear distances, H-C or D-C, as the case may be. R_2 represents the displacement from equilibrium of the C-C internuclear distance. A suitable set of symmetry coordinates for either HCCH or DCCD is:

$$\begin{aligned} S_1 &= \left(\frac{1}{2}\right)^{1/2} (R_1 + R_3) \\ S_2 &= R_2 \\ S_3 &= \left(\frac{1}{2}\right)^{1/2} (R_1 - R_3) \end{aligned} \tag{1}$$

S_1 and S_2 have the symmetry Σ^+g and S_3 has the symmetry Σ^+u.

Assuming the forces to be harmonic and neglecting all cross terms, the potential, V, in internal coordinates is:

$$2\,V = k_1 R_1^{\,2} + k_2 R_2^{\,2} + k_1 R_3^{\,2} \tag{2}$$

where k_1 is the force constant for a C-H displacement and k_2 the force constant for a C-C displacement. In symmetry coordinates the potential becomes:

$$2\,V = k_1 S_1^{\,2} + k_2 S_2^{\,2} + k_1 S_3^{\,2} \tag{3}$$

The non-vanishing elements of Wilson's (J. Chem. Phys. 9, 76 (1941)) inverse kinetic energy matrix, G, in symmetry coordinates are:

$$\begin{aligned} G_{22} &= 2/m_c \\ G_{12} &= G_{21} = -(2)^{1/2}/m_c \\ G_{11} &= G_{33} = (1/m_c) + (1/m_x) \end{aligned} \tag{4}$$

where m_c is the mass of a carbon atom and m_x is the mass of a hydrogen or deuterium atom, depending on which molecule is being considered.

The secular equation in symmetry coordinates for HCCH or DCCD factors in the two equations:

$$\begin{vmatrix} -(2)^{1/2}\, k_2/m_c & (k_1/m_c) + (k_1/m_x) - \lambda \\ (2k_2/m_c) - \lambda & -(2)^{1/2}\, k_1/m_c \end{vmatrix} = 0 \tag{5}$$

and $$(k_1/m_c) + (k_1/m_x) - \lambda = 0$$

Where $\lambda = 4\pi^2 c^2 \nu^2$, ν is a fundamental frequency in wave numbers.

HCCD is linear but unsymmetrical and has the point symmetry $C_{\infty v}$. All three of the stretching vibrations are of symmetry species Σ^+, and the secular equation is a cubic. There is no need to use symmetry coordinates. Choose as internal coordinates R_1, R_2, R_3. R_1 is the displacement of the H-C internuclear distance from equilibrium, R_3 is the displacement of the D-C internuclear distance from equilibrium, and R_2 is the same as above. In internal coordinates the non-vanishing elements of G are:

$$\begin{aligned} G_{11} &= (1/m_H) + (1/m_c) \\ G_{12} &= G_{21} = G_{23} = G_{32} = -1/m_c \\ G_{22} &= 2/m_c \\ G_{33} &= (1/m_D) + (1/m_c) \end{aligned} \tag{6}$$

where m_H is the mass of a hydrogen atom and m_D is the mass of a deuterium atom.

The secular equation for HCCD assuming the potential given by equation (2) is:

$$\begin{vmatrix} (k_1/m_H) + (k_1/m_c) - \lambda & -k_2/m_c & 0 \\ -k_1/m_c & (2k_2/m_c) - \lambda & -k_1/m_c \\ 0 & -k_2/m_c & (k_1/m_D) + (k_1/m_c) - \lambda \end{vmatrix} = 0 \tag{7}$$

The Normal Coordinates

The infrared and Raman spectra have been thoroughly investigated (G. Herzberg, Infrared and Raman Spectra of Polyatomic Molecules. D. Van Nostrand, New York,

1945; E.E. Bell and H.H. Nielsen, J. Chem. Phys. 18, 1382 (1950)) and vibrational assignments are well established. Rather than a different set of force constants for each molecule, as Herzberg chose, a single set of force constants was tried. The force constants were adjusted to give the best agreement with the observed frequencies. Values for the fundamental frequencies, calculated by the use of the secular equations (5) and (7) and a single set of force constants, are compared to observed values in Table 1. The average deviation between observed and calculated values is 0.3%. This agreement indicates that the potential used is a good approximation to the true potential.

Table 1

Observed and Calculated Values of the Fundamental Frequencies for Some Isotopic Acetylene Molecules

Wave Numbers	HCCH		HCCD		DCCD	
	Observed[a]	Calculated	Observed[b]	Calculated	Observed[b]	Calculated
ν_1	3373	3381	3335	3345	2700	2688
ν_2	1974	1979	1851	1853	1762	1760
ν_3	3282	3300	2584	2569	2427	2423

[a]Values according to Bell and Nielsen.
[b]Values according to Herzberg.

The normalized coefficients, L_{ij}^{-1}, in the transformation from internal to normal coordinates,

$$Q_i = \Sigma_j L_{ij}^{-1} R_j \tag{8}$$

are given in Table 2. The L_{ij}^{-1} values were calculated by the method outlined by Wilson.

Table 2

Values of L_{ij}^{-1} for the Stretching Modes of Vibration of HCCH, HCCD and DCCD

Normalized Coefficients ($\times 10^{-12} g^{1/2}$)	HCCH	HCCD	DCCD
L_{11}^{-1}	0.826	1.197	0.884
L_{12}^{-1}	-0.528	-0.418	-1.421
L_{13}^{-1}	0.826	0.0664	0.884
L_{21}^{-1}	0.392	0.350	0.944
L_{22}^{-1}	3.244	3.095	3.101
L_{23}^{-1}	0.392	1.071	0.944
L_{31}^{-1}	0.879	0.2366	1.197
L_{32}^{-1}	0	1.203	0
L_{33}^{-1}	-0.879	-1.394	-1.197

The transformation from normal to internal coordinates:

$$R_l = \Sigma_j L_{ij} Q_j \qquad (9)$$

has the normalized coefficients listed in Table 3.

Table 3

Values of L_{ij} for the Stretching Modes of Vibration of HCCH, HCCD and DCCD

Normalized Coefficients ($x10^{12}g^{1/2}$)	HCCH	HCCD	DCCD
L_{11}	0.562	0.797	0.380
L_{12}	0.0914	-0.071	0.174
L_{13}	0.569	0.093	0.418
L_{21}	-0.136	0.105	-0.231
L_{22}	0.286	0.239	0.217
L_{23}	0	0.179	0
L_{31}	0.562	-0.044	0.380
L_{32}	0.0914	0.219	0.174
L_{33}	-0.569	0.547	-0.418

These transformations completely define the normal coordinates in terms of internal coordinates.

The Relative Abundances of the Isotopes of Krypton and Neon (5311)

O. A. Schaeffer

Recently A.O. Nier (Phys. Rev. 79, 450 (1950)) has remeasured the abundances of the isotopes of the rare gases and has corrected for systematic errors by using a known mixture of separated argon isotopes. The abundances of the krypton isotopes were measured independently at this Laboratory by a method that was thought to be free from systematic errors. The comparison in Table 1 of Nier's recent values with those of this Laboratory shows that such was indeed the case.

The relative abundances of the neon isotopes have been measured at this Laboratory by the same method used to measure the krypton abundances, magnetic scanning and a high ion accelerating voltage. The results of these measurements are compared to Nier's values in Table 2. In this case the values found here do not agree, within the precision of the measurements, with Nier's results. The disagreement may be caused by the fact that Nier's measurements were complicated for the case of neon by the interference of residual water vapor in the mass spectrometer, causing a possible error in the measurement of the $(A^{36}/A^{40})^{++}$ ratio of the calibrating gas. The comparison in Table 2 of the molecular weights computed from the relative abundances to the international value, based on a gas density measurement, indicates that abundances found in this research are probably more nearly correct that Nier's values. The molecular

Table 1

Relative Abundances of the Krypton Isotopes[a]

Mass	BNL	Nier
78	0.353 ± 0.001	0.354 ± 0.002
80	2.29 ± 0.01	2.27 ± 0.01
82	11.58 ± 0.01	11.56 ± 0.02
83	11.51 ± 0.02	11.55 ± 0.02
84	56.95 ± 0.04	56.90 ± 0.10
86	17.31 ± 0.03	17.37 ± 0.02

[a]The errors listed are probable errors.

Table 2

Relative Abundances of the Neon Isotopes[a]

Mass	BNL	Nier
20	90.49 ± 0.03	90.92 ± 0.04
21	0.257 ± 0.001	0.257 ± 0.001
22	9.25 ± 0.03	8.82 ± 0.04
Atomic Weight[b]	20.181	20.172

[a]The errors listed are probable errors.
[b]International atomic weight = 20.183.

weights of neon were calculated on the assumption that the neon isotopes, Ne^{20}, Ne^{21}, Ne^{22} have the masses 19.9987, 20.9986, 21.9986, respectively, and that the conversion factor from the chemical to the physical atomic weight scales is 1.000278.

The Determination of Deuterium in Water (5311)

L. Friedman and A.P. Irsa

Abstract

An improved method for determining the deuterium content of water samples has been developed. The method is based on quantitative conversion of the hydrogen to ethane, through reaction of the water

with zinc diethyl. The ethane is analyzed in a mass spectrometer. The method is applicable above ~0.5 M% deuterium. The accuracy is ~±2% of the percent composition in this range on routine analyses.

The conventional analytical procedure for the rapid determination of deuterium in water samples of limited size, of the order of 10 mg, involves its conversion to hydrogen by reaction with a suitable metal at elevated temperature (D. Rittenberg, Preparation and Measurement of Isotopic Tracers. Edward Bros., Ann Arbor, Mich., 1946) followed by mass spectrometer analysis (R.B. Alfin-Slater, S.M. Rock and M. Swislocki, Anal. Chem. 22, 421 (1950)). This method suffers from "memory effects" resulting from heterogeneous exchange of hydrogen with water in the mass spectrometer and the conversion apparatus. Fractionation of the isotopes and voltage discrimination in the mass spectrometer make frequent empirical calibration of the instrument necessary for accurate results.

A more efficient procedure would be the quantitative conversion of water to molecules which would not exchange hydrogen with water and which would be of sufficiently high molecular weight so that fractionation and voltage discrimination effects in the mass spectrometer would introduce negligible errors when the isotopic species were determined. A preliminary investigation of the reaction of water with aluminum carbide

$$6\ H_2O + Al_4C_3 \longrightarrow 3\ CH_4 + 2Al_2O_3 \qquad (1)$$

revealed that a side reaction producing hydrogen was very difficult to eliminate. In addition, it was found that the methane-methyl deuteride system was unsatisfactory for spectrometer analysis. In spite of the fact that the conditions of molecular weight and nonexchange with adsorbed water are fulfilled, the analysis is interfered with by the very same adsorbed water that introduces the memory effects mentioned above. Any hydroxyl-containing molecule that ionizes on electron impact to produce masses of M/e = 17 and M/e = 16 must be kept out of the spectrometer if the instrument is to be used for deuterium analysis via the methane-methyl deuteride system.

Orchin, Wender and Friedel (Anal. Chem. 21, 1072 (1949)) have adapted the Zerewitinoff active hydrogen determination (Ber. 40, 2023 (1907)) for the analyses of deuterium in water. They found that the reactions

$$CH_3MgI + H_2O \longrightarrow CH_4 + Mg\begin{matrix}OH\\ I\end{matrix} \qquad (2)$$

$$CH_3MgI + Mg\begin{matrix}OH\\ I\end{matrix} \longrightarrow CH_4 + MgO\cdot MgI_2 \qquad (3)$$

did not produce quantitative yields of methane. They assumed no fractionation of isotopes in this process and this assumption seems to be borne out by their results.

The conversion of water to ethane by reaction with zinc diethyl

$$H_2O + Zn(C_2H_5)_2 \longrightarrow ZnO + 2C_2H_6$$

showed some promise of virtually eliminating many of the difficulties associated with both the hydrogen procedure and the Zerewitinoff reaction. This paper describes a procedure for the quantitative conversion of water to ethane and the mass spectrometric

determination of ethane ethyl deuteride mixtures.

Experimental

Standard samples of water are converted to ethane in the apparatus shown in Figure 1. Flask A is carefully dried, cooled to room temperature and a 10 λ sample of water is introduced into it using a carefully dried micropipette which has been flushed several times with samples of the water to be analyzed. The flask, a 1-cc bulb on the end of a standard taper 12/30 joint, is then attached to the apparatus, cooled with liquid nitrogen and evacuated. After all the air is removed, the droplet of water should be in the bottom of the bulb; if not, the flask is warmed and the water is condensed on the bottom of the bulb using liquid nitrogen. Zinc diethyl is then distilled from the reservoir flask B into the reaction flask A. Approximately 1/2 to 1 cc of liquid is transferred for a run using 10 λ of water. The excess can be almost quantitatively recovered when the reaction is completed. The liquid nitrogen bath surrounding it is removed and as soon as the zinc diethyl starts to melt, bubbles of ethane may be observed evolving from the liquid. A large excess of zinc diethyl is desirable to avoid local overheating which may induce a violent decomposition reaction. Although samples of water as large as 0.1 cc have been decomposed, the hazard of a reaction in which the zinc ethyl itself decomposes increases with sample size.

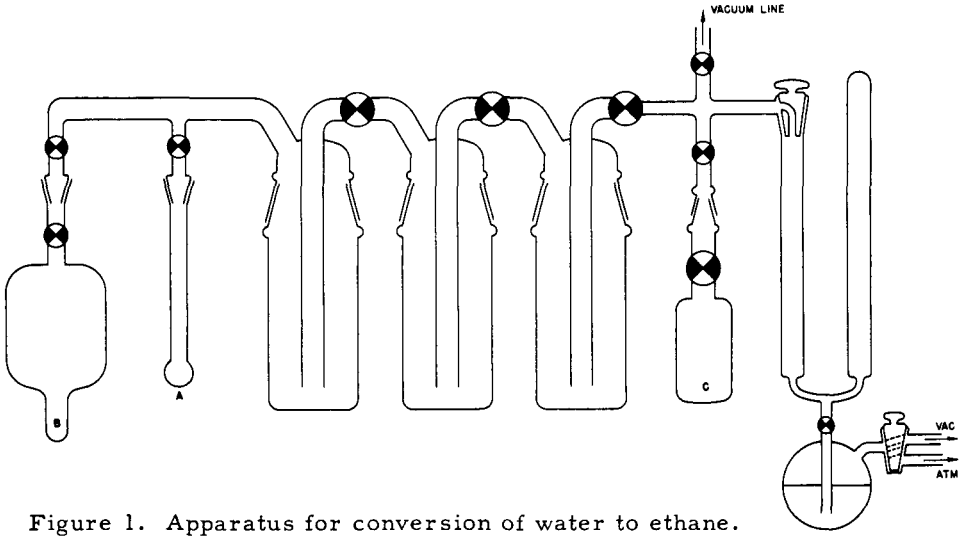

Figure 1. Apparatus for conversion of water to ethane.

The reaction appears to proceed in two steps. Conversion proceeds smoothly to 50-75% of completion as A gradually warms to room temperature. At this point bubbles may cease to evolve and the liquid assumes a viscous gelatinous appearance. Gentle warming with the hand or warm water will initiate further reaction which proceeds vigorously for several minutes. The zinc diethyl becomes more fluid and some zinc oxide may precipitate from the solution. In order to insure complete reaction, the zinc ethyl is refluxed four or five times for 5- to 10-sec intervals by heating cautiously with the luminous flame of a microburner after the second phase of the reaction has stopped. The ethane and any water vapor entrained by it is then condensed into A using a liquid nitrogen bath. This is replaced with a dry ice acetone bath and the ethane is condensed

in the first trap using liquid nitrogen. The stopcock between A and the rest of the apparatus is closed and A is gently heated with a luminous flame refluxing the zinc ethyl again.

The three traps in series are cooled with acetone dry ice, secondary butyl chloride-liquid nitrogen slush and liquid nitrogen. The ethane is taken through these traps and any entrained zinc ethyl is separated by condensation. Traces of ethane in A produced by the last heating are also collected in the third trap. Finally, the liquid nitrogen bath on the third trap is replaced by the sec-butyl chloride bath and the product ethane is condensed in the evacuated sample bulb C. The time required for the conversion of 10 λ of water, following the procedure outlined above, is approximately 1/2 hr.

The product ethane was analyzed in a Consolidated-Nier model 21-201 mass spectrometer. Patterns for ethane and ethyl deuteride were determined at 1500 v ion accelerating potential using magnetic scanning. A ratio of the sensitivity coefficients of the two gases is required for the superposition method of analysis. The model 21-201 may be adapted for the determination of sensitivity coefficients in the following manner: A 200-cc bulb is attached to one of the two sample inlets to serve as a gas reservoir. Ethane is introduced through the other inlet and compressed to a pressure of 100-110 mm by raising the Toepler pump to the point at which the check valve is seated by the mercury. Gas pressure is then read and recorded. The gas is then expanded into the reservoir bulb and a final pressure, compatible with the requirements of the spectrometer tube and leak, is obtained. The sensitivity coefficient is then determined with a precision limited by the precision in reading a pressure of between 100 and 110 mm on the sample system manometer, approximately 0.5%.

The pump-out time of ethane in the spectrometer, using acetone dry ice refrigerant on the spectrometer trap, was 2 min. Samples of light ethane run directly after 99.8% ethyl deuteride on this pumping schedule showed less than 0.1% contamination due to memory effect or holdover of the ethyl deuteride. Memory effects in the conversion apparatus were not observed carried to completion. After a large number of runs a grayish white deposite of zinc oxide is observable on the glass, and at this point it is profitable to clean the apparatus.

Discussion and Results

Typical calibration data, required for analysis of the ethane-ethyl deuteride system is presented in Table 1. Data obtained by Turkevich et al. (J. Am. Chem. Soc. 70, 2638 (1948)) and Stevenson and Wagner (J. Chem. Phys., in press) from samples prepared by the Grignard reaction are included for comparison. The differences in the sets of data are considered to be for the most part instrumental. It is important to note that the ratios of the sensitivity coefficients for deuterium substituted hydrocarbon and their protium analogues are not necessarily unity, and that these ratios may vary instrumentally.

The results obtained from analysis of a series of water standards prepared by weight dilution from distilled water and 99.8% D_2O are presented in Table 2. Each value reported in the table represents a separate conversion of a .01-cc water sample. Mass spectrometer precision in analysis of any particular gas sample was found to be better than 0.3%. The M% D was calculated from the relative ion intensities of the 30

Table 1

Mass Spectra and Sensitivities for Ethane and Ethyl Deuteride

Mass	C_2H_6			C_2H_5D		
	F	S	T	F	S	T
31	-	-	-	1.00	1.00	1.00
30	1.00	1.00	1.00	0.701	0.608	0.731
29	0.74	0.765	0.676	3.06	2.47	3.304
Sensitivity at Parent Mass	1.06	1.00	-	1.00	1.00	-

Table 2

Analyses of Deuterium in Water

Sample	Experimental M % D	Calculated M % D
1	0.560 0.567	0.563
2	1.90	1.89
3	3.99 4.01	4.025
4	4.91	4.94
5	10.4 10.9 10.8	10.95
6	30.6 31.2	31.2
7	48.8 49.4	49.0
8	68.0 68.6	68.8
9	78.6	79.0
10	84.6 84.5	84.45

and 31 peaks in the observed spectra using the calibration data presented in Table 1.

This method can be used over a wide range of deuterium concentration. The lower limit is set at between 0.5 and 1.0 M% because of natural C^{13} interference. The upper limit depends essentially on the pattern stability in the mass spectrometer and the quality of heavy water available for calibration purposes. Samples containing 95% D require a spectrometer precision of 0.1% to obtain an accuracy of 2%.

A study is in progress to determine the precision and accuracy that may be expected in this concentration range of 0.5-5.0% if the procedure as outlined is used as a routine method of analysis.

It is evident that most errors in the method arise in the chemical conversion of water to ethane. If reasonable care is taken, errors in sampling and handling the 10 λ of water can be readily eliminated. The problem of decontamination of the ethane from unreacted zinc diethyl is easily disposed of if the procedure is carefully followed. The most difficult error to eliminate is the problem of fractionation of the isotopes in the conversion, i.e., driving the reaction to completion.

An investigation of the relative rates of the reaction of H_2O and HDO with zinc ethyl under the condition of the conversion was made using water containing 4 M% HDO. The reaction was run with separate samples of water, quenched (by cooling with liquid nitrogen) at appropriate degrees of completion; the extent of reaction in each case was determined by measuring the pressure of gas produced in the initial and final stages. It was assumed that the concentration of D_2O in the water was negligible and that the amount of C_2H_6 produced from reaction of HDO could also be neglected. Since in all cases a large excess of zinc diethyl was used the reaction is kinetically first order and the following expression is obtained:

$$\frac{k_{HDO}}{k_{H_2O}} = \frac{\ln \frac{1}{1-xf}}{\ln \frac{1}{1-f}}$$

where f is the fraction of the total water converted and x is the fraction of total deuterium converted.

The results of this fractionation study are presented in Table 3. During the first half of the conversion the reaction is primarily between zinc diethyl and ice, k_{HDO}/k_{H_2O} is approximately 0.9. This relatively small value for a protium-deuterium system

Table 3

Fractionation of D in the Water Conversion

% Reaction	% D Converted	k_D/k_H
6.3	42.0	.88
23.8	44.0	.84
46.0	50.6	.86
54.2	56.2	.92

(J. Bigeleisen, Science 110, 14 (1949)) at temperatures 0°C and below may be a result of the heterogeneous nature of the reaction in which surface layers of ice are removed by the reagent. Essentially complete reaction occurs in successive elements of volume. Only one point was determined for almost complete reaction (95% reaction, 89.2% deuterium converted). Assuming that the reaction proceeds stepwise and that, in the last half, ethane is produced homogeneously from the reaction of zinc diethyl with $(C_2H_5)Zn(OH)$ or a similar intermediate, the ratio of rate constants calculated from the 95% point for this mechanism is $k'_{OD}/k'_{OH} \tilde{=} 0.2$. A considerably greater fractionation of isotopes occurs in the last half of the reaction and consequently serious errors are made if the reaction is not driven to completion.

Szilard-Chalmers Separations with Metal-TTA Complexes (5311)

J.A. Miskel

In connection with experiments on the chemical separation of nuclear isomers, the use of TTA (thenoyl trifluoroacetone) complexes of metal ions for Szilard-Chalmers separations has been tried. Metal TTA complexes were prepared by extraction of aqueous solutions of metal ions with a 0.05 M solution of TTA in benzene. The benzene layer was separated from the aqueous one and evaporated to dryness; the solid was then heated with an infrared lamp to remove any uncombined TTA remaining. Complexes of Fe(III), Cu(II) and Hf(IV) were prepared.

The solid complexes were irradiated in the reactor, dissolved in benzene and the solution extracted with H_2O. The specific activities of both fractions were compared and the total activity determined. The results are presented in Table 1.

Table 1

Solid Complexes	Yield	Enrichment Factor*
$Fe(TTA)_3$	50-80%	100
$Hf(TTA)_4$	20-30%	10
$Cu(TTA)_2$	no separation	

*$\frac{\text{Specific activity aqueous phase}}{\text{Specific activity benzene phase}}$

An experiment was made to determine if the exchange of $Hf(IV)_{aq}$ with $Hf(TTA)_4$ (benzene) would account for the low yield and enrichment of the hafnium compared to iron. An irradiated sample of $Hf(TTA)_4$ was dissolved in benzene and three aliquots prepared. These aliquots were then extracted with aqueous solutions of the following compositions:

Extraction solution 1: 1 ml $Hf(IV)_{aq}$ solution + 3 ml H_2O
Extraction solution 2: 2 ml $Hf(IV)_{aq}$ solution + 2 ml H_2O
Extraction solution 3: 4 ml $Hf(IV)_{aq}$ solution + 0 ml H_2O

The specific activities of the HfO_2 obtained from these extractions were found to be in the ratio 4:1.4:1. This indicates that exchange between $Hf(IV)_{aq}$ and $Hf(TTA)_4$ (benzene) is not large during the separation time.

Half-Life of I^{129} and the Age of the Elements (5311)

S. Katcoff, O.A. Schaeffer and J.M. Hastings

Abstract

The specific activities of several samples of methyl iodide containing I^{129} were measured with proportional counters and the ratios of I^{129} to I^{127} were determined with a 60° sector type mass spectrometer. The half-life of I^{129} was found to be $(1.72 \pm 0.09) \times 10^7$ yr. The time interval between the formation of the elements and the formation of the earth calculated from this value is 2.7×10^8 yr. It was assumed that most of the Xe^{129} now present on the earth, originated from decay of I^{129} after the formation of the earth and that the original cosmic abundance of I^{129} was about equal to that of the stable I^{127}.

The half-life of I^{129} was found by measuring the absolute disintegration rates, isotopic compositions, and total iodine contents of several samples obtained from fission product iodine. This latter was separated from a uranium slug that had received a 4-yr irradiation in the Oak Ridge reactor and had cooled for 21 months.

For the chemical separation, the uranium was dissolved in concentrated hydrochloric acid to which a few mg of iodine carrier had been added. After oxidation with hydrogen peroxide, the elementary iodine was removed by counter-current extraction into carbon tetrachloride. It was purified by six or eight (see below) chemical cycles consisting of reduction to iodide, extraction into water, re-oxidation to iodine and re-extraction into carbon tetrachloride. The iodine was finally precipitated as PdI_2 which was washed and dried. Then it was decomposed by heating to 350° in an evacuated glass system; the evolved iodine vapor was collected in a tube containing methanol and red phosphorus. This mixture was heated to 110° for 1 hr to make methyl iodide, which was then passed over anhydrous calcium chloride to separate it from excess methanol. The methyl iodide was used for the activity measurements and the isotope ratio determinations.

The counters (W. Bernstein and R. Ballantine, Rev. Sci. Instr. 21, 158 (1950)) were 2 cm in diameter and 30 cm long with silver cathodes and 2 mil wolfram center-wires. They were operated in the proportional region with a 5000 v power supply, a non-overloading pulse amplifier and an Atomic Instrument Co. scaler, model 101A. The counter gas was methane at 1 atmosphere. Preliminary experiments were performed to study the effect of adding small amounts of methyl iodide to the methane. It was found that the counter plateau disappeared and that the counting rate of a Co^{60} gamma-ray standard started to decrease as the partial pressure of methyl iodide was increased above 50 μ. Therefore, the measurements were made with the radioactive methyl iodide

samples at partial pressures between 17 and 38 μ and with the counters operating at 3800 v on both voltage and gain plateaus. Each sample was counted at least twice for periods of 20 to 150 min for total recorded counts $>10^4$. Then the counter was cooled to -195° for 1 hr and the methane pumped off leaving the methyl iodide behind. By warming the counter to room temperature, the methyl iodide was distilled into a small tube containing a 30-mg piece of sodium and cooled with liquid nitrogen. This tube was set aside for the quantitative iodine determination.

The counter was refilled with methane and the background counting rate determined. This was usually found to be somewhat higher than it had been before the active methyl iodide had been in the counter. Apparently anywhere from 0-12% (average 5%) of the methyl iodide remained in the counters. The backgrounds used in the calculations were those measured after the methyl iodide was distilled out. The operation of the counters was always checked by means of the Co^{60} standard. Its counting rate, corrected for I^{129} activity and background, remained the same within 1%, independent of the counter used and the amount of active methyl iodide therein. The total volumes and cathode volumes of the counters were measured at the conclusion of the experiments by adding water to them from a buret. It was shown by Bernstein and Ballantine that for C^{14}, the cathode volume is equal to the sensitive volume and that within this volume, the observed counting rate is very nearly equal to the actual disintegration rate. In the present work, it was assumed that these conditions apply also.

The small tube, containing the methyl iodide transferred from the counter, was heated with the sodium to 250° for 20 min in order to form NaI. Then water vapor diluted with helium was passed in to react with the excess sodium. The mixture in the tube was dissolved in 3 ml of water and its iodine content determined quantitatively by a potentiometric titration with 1.01×10^{-4} M silver nitrate solution against a calomel electrode. This analytical method was first tested by titrating eight 22-μg samples of iodide from a stock solution. The mean deviation from the average was less than 2%, and the agreement with a gravimetric analysis of the stock solution in which two 13.5-mg samples of silver iodide were precipitated was better than 4%. The analytical method was also tested by filling counters with amounts of inactive methyl iodide measured with a manometer and expanded by a known amount, adding an atmosphere of methane, and then proceeding as in the final experiments. In five samples, with methyl iodide pressures between 16 and 142 μ the average agreement was 7%, but the methyl iodide pressure determinations were not very accurate and no correction was made for the methyl iodide that remained behind in the counter. In one run, when no methyl iodide was added, a zero blank was obtained.

Two different isotopic analyses were performed. The first, no. 1, was done with the CH_3I prepared from the iodine that had been through six purification cycles and from which samples 1a-1d were taken. Isotopic analysis no. 2 and samples 2a-2e were taken from the iodine that had undergone eight purification cycles. The single collector 60° sector-type mass spectrometer (O.A. Schaeffer and J.M. Hastings, J. Chem. Phys. 18, 1048 (1950)) that was used had 70-v ionizing electrons, a 4000-v ion accelerating potential, and magnetic scanning. Several preliminary runs were made with ordinary CH_3I (only I^{127}). For analysis no. 1, the ratios of the ion current at mass 129 to that at mass 127 (I^+ peaks) in six successive runs were: 0.0707, 0.0703, 0.0701, 0.0701, 0.0713 and 0.0702. The average was 0.0704. In analysis no. 2, the ratios in four runs were: 0.0714, 0.0691, 0.0685, 0.0682; average: 0.0694. Since a compensating hairpin-type leak was used, a correction for fractionation had to be made. The ratios were multiplied by $(\text{mass of } CH_3I^{127}/\text{mass of } CH_3I^{129})^{1/2}$. Thus the corrected ratios for

analyses no. 1 and no. 2, respectively, are: 0.0699 and 0.0689; or 6.53 and 6.45 atomic % I^{129}. For some of the runs, the complete spectrum was computed using these ratios and the standard pattern for ordinary CH_3I. The maximum deviation was less than 2% for any mass. Even considering the possible systematic errors, the isotopic ratios found are probably accurate to $\pm 2\%$.

Table 1 gives the data and results for each sample. The average of the nine values for the half-life of I^{129} is 1.72×10^7 yr with an over-all estimated probable error of 5%. This figure supercedes earlier tentative estimates (S. Katcoff, O.A. Schaeffer and J. Hastings, BNL 64 (S-6), p. 87) which ranged from 0.7×10^7 to 1.7×10^7 yr. A half-life of $(3 \pm 1) \times 10^7$ yr based on experiments in which the activity of solid samples of AgI containing I^{129} was measured has been reported by Parker, Creek, Herbert, Lantz and Martin (Oak Ridge National Laboratory Report No. 286 (1949)). They also report a maximum beta-ray energy of 100-135 kev in good agreement with the value of 130 kev found in this work by observing that the range of the beta rays in aluminum is about 22 mg/cm^2.

It was first pointed out by H.E. Suess (Zeit. f. Physik 125, 386 (1948)) that a lower limit for the time interval, t, between the formation of the elements and the formation of the earth's atmosphere could be calculated if the half-life of I^{129} were known. Any I^{129} still in existence when the earth was first able to retain its atmosphere, must have decayed to Xe^{129} and therefore increased the abundance of this isotope over its primeval value. By making the plausible assumption that the original abundance of I^{129} was approximately equal (H.E. Suess, Zeit. f. Naturforsch. 2a, 311 (1947); J. Mattauch and S. Flügge, Nuclear Science Tables, Interscience Publishers, Inc., New York, p. 104) to that of I^{127} it is only necessary to compare the present abundance in the earth's crust of I^{127} with that of Xe^{129}. Suess used 1 g/cm^2 and 10^{-4} g/cm^2, respectively, for these abundances and calculated a lower limit for t of 10 I^{129} half-lives. From the systematics of nuclear abundance data, he thought that Xe^{129} does not have an abnormally high abundance compared to the other Xe isotopes.

A.H.W. Aten, Jr. (Phys. Rev. 73, 1206 (1948)), however, has pointed out that in all cases where an odd isotope occurs between two even ones, the odd one is always less abundant than the sum of the abundances of the other two. The only exception is Xe^{129}. Its abundance is 26.23% while Xe^{128} and Xe^{130} have abundances of 1.90% and 4.07%, respectively. It is likely, therefore, that most of the Xe^{129} present in the atmosphere today originated by decay of I^{129} after the formation of the earth as did the A^{40} originate from decay of K^{40}.

It was suggested by Dr. Maurice Goldhaber of this Laboratory that t probably could be calculated more accurately by comparing the I^{127}/K^{40} abundance ratio with the Xe^{129}/A^{40} abundance ratio. In this way, the terrestrial abundance data, given by V.M. Goldschmidt (Geochem. Verteilungsgesetze IX, Videnskapsakademien, Oslo (1937)) can be applied directly; as a first approximation it can be assumed that the atmosphere contains the same fraction of the earth's Xe^{129} that it does of the earth's A^{40}. The following equation was used:

$$(I^{127} \; e^{-\lambda t} / K^{40})_T = (Xe^{129} / A^{40}).$$

I^{127} refers to an abundance of 0.24 atoms per 10^6 atoms of Si; λ is the disintegration constant of I^{129}; K^{40} refers to the number of atoms (per 10^6 atoms of Si) which have decayed to A^{40} in time T, the age of the earth (3.35×10^9 yr (A. Holmes, Nature 159,

127 (1947))). Its present abundance was taken as 0.0119% of the total K abundance of 44,200 atoms per 10^6 Si atoms. Its half-life was taken as 1.27×10^9 yr (G.A. Sawyer and M.L. Wiedenbeck, Phys. Rev. 79, 480 (1950)), with 12% decaying to A^{40}. The A^{40}, in the equation, refers to its abundance in the atmosphere by volume, 0.93%; Xe^{129} refers to the radiogenic Xe^{129} which is assumed to be 20% of the total Xe abundance in the atmosphere (8×10^{-6}% Xe by volume (G. Damköhler, Z. Elektrochem 41, 74 (1935))). This leaves 6.23% Xe^{129} which is not radiogenic. Thus the rule of Aten is approximately satisfied and the rule that two odd isotopes of an element have roughly the same abundance is not seriously violated (abundance of Xe^{131} is 21.2%).

Table 1

No. of Sample	No. of Counter	Cathode Vol. / Total Vol.	CH_3I in Counter ($M \times 10^{-7}$)	Counter Bkd. (c/m)	Activity of I^{129} (c/m) (Corr. for Bkd.)	Half-Life (Yr $\times 10^7$)
1a	7	0.859	1.698	127	467	1.62
1b	8	0.867	1.468	117	376	1.75
1c	7	0.859	1.838	183	470	1.74
1d	8	0.867	1.995	137	506	1.77
2a	6	0.864	0.970	169	250	1.71
2b	7	0.859	0.925	148	238	1.71
2c	8	0.867	1.434	119	370	1.72
2d	10	0.864	1.810	95	462	1.73
2e	8	0.867	1.688	131	427	1.75

Solving the equation for t gives 15.4 half-lives of I^{129} or 2.7×10^8 yr for the time between the formation of the elements and the formation of the earth. Thus the age of the elements (T + t) is 3.6×10^9 yr. This calculation of t is very insensitive to the accuracy of the assumptions and approximations that were used. For example, if the amount taken for radiogenic Xe^{129} is wrong by a factor of 10 the error in t is only 22%.

Emission of Lead X-Rays in the Decay of Po^{210} (5311)

W. Rubinson and W. Bernstein*

Abstract

The low energy photons from Po^{210} sources have been investigated by means of a proportional counter pulse analyzer. The photons have energies corresponding to the K, L, and M X-rays of atoms with atomic number in the neighborhood of Pb. By comparison of the L_α

*Electronics Division.

line from the Po^{210} source, with the corresponding lines excited by alpha particle bombardment of Tl, Pb and Bi, and by critical absorption experiments on the L_β line, it has been established that the L lines, at least, are characteristic X-ray lines of Pb. The yield of L photons per nuclear decay is: L_α, 5.2×10^{-4}; L_β, 2×10^{-4} (with an error of perhaps 25%). Assuming a Pb fluorescence yield of ~ 0.5, this means that when a Po^{210} nucleus decays, the chance that its electronic cortege emits an L electron is $\sim 0.14\%$. This is above five times as great as predicted by Migdal's theory.

Part I

The emission of low energy photons from Po^{210} sources was first observed and studied experimentally by Curie and Joliot (J. Phys. Radium VII 2, 20 (1931)) and it has been noticed by others (S. DeBenedetti and E.H. Kerner, Phys. Rev. 71, 122 (1947)); B. Zajac, E. Broda and N. Feather, Proc. Phys. Soc. 60, 501 (1948)). Curie and Joliot used ionization chambers, with an electroscope to detect these photons and absorption coefficients to identify the photon energies. They found that, within experimental error, the photon energies were those to be expected for the L and M X-radiations of Po. Further, they thought that the intensity of the radiations increased with the thickness of the Po^{210} source. Since they used sources of roughly constant area and up to ~ 50 mc in strength, they were inclined to believe that the radiations were Po X-rays excited by alpha particle bombardment of the undecayed Po atoms in the source. However, it might well be expected that the radiations are Pb X-rays; the emission of an alpha particle from a Po^{210} nucleus may be accompanied by ejection of an electron from the electronic cortege of that nucleus; the subsequent electronic transitions, taking place in the field of a Pb^{206} nucleus, would give rise to radiations characteristic of Pb. This possibility was recognized by Curie and Joliot, but their absorption technique could not distinguish between Po and Pb X-rays.

The theory (A. Migdal, P. Phys. (U.S.S.R.) IV, 449 (1941); E.L. Feinberg, ibid., p. 424; J.L. Levinger, Thesis, Cornell University, June, 1948) of the ejection of an electron from the electronic cortege, on emission of a charged particle by the nucleus, recognizes two processes that can cause such ejection of an electron. The first of these processes is "collision" between the decay particle and the orbital electron, similar to the collision of a charged particle from an external source with an orbital electron. The second process is the "sudden" perturbation (in the quantum mechanical sense) on the motion of the orbital electron by the sudden change in nuclear charge.

The probability of transition of an orbital electron from a given state $\psi_n{}^z$ in an atom of nuclear charge z to a final state $\psi_E{}^{z'}$ of continuum energy E in the field of an atom of nuclear charge z', the transition being induced by the nuclear decay, is computed by standard perturbation theory. The approximations that are made by the three authors restrict the applicability of the results to cases of beta particles with very large speed, or alpha particles with very small speed as compared to the speed of the orbital electron. Also, hydrogenic wave functions are used, so that the theory is applicable only to electrons in the deepest shells. The change of nuclear charge must be small compared to the nuclear charge itself if perturbation theory is to be applied.

Within these restrictions, Migdal shows that for beta decay the ejection of electrons

by collision will be small compared to ejection by "sudden" change of nuclear charge if

$$\left(\frac{Z^* e^2}{hc}\right)^2 \ll 1$$

where Z^* is the effective nuclear charge (of the product nucleus) seen by the electron concerned. All three theories show that the efficiency of ejection of orbital electrons in beta decay is proportional to $1/Z^{*2}$. The proportionality constants computed in the theory are different for electrons in different initial states. In a subsequent paper, the current experimental study of the beta effect will be reported.

This paper is concerned with the ejection of orbital electrons in alpha decay. The theory is applicable to this case since for all known alpha-active nuclides the speed of decay alphas is much less than that of the orbital electrons in inner shells. Migdal treats the problem by means of the small perturbation potential $-2e^2/r(t)$ of the alpha particle, and using hydrogenic wave functions, computes the matrix elements of the electronic transitions. Levinger makes a similar calculation, but in addition to this, he makes a separate computation of the effect of the perturbation due to sudden change of nuclear charge and simultaneous nuclear recoil. In this latter case, according to Levinger, it is not the alpha velocity, but the velocity of the center of charge of the alpha particle and the nucleus, that must be taken into account. The theory shows that in alpha decay the effect of the sudden perturbation is much less than the collision effect.

Part II

As part of a program to study experimentally the ejection of orbital electrons on emission of a charged particle from a nucleus, the X-rays from Po^{210} sources have been investigated. For that purpose an improved verision of a proportional counter X-ray spectrometer has been used (W. Bernstein, H.G. Brewer, Jr. and W. Rubinson, Nucleonics 6, 39 (1950)). The improvements consist of better stabilization of high voltage supply and filament supply, and more carefully constructed counter tubes. By this means, the stability of the instrument has been greatly improved and the resolution considerably bettered. With the 10.5-kev As K X-rays from a Se^{75} (K capture) source, peaks can now be had with full width at half-height of $\sim$15%. With the instrument in its previous state it could not be done better than $\sim$20%. The present counter tubes are brass or aluminum coated glass, 12 in long and 4 in. in diameter, with a center wire of 4 mil wolfram or stainless steel. The window is a 1-in diameter hole in the center of the cylindrical counter wall, covered with 5 mil Be. As counter gas, a 10:1 mixture of argon and methane has been used mainly at a total pressure of 1 atmosphere.

The Po^{210} was obtained from Oak Ridge. It was not tested for radiochemical purity beyond checking that a source of $\sim 10^8$ alpha decay/min covered with 3 mg/cm^2 of cellophane and 5 mg/cm^2 of Al gave a counting rate only a few times background on the Geiger counter, and that the half-life was correct. The Po^{210} was dissolved in 0.5N HNO_3 solution, and a source was prepared by evaporating (with a heat lamp) an aliquot of this solution in a shallow depression, 1 mm deep and 15 mm in diameter, in a polystyrene disk. The disk was then fitted into a well in an aluminum plate, and covered with cellophane 2.7 mg/cm^2 in thickness. The strengths of most of the sources were initially of the order of 1 mc, and the sources showed practically no visible deposit.

In Figure 1, the curve "No As_2O_3 absorber" shows the L X-ray peaks from a

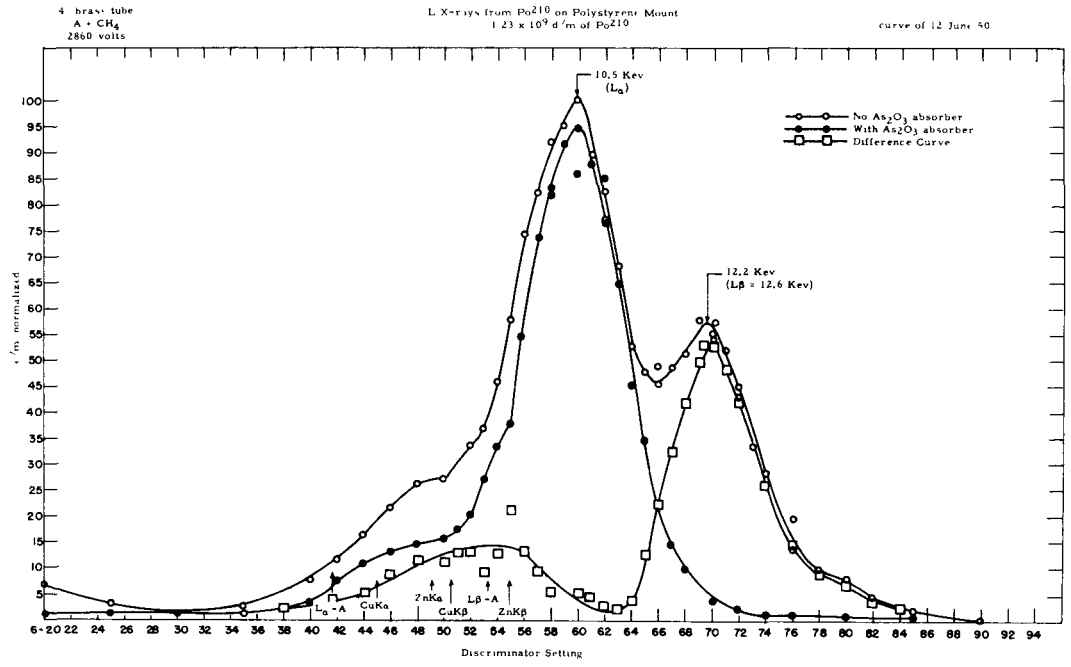

Figure 1. L X-rays from Po^{210} on polystyrene mount.

Po^{210} source of alpha decay rate 1.23 x 10^9 d/m, set at a distance of 1 3/8 in from the counter window. The counting rate at the top of the main peak was 960 c/m.

It has been established that these peaks are from Pb L X-rays by the following experiments.

The Pb and Bi L lines, as listed in Compton and Allison (X-rays in Theory and Experiment. D. Van Nostrand and Co., New York, 1935, Appendix V, Table II) and the corresponding lines of Po obtained by extrapolation are listed in Table 1.

Table 1

Energies in Kev of L Lines of Pb, Bi, and Po

Siegbahn Notation	L_{α_2}	L_{α_1}	L_{β_1}	L_{β_2}	L_{γ_1}
Transition	L_{III}-M_{IV}	L_{III}-M_V	L_{II}-M_V	L_{III}-N_V	L_{II}-N_V
Element					
$_{82}Pb$	10.466	10.568	12.634	12.634	14.787
$_{83}Bi$	10.748	10.856	13.044	13.000	15.272
$_{84}Po$	(10.99)	(11.14)	(13.45)	(13.39)	(15.7)

(1) The position of the main peak in Figure 1 is experimentally identical with that of the As K peak from a Se^{75} (K capture) source, which has energy 10.53 kev. Therefore

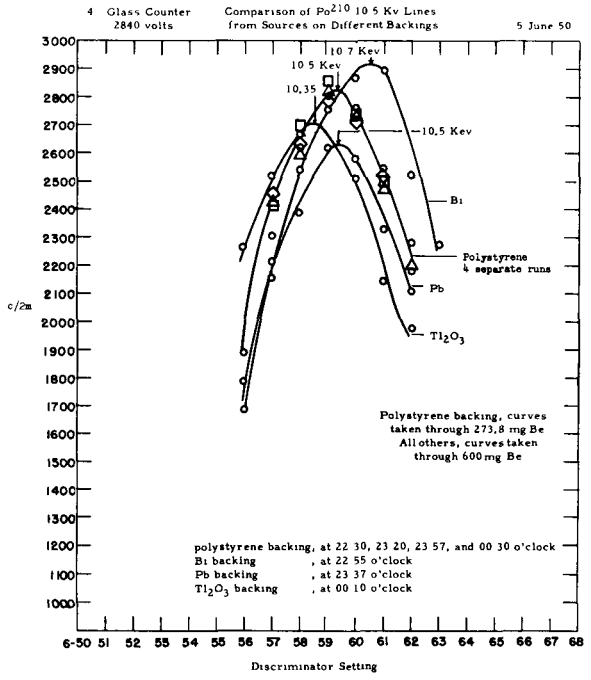

Figure 2. Comparison of Po^{210} 10.5 kev lines from sources on different backings.

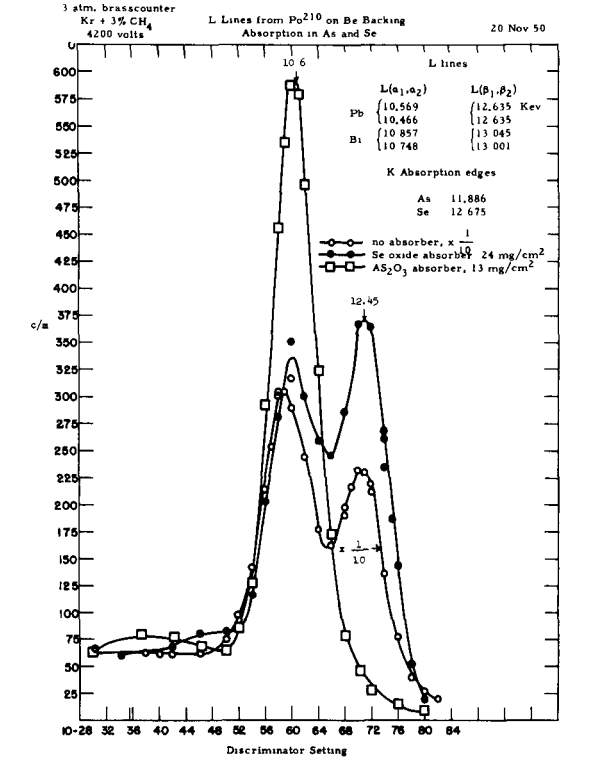

Figure 3. L lines from Po^{210} on Be backing absorption in As and Se.

the main peak has approximately the correct energy to be the L_α line of Pb. But the resolution of the instrument is not good enough to allow rejection of the possibility that these lines are Bi or even Po lines.

(2) Four Po^{210} sources of identical strength (~ 1 mc) were prepared and mounted, respectively, on thick backings of polystyrene, Pb, Bi and Tl_2O_3. The alpha bombardment of the heavy-element backings excites them to emit their characteristic X-rays, which are superposed on the X-rays from Po. The intensity of the heavy element L radiations produced in this way is about equal to the intensity of the L radiations from the Po^{210}. Figure 2 shows the main L peak for each of these four sources. In order to ascertain that the instrument did not drift while the different curves were being taken, a curve with a polystyrene-backed source (which has no fluorescent radiations in this energy region) was taken on heavy-element backing immediately before and after each of the curves of Po. Be absorber was used to decrease the X-ray intensity (if the intensity gets too high, the resolution becomes poorer). Since the Be counting rate was about twice that of the other sources, a lesser thickness of Be was used for the polystyrene-backed source in order that its total counting rate should be approximately equal to that of the others. This was done because it was found that, due to an instrumental effect, the apparent peak position shifts somewhat toward lower energies if the counting rate is greatly increased. It is seen in Figure 2 that the polystyrene-backed source gives a peak identical in position with that of the Pb-backed source, and lying between the other two. Hence the L_α line from the Po source is a characteristic line of Pb.

(3) There is no element with an absorption edge of energy lying between the L_α energies of Pb and Bi, but Se has an absorption edge of 12.675 kev, which lies between the Pb L_β (12.634 kev) and the Bi L_β (13.00 and 13.044 kev). Therefore, if the L_β lines from Po are those of an

element higher than Pb, they will be critically absorbed in Se. Figure 3 shows curves without absorber, with 24 mg/cm^2 of Se oxide absorber, and with 13 mg/cm^2 of As_2O_3 absorber. It is seen that the Se absorber absorbs a smaller fraction of the L_β than of the L_α, as is to be expected for Pb L radiations. The As absorber, with an absorption edge at 11.886 kev, takes out the L_β line completely, as is to be expected.

(4) Before the experiments described under (2) and (3) were done, the following experiment eliminated the possibility that the observed radiations were Po X-rays excited by alpha particles. Two Po^{210} sources were prepared which differed only in that in preparing one of them, 1 mg of Bi in HNO_3 solution was added to the Po^{210} aliquot before evaporation. There were about 4×10^4 times as many Bi atoms in this source as Po atoms, and the total quantity of solids on this source was visibly much greater than in the source free of Bi. However, the intensity of the X-radiations from the source containing Bi was only slightly greater than that from the source containing no Bi. This is not in contradiction with the experiments described under (2), where Po^{210} was mounted on a heavy Bi backing. This fairly well eliminates the possibility that the X-radiations from Po sources are Po X-rays excited by alpha particle bombardment.

It is unlikely that the electron ejections giving rise to these Pb X-rays can be caused by any process other than the ones considered here. Internal conversion of the well-known 0.8 Mev gamma of Po^{210} has been shown to be of the order of 10% in the K shell, and $\sim 2\%$ in the L shell (D.E. Alburger and G. Friedlander, Phys. Rev., in press). Since there is only one 0.8 Mev gamma emitted per 10^5 alpha decays, this would allow of an L X-ray yield of less than 10^{-6} per alpha decay, which is about 1/1000 of what has been measured.

It might still be argued that some nuclear gamma of lower energy is being completely converted. This would have to be a very general phenomenon, because X-rays have been observed from all of the several nuclides tried. In any case, it is rather too fortuitous that the intensity of this hypothetical completely converted gamma be such as to give an X-ray intensity of the same order of magnitude as that predicted theoretically for particle decay.

Part III

To determine the efficiency of production of Pb L_α and L_β radiations in Po^{210} decay requires a measurement of the alpha disintegration rate of the source, a measurement of the number of photons per min of each kind detected by the counter, and a computation of the counter efficiency and geometry for each kind of photon.

The alpha disintegration rate of the source was determined by alpha-counting three 100 λ aliquots of a 5×10^5-fold dilution of the Po^{210} stock solution, evaporated onto Pt disks. A reliable methane-flow alpha counter was used, and alpha-counting geometry was assumed to be 51%. The precision of this measurement was very good. The stock solution proved to have a disintegration rate of 1.47×10^{10} decay/min/ml on 10 May 1950.

The number (per min) of L_α and L_β photons detected by the counter was determined by graphical integration of the curves in Figure 1. The curve without added absorber was normalized to 100 at the L_α peak. The curve taken through As_2O_3 absorber, which

extinguishes the $L\beta$, was normalized to 94, since a graph in which both curves were normalized to 100 showed that the $L\beta$ lines make a contribution of about 6% to the $L\alpha$ peak height. The difference curve, excluding the bump at discriminator setting ~54 (which is due primarily to fluorescence radiations from the counter walls) gives the $L\beta$ line completely separated from the $L\alpha$. The $L\alpha$ intensity is proportional to the area under the curve taken through As_2O_3, and $L\beta$ intensity is proportional to the area under the difference curve. These areas must be corrected. As the graph stands, unit area is counts/min/channel-width x unit of discriminator setting. The channel was 1.5 volts wide, and a unit of discriminator setting was 0.5 volts. Therefore unit area is counts/min x 1/3.

The over-all counting efficiency (including the geometry) of the counter was achieved by a tedious numerical integration. Suppose that the source is a point source at the origin of rectangular axes, with the z axis meeting the center of the window at a distance h from the source, and the counter axis parallel to the y axis and distant p from it. Then, if ν photons/min (of a given energy) are emitted by the source, the counting rate J registered by the counter will be

$$J = \frac{\nu}{4\pi} \int_0^{2\pi} d\phi \int_0^{\theta_{max}} \sin\theta \, e^{-\sec\theta(\mu_c C + \mu_a h + \mu_w t)} \left(1 - e^{-\mu g \sec\theta (z-h)}\right) d\theta$$

Here:

θ and ϕ are spherical coordinates of the path of a photon.

$\mu_c C$ is the absorption coefficient of cellophane times the thickness of the cellophane cover of the source.

$\mu_a h$ is the absorption coefficient of air times the distance from source to window.

$\mu_w t$ is the absorption coefficient of the window material (here Be) times window thickness.

μ_g is the absorption coefficient of the counting gas, and z is given by

$$z = \frac{p + \sqrt{p^2 - (p^2 - a^2)(\tan^2\theta \cos^2\phi + 1)}}{\tan^2\theta \cos^2\phi + 1}$$

where p is the distance between the counter axis and the y axis, and a is the counter radius (1.94 in).

θ_{max} is easily computed as the arc tan of the ratio window radius; distance of source from window.

The numerics used in the integration are given in Table 2. The absorption coefficients were obtained by interpolating data given in Compton and Allison's book, or from empirical formulas that may be found there.

For the numerical integration, a quadrant of the solid angle subtended by the window with respect to the source was divided into 6 pieces (not all equal in size). The probability of counting a photon passing through the center of each piece was computed, these probabilities were weighted by the areas of the corresponding pieces, and the sum of the 6 weighted probabilities multiplied by 4 (4 quadrants!) is the integral.

Computing for a point source 1 3/4 in from the counter window, the ratio of

Table 2

Numerics Used in Computing Counting Efficiency of Counter

Absorption Coefficients	L_α (10.5 kev)	L_β (12.6 kev)
$\mu_a h$	.0176	.0105
$\mu_c C$	.0136	.0083
$\mu_w t$	.0180	.0112
μt/in of Argon (.9 atm)	.205	.122
μt/in of Methane (.1 atm)	.00034	.00021

observed photons to emitted photons is

$$J/\nu = .0153 \text{ for } L_\alpha, \ .0106 \text{ for } L_\beta$$

The assumption of a point source (the source here was 7 mm in radius) introduces a completely negligible error, as shown by a calculation using Blachman's equation (see the Appendix in B. Burt, Nucleonics 5, 28 (1949)) for the geometry of an extended source.

These computed values of the counting efficiency, together with the integrated counting rates of 10480 counts/min for L_α and 2810 counts/min for L_β and the alpha disintegration rate of 1.23×10^9 decay/min of our Po^{210} source give as the probability for emission of photons per alpha decay

$$L_\alpha = 5.15 \times 10^{-4}$$
$$L_\beta = 2.07 \times 10^{-4}$$
$$L_\alpha + L_\beta = 7.2 \times 10^{-4}$$

The error on this is probably not greater than 25%. Curie and Joliot found that 4×10^{-4} "Po" L photons were emitted per alpha decay. To get the probability of ejection of an electron from one of the L shells, the photon probability must be divided by the fluorescence yield of the shell concerned. Such fluorescence yields for the L shells of Pb do not seem to have been measured, but from Stephenson's results with U, and from theory (Compton and Allison, p. 490) one can assume a fluorescence yield of ~ 0.5. Therefore, the measured probability of the ejection of an L electron in Po^{210} alpha decay is $\sim 0.14\%$.

It will be noted that in this calculation, the production of holes in the L shell by electron transition to decay-induced holes in the K shell has been neglected. However, both theory and the little experimental evidence available indicate that the ejection of electrons from the K shell by decay is about one-tenth as frequent as ejection of L electrons.

In Midgal's theory, the probability P_{nl} that an electron with quantum numbers n and l be ejected when the nucleus emits an alpha particle is

$$P_{nl} = \left(\frac{v}{v}\right)^2 \frac{C_{nl}}{Z^{*2}}$$

Table 3

Probabilities of Electron Ejection from Different L Shells According to Migdal's Theory

Level	$\frac{C_{nl}}{Z^{*2}}$	$\left(\frac{V}{v}\right)^2$	P_{nl}
L_I	$\frac{7.2}{3969} = 1.8 \times 10^{-3}$	.048	8.6×10^{-5}
L_{II}, L_{III}	$\frac{13.3}{3697} = 3.6 \times 10^{-3}$	.051	18.4×10^{-5}
			2.7×10^{-4} = total probability

where V is the speed of the alpha particle, v is the speed of the electron concerned, and the C_{nl} are constants. Z^* is the effective charge of the product nucleus, in this case, Pb.

In order to compute these theoretical probabilities for the case of Po^{210} decay, the following process was used:

$$\left(\frac{V}{v}\right)^2 = \frac{E_\alpha}{E_e}\frac{m}{M} = \frac{.726}{E_e \text{ (in kev)}}$$

where E_α is the kinetic energy of the Po^{210} α, 5300 kev.

E_e is the kinetic energy of the orbital electron concerned, which is equal to its ionization energy.

$$\frac{m}{M} = \frac{\text{electron mass}}{\alpha \text{ mass}} = 1.37 \times 10^{-4}$$

For Z^*, 82- σ is used where σ is the screening constant for an electron in the shell concerned. The screening constants were read carefully from Figure 16.16 of White's book, "Introduction to Atomic Spectra", McGraw-Hill, New York, 1934.

The theoretical probabilities computed in this fashion are given in Table 3.

It is this total probability that must be compared with the experimentally determined total probability, even though none of the lines measured has L_I as its lowest state. If an L_I electron is ejected from the atom, the L_I hole will be filled by a radiationless transition of an electron from L_{II} or L_{III}, and the subsequent transition to fill the hole in L_{II} or L_{III} will give rise to a satellite line of the corresponding diagram line (F.R. Hirsch, Jr., Rev. Mod. Phys. 14, 45 (1942)). Our instrument cannot distinguish between a diagram line and a satellite line.

It appears, then, that Migdal's theory gives a result that is too small by a factor of about five.

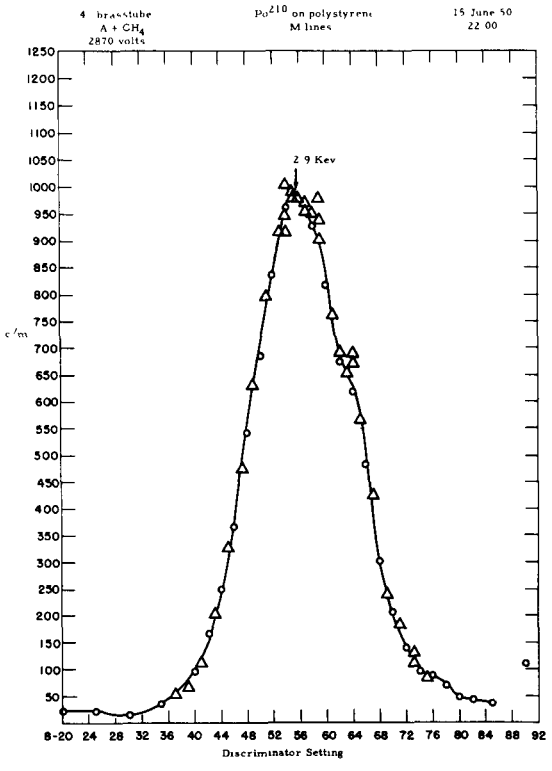

Figure 4. Po^{210} on polystyrene M lines.

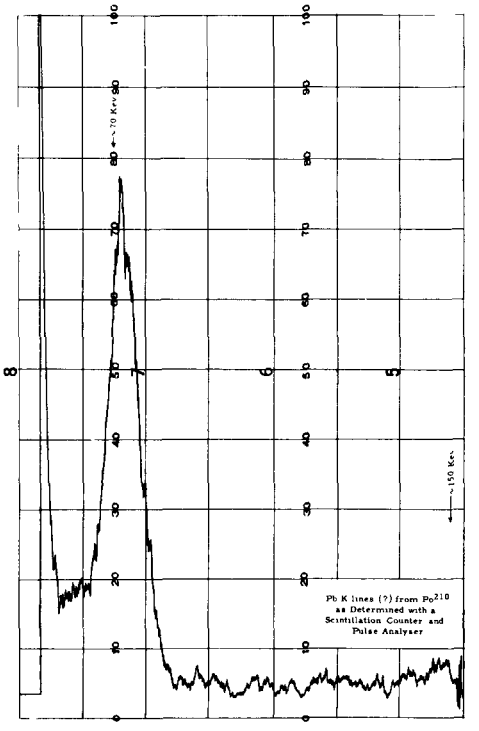

Figure 5. Pb K lines (?) from Po^{210} as determined with a scintillation counter and pulse analyzer.

These results will not be compared with Levinger's theory, since his thesis contains some errors that he has not yet rectified (J.L. Levinger, private communication).

Part IV

Photons of energy ~3 kev emitted by the Po^{210} sources have also been observed (see Figure 4). These are presumably Pb M lines. The peak of Figure 4 is doubtless a composite of several peaks, including satellite lines, as can be seen from the large half-width. Since these lines have not been unravelled, a numerical probability for their production cannot yet be given. These X-rays are doubtless the "Po" M lines observed by Curie and Joliot, who measured their frequency of production as 15×10^{-4} per alpha decay.

Figure 5, obtained with a Po^{210} source by use of a scintillation counter (NaI(Tl) crystal) in conjunction with a pulse analyzer, a counting rate meter, and a Brown recorder, shows a peak at ~70 kev. This is most likely a composite of Pb K lines, as indicated by some experiments using critical absorbers, but these studies are not yet completed.

It may be noted in Figure 5 that there is no sign of a peak at 105 kev, such as Zajac, et al, thought they observed with an intensity abut 1/4 that of another peak at 84 ± 4 kev (presumably this Laboratory's 70 kev peak).

REACTOR SCIENCE AND ENGINEERING DEPARTMENT

Reactor Operations

During this review period, the reactor has been brought up to the point where it is operated routinely for the benefit of the research programs throughout the Laboratory. It is now running at a power of about 10 megawatts with a maximum central flux of better than 2 x 10^{12} neutrons/cm^2/sec. The full loading has not yet been achieved and various operating difficulties must be overcome before full power will be achieved. The data taken on startup of the reactor is still being worked up, and memoranda are issued from time to time as some phase is completed. This work, and other classified programs of the Department, is being reported in a separate classified progress report. The unclassified programs of the Department are covered in the succeeding items.

Reactor Physics

Long-Lived Delayed Neutrons (5263)*

During October and November, observations taken with a BF_3 counter after shutdowns in the reactor seemed to indicate the presence of delayed neutrons with periods considerably longer than 1 min. A preliminary investigation was subsequently made with a series of rhodium and indium foils inserted near the center of the reactor during the period following shutdown. A long decay to the equilibrium level of the subcritical reactor was observed. The first part of the decay had a period of 5 or 10 min, and the second part was much smaller in intensity and seemed to have a period of the order of hours. The yield of these long-lived delayed neutrons is estimated roughly to be 1 per 10^6 neutrons found in fission, or about 1 per 10^4 delayed neutrons.

In December the apparatus was revised and improved, and investigations into periods and yields are being continued. The possibility that these long-period delayed neutrons are photo-neutrons produced by fission-product gamma-rays will also be investigated. (J.W. Kunstadter, J.J. Floyd)

Double Beta Decay and Other Rare Types of Nuclear Events (5263)

A program to investigate very rare types of nuclear disintegrations involving ionization of soft particles (e.g., double beta decay, pair creation in H_2 and D_2, etc.) has been started. A cylindrical self-triggering cloud chamber counter[1] (12-in diameter and 4 1/2-in depth) has been constructed. This chamber has been made to operate with H_2 and He gas at 1 1/3 atmosphere pressure. Helmholtz coils for this chamber which will produce a magnetic field of 1200 gauss, uniform to 1% over the chamber volume, are now being constructed. Apparatus for viewing and measuring track

*For explanation of these numbers, see Foreword.

[1] E.L. Fireman and G.M. McHaney, Rev. Sci. Instruments 21, 813-5 (1950).

curvatures in stereoscopic photographs is now being designed. (E.L. Fireman)

Scattering Cross Section (5263)

Apparatus for the measurement of scattering cross sections in the thermal and epi-thermal region is now being installed. This apparatus is similar in principle to the Raman tube for optical spectra. It consists of an evacuated tube which runs completely through the reactor. The scattering sample is placed in the tube at the center of the reactor and neutrons from the sample pass out through a collimating system at one end of the pipe. The collimation is so fine that only neutrons scattered from the sample can emerge and enter the detecting system. This apparatus will give a "bright line" type of scattering spectrum. (L.B. Borst, V.L. Sailor)

Double Crystal Spectrometer (5263)

Construction and installation of a double crystal spectrometer for neutrons is nearing completion. The collimation system, the heavy-duty second crystal table, and the counting apparatus are complete and have been used during the past month as a single crystal spectrometer. The shielding is partly in place and the first crystal table is ready for installation. Studies of the eccentricity and errors in the graduated circles, reproducibility of angular settings, and alignment of the various axes and planes show that the instrument meets design specifications with minor exceptions.

Preliminary experiments, using the instrument as a single crystal spectrometer, have included transmission vs. neutron energy measurements for indium, studies of the energy spectrum of the thermal neutrons from the reactor, and rocking curves for calcite (cleavage) and LiF (111) crystals. It is planned to use the instrument for activation and transmission studies of several elements in the rare earth region to start the research program. (V.L. Sailor)

Radioisotope Production (I^{132}) (6400)

The equipment rack was placed in Hot Cell #1 and several runs were made, at both cold and tracer levels. The remote operation of the equipment was quite satisfactory and no difficulty was experienced in following the planned procedure. The periscopes proved to be convenient to use and to give an adequate view of all the equipment; much has been learned about the proper placing of equipment and lines for optimum visibility.

The tellurium separation process, as modified by the result of runs in the equipment and work in the laboratory, has been demonstrated to work successfully and is essentially frozen. Sufficient decontamination from fission products is indicated and yield should be satisfactory. It is estimated that the time for a complete cycle from introduction of the jacketed slug to removal of the iodine generator from the hot cell will be of the order of 14 hr. A new equipment rack has been built incorporating changes found to be desirable from experience gained in the operation of the first rack. The new rack will be safer and more convenient to operate. After it is tested, it is planned to undertake a full-scale hot run using material irradiated in the nuclear reactor.

The iodine generator was built and operated successfully. The model, as originally designed, incorporated a sintered stainless steel frit; this was found to corrode excessively, and an improved model has been built. There is still some corrosion, but the technique of operation and the materials of construction are under investigation and it is felt that the corrosion problem will be eliminated.

The mock-up of the shipping container and its auxiliaries was completed and design carried to a point from which detail drawings and construction can proceed. The container is compact and will require a minimum number of connections for operation. A temperature regulator for the iodine generator has been selected which will give adequate control for safe and fool-proof operation at moderate cost. (L.G. Stang, Jr., W.D. Tucker)

Permanent Disposal of Radioactive Wastes (4582)

Work is continuing in an effort to determine the degree of fixation achieved when montmorillonite clays, containing radioactive ions, are subjected to high temperatures. Tests are being carried out using clays containing 4-year-old mixed fission products. It has been found that some clays when heated to 800-900°C for 24 hr retain 95%, 99.8% and 99.97% of their activity after being treated for several months with nitric acid, sea water, and distilled water, respectively.

We are now in the process of determining the fixation characteristics of each of the long-lived isotopes that occur in fission. Replacement tests using clays containing Ce^{144}-Pr^{144} and Zr^{95}-Nb^{95} in contact with distilled water and sea water are now in progress. Similar experiments employing Cs^{134} and Ru^{103}-Rh^{103} are due to be started shortly. (Tests involving Sr^{89} were reported previously.)

Some preliminary work is being done on the effect of added carrier ions on the pick-up activity on clays, and the degree of fixation as a function of temperature. Initial results in the case of Ce^{144}-Pr^{144} indicate that fixation is more efficient when carrier is added than when carrier-free Ce^{144} is used.

In collaboration with J.E. Atherton of the Metallurgy Group, we are attempting to determine the structural changes induced in the clay as a result of the high-temperature treatment, and possibly, the position of the fixed ions. This is being done by means of X-ray diffraction studies on barium-saturated clays that had been heated to various temperatures. (L.P. Hatch, W.S. Ginell)

A number of ion exchange experiments utilizing columns containing beds of montmorillonite supported on asbestos have been performed. Some of the factors under investigation are (a) the determination of optimum flow rates sufficiently slow to permit equilibrium to be established and (b) the effect of cation concentration and clay-to-asbestos ratios on the observed exchange capacity. The calcium-saturated montmorillonite is being treated with solutions containing Cs^{137} and Na^{22} as tracers. (J.A. Faucher, R.W. Southworth, H.C. Thomas (work performed at Yale University))

Waste Concentration (4582)

The problem of the Waste Concentration Group has been to develop a process that will result in an effluent that can be safely discharged to the environment (3×10^{-12} curies/ml). It has been estimated that this latter requirement will involve a decontamination factor of the order of 10^7 from concentrate to effluent. Several processes have been developed which involve simple evaporation followed by very efficient de-entrainment. Development work on these processes is described in BNL I-10, BNL 49 (T-16), and BNL 59 (C-12). During the last quarter a summary report was prepared and published covering the work to date (BNL 90 (T-20)).

It has been found that a decontamination factor of at least 10^7 (concentrate to effluent) can be obtained by simple evaporation followed by de-entrainment using a fiberglass filter (B.N.L. Filtration Process). The efficiency of the process is relatively insensitive to observed changes in operating variables. The presence of fine suspended solids that may adsorb activity in the concentrate, be entrained in the vapor, and later impart contamination to the condensate by desorption is a limiting factor to the decontamination of non-volatile fission products by this process.

The following expression is considered to be adequate for a conservative design of a simple submerged coil evaporator with offset condenser when evaporating a non-volatile fission product solution containing fine suspended solids:

$$\text{D.F.} = 42\ G^{0.9} \quad (G = 5 \text{ to } 50)$$
$$\text{and} \quad \text{D.F.} = 2.9 \times 10^5\ G^{-1.3} \quad (G = 50 \text{ up})$$

where D.F. = concentrate activity (stillpot)/effluent activity (condensate)
and G = Boil-up rate (lb/hr/ft^2 of disengaging area)

For cases of liquid entrainment only, i.e., no suspended solids present or suspended solids that do not readily adsorb the activities present, the following expression is considered to be adequate:

$$\text{D.F.} = 6.4\ G^{0.76} \quad (G = 10 \text{ to } 30)$$
$$\text{and} \quad \text{D.F.} = 3.5 \times 10^{11}\ G^{-3.7} \text{ from } G = 30 \text{ up}$$

where D.F. and G have the same meaning as above.

Economic studies (BNL 59 (C-12)) have indicated that compression distillation would be an advantageous evaporative method for Brookhaven Laboratory conditions. A semi-works scale compressive still, including a fiberglass filter, has been designed, fabricated, and installed. During the review period an experimental program has been initiated which will include a decontamination evaluation of the filter, a decontamination evaluation of the 85 gal/hr vertical tube evaporator, and an engineering evaluation of the entire unit. (B. Manowitz, R.V. Horrigan)

Meteorology

October 1950 marked the beginning of the final phase of development of the meteorological control program, for during that month the nuclear reactor reached

sufficient power to cause perceptible radiation dosage at ground level. Although the dose-rates were sufficiently intense to be differentiated from fluctuations in natural background radiation, the data cannot be used for a quantitative comparison with meteorological calculations. Such comparisons must await sustained operation at higher power.

A summary was made of the dates and times during the month at which radiation from A^{41} might have been observed at each of the Health Physics monitoring stations on the basis of observed weather conditions. Simultaneously, the Health Physics Division prepared a detailed analysis of their records for the month. In all, 27 dose-rate peaks or groups of peaks were reported by Health Physics, of which 21 were in close agreement with meteorological calculations. Of the remaining six, five were almost certainly not caused by reactor operations, either because the reactor was inoperative or because the wind flow was from a different quadrant. From the meteorological point of view, dosage would have been anticipated in a number of additional cases, where none is evident in the Health Physics records. This is not at all surprising, since the peak readings in the most favorable situations were only slightly above background.

Sustained reactor operations at the higher power levels that have been reached in the recent past will permit quantitative comparisons between meteorological calculations and radiation data during the next several months. (P.H. Lowry, M.E. Smith)

A series of experiments have been undertaken in cooperation with the Health Physics Division to determine the reaction of the radiation monitoring instruments to an elevated source of unknown intensity. The geometry of the instruments, the absorption of gamma radiation in air, and the scattering induced by terrain features and vegetation are all factors influencing the accuracy of the measurements that will be used for comparison with meteorological calculations.

Cobalt-60 has been chosen as the radiation source, because of the similarity of the gamma radiation from A^{41} and Co^{60}. A 500-lb test nylon line has been suspended between the tops of Ace and King towers, and a pulley system is used to raise the source without danger to personnel. Data have been obtained at slant ranges (instrument to source) from 72 to 500 ft and elevation angle from 12^{o} to 90^{o}. These data are currently being processed. (P.H. Lowry, D.A. Mazzarella, M.E. Smith)

The instrumentation used in measuring oil-fog concentrations has been considerably improved and expanded. The new ground level densitometer (#3), designed and constructed by the Electronics and Instrumentation Division, has proved to be so sensitive and reliable that another identical unit has been completed. These two instruments now serve as the basic measuring devices for all oil-fog runs.

A transmission fluorometer has recently been completed as an experimental device for obtaining oil-fog concentration measurements. The basic design of the device is relatively simple. Ultraviolet light is passed through a section of filter paper on which oil has been collected. The fluorescent light from the oil particles then passes through a second optical filter and is picked up by a photoelectric cell. The amplifying circuit is identical to that used in the new densitometers. Initial tests of the device have been completed with definitely promising results. (D.A. Mazzarella)

The wind speed records given by standard D.C. generator units are no longer

completely suitable for the work of the Group. In the early stages of the program there was considerable advantage in having a continuous record of instantaneous speed for every level on the towers, so that a complete study of gustiness could be completed. Now that 2 full years of data are available, wind speed records in the form of short-term averages are more valuable for most levels, especially since they reduce the processing time by a large factor.

The Friez Aerovane assembly is used as the standard wind equipment by the Group and a new contacting anemometer unit has been designed to fit inside the Aerovane housing. This unit will utilize the standard Aerovane propeller, and will not alter the moment of inertia of the vane. Thus, the character of the records will be changed, but the measuring unit will remain the same. (P.H. Lowry)

Atmospheric Stability

The U.S. Weather Bureau research unit at the Laboratory is investigating the transition from stable to unstable atmospheric flow in the lowest 410 ft which occurs following sunrise on cloudless mornings. Values of the critical Richardson number, a generally accepted criterion for the condition of "just-no-turbulence" in a compressible fluid having a vertical gradient both in density and wind speed, have been found to lie between 0.28 and 0.55 for air layers above 150 ft. Transient changes in the density and speed gradients are observed, which indicate that these "critical" values are somewhat larger in magnitude than the actual critical number applying strictly to the layer in which turbulence is increasing. It is supposed that, in general, measurements on towers with instruments at fixed and widely separated levels yield overestimates of the critical number. (R.C. Wanta)

Geology

Most of the review period was spent in preparing for and in running a pumping test at Laboratory supply well # 2. A total of 9 special observation wells was used. One of these was a 4-in well, equipped with a standard float type of recorder. The other 8 wells were 2 1/2 in or less in diameter and float recorders could not be used. However, two of these wells were equipped with electrically operated recorders, rebuilt to operate from storage batteries. The pumping test was entirely successful and when the calculations have been finished, should provide much better quantitative values for the hydrologic properties of the glacial aquifer than now exist.

In the course of the test, 16 gal of ammonium chloride-alcohol tracer solution was introduced into an observation well 30 ft from the pumping well. The arrival of the tracer was detected with a "flow through" conductivity cell which drew water from the pump discharge at a rate of about 1 gal/min. The conductivity of the cell was measured with a 1,000 cycle electronic bridge. The tracer was easily detected at a dilution of 1 to 10,000 and could just be detected at a dilution of 1 to a million. The arrival curve was sharp enough so that the travel time could be determined to within ~2%. It will probably not be possible to check this observed time against a travel time calculated from the observed values of permeability and head loss, for the area covered was well within the zone of converging flow lines around the screen of the pumped well. As nearly as could be determined, 85% of the tracer introduced into the

observation well arrived at the pumped well, but this determination was not so exact as the other measurements. Probably not less than 10 % of the tracer was adsorbed, however. What effect this adsorption had on the travel time is of course not known.

It was noted in the study of the arrival curve that it took as long for the tracer to pass through after it had once shown up as it did for the tracer to put in its first appearance. In this case, the first arrival appeared 7 1/2 hr after introduction and the last of the tracer was pumped through after 15 hr. Going back over the other curves of tracer runs using the natural ground-water flow, where the time intervals were days instead of hours, the same relation appeared to hold within the experimental error. (W. deLaguna, N.J. Lusczynski)

Biological Effects of Radiations

Relation Between Chromosome Breakage and Mitotic Inhibition (6400)*

A possible relationship between chromosome breakage and the increase in time required to pass through certain stages in the nuclear cycle has been studied in Trillium. The time required to go from first meiotic metaphase and from early interphase to microspore division has been determined in control and irradiated anthers. Preliminary results indicate that sensitivity to inhibition varies the same way and approximately to the same degree as break sensitivity -- i.e., metaphase is much more sensitive to radiation-induced inhibition than is early anaphase. It has also been shown that in a population of microspores those showing the most severe break damage tend to go through division later than those showing a smaller amount of breakage. These observations indicate a relationship between chromosome breakage (without loss of chromatin) and the degree of mitotic inhibition. However, it has not yet been shown that the two are causally related. (A.H. Sparrow)

Regeneration of Irradiated Tradescantia (6400)

Regeneration of Tradescantia plants removed from the gamma field in late September is being studied. Speed of regeneration following removal of most of the foliage is proportional to field exposure. Plants exposed to 128, 82 and 67 r per day have shown no regeneration except for underground portions that were partially shielded by soil, but the plants are still alive. Plants with abnormal terminal growths (those exposed to 50, 30.5, 22 and 15 r per day) have shown multiple shoot growth after removal from the radiation field. In extreme cases, as many as 30 shoots have been produced from a single terminal proliferation (see Figures 1-4). When rooted, these shoots behave as normal shoots except that growth seems to be somewhat slower than usual. This implies that the abnormal terminals, both vegetative and reproductive types, are due to physiological disturbances rather than to mutation. (A.H. Sparrow, E. Christensen)

Cytochemical Analysis of X-ray Effects (6400)

In the last progress report it was shown that, in both living and fixed Trillium pollen mother cell nuclei, there is virtually no change in nucleic acid content following irradiation. However, it was further shown that, if the cells are subjected to a slow hydrolysis that brings about the degradation of the nucleic acid molecule, the nucleic acids of the cells irradiated after fixation are hydrolyzed many times faster than the controls, while the cells irradiated in the living state are hydrolyzed much slower than the controls. Furthermore, in fixed Trillium cells there is a decrease in the methyl green reaction (depolymerization).

*For explanation of these numbers, see Foreword.

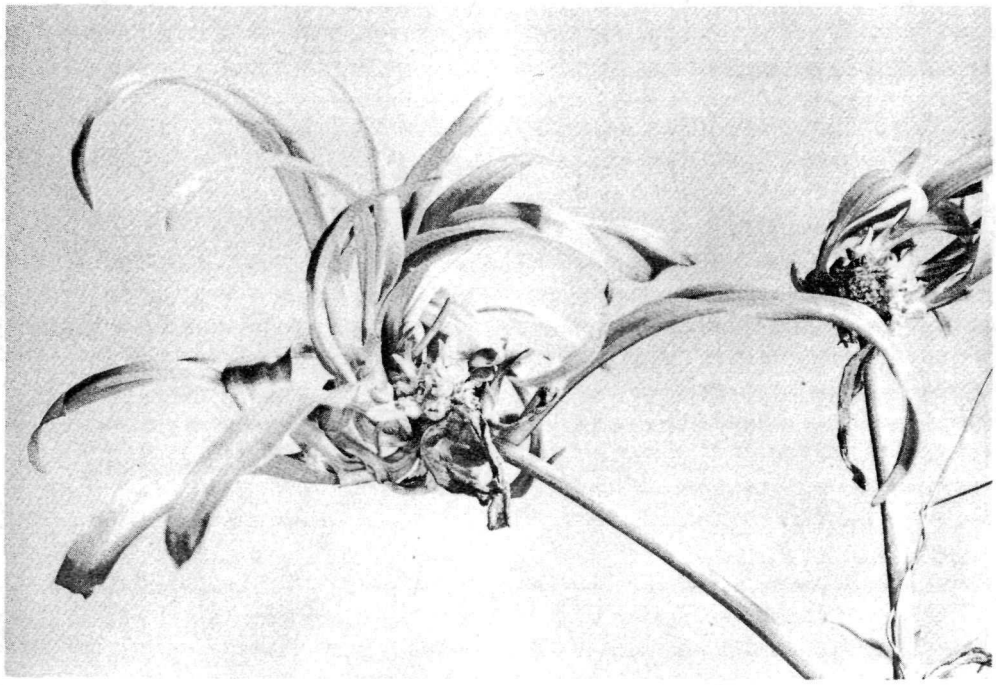

Figure 1. Abnormal regrowth in Tradescantia during recovery from chronic irradiation. After 114 days of constant exposure to 30 r/day of gamma irradiation, a much inhibited flower bud development began regrowth with abnormal formation of new leafy shoots during a 39 day recovery period.

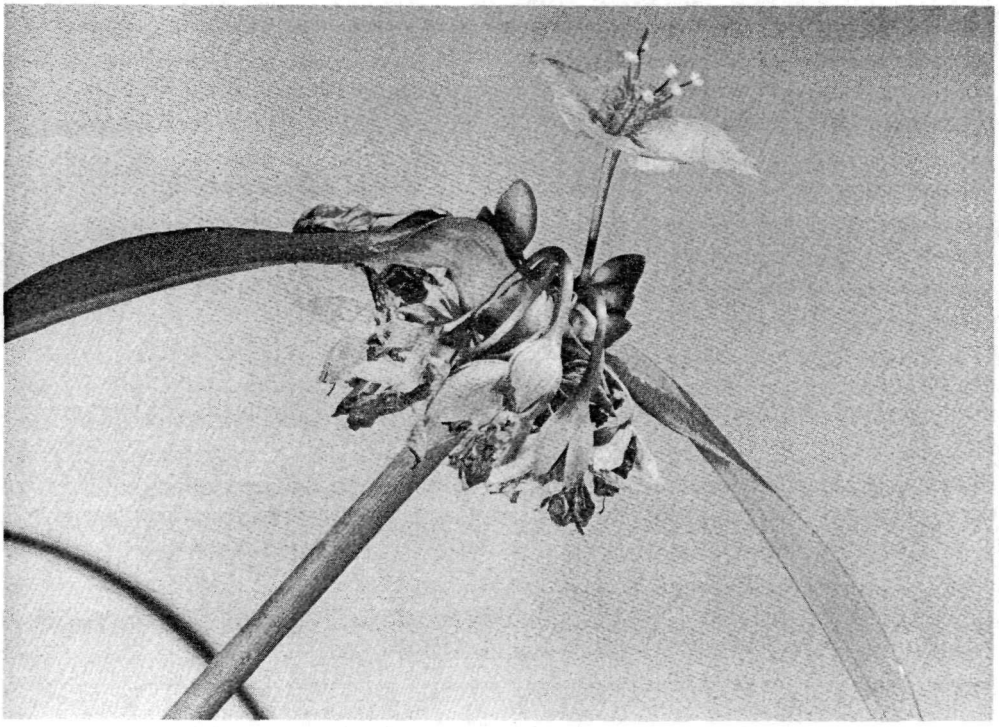

Figure 2. Normal Tradescantia inflorescence at maturity. No additional leaf growth is made from such a cluster under normal conditions.

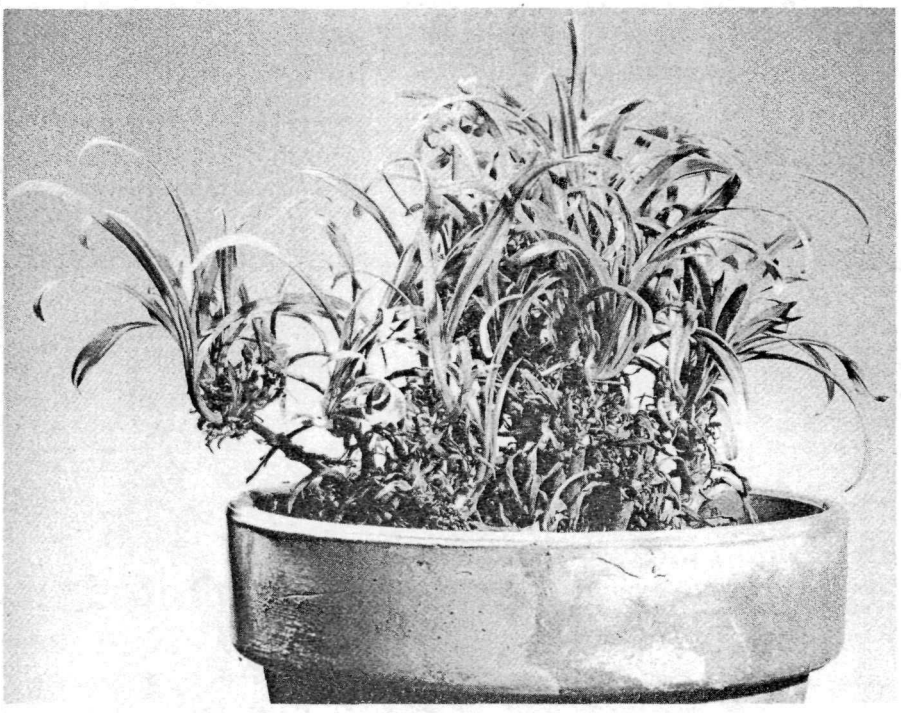

Figure 3. Abnormal growth of irradiated Tradescantia plant during recovery period following 114 days of gamma irradiation at 30 r/day. Length of recovery period: 47 days. New growth in this plant is arising entirely from previously formed, but much modified, flower bud clusters.

Figure 4. Unirradiated Tradescantia showing normal flowering and growth of new shoots from underground portions of plant.

Work has continued on this problem in an effort to see if this is an effect common to different tissues, and the frog liver was chosen as a suitable test tissue. Preliminary indications are that in this material, contrary to the observations in Trillium, there is little or no change in the methyl green reaction following irradiation of the fixed material. However, there does appear to be an increased susceptibility to acid hydrolysis, although it is not as marked as in Trillium.

It has been suggested that one of the significant methods of X-ray damage in living systems is the production of free hydroxyl radicals from H_2O_2 formed in water as a result of the irradiation. The nucleic acid reactions offer a possibility of testing this hypothesis. Free OH groups formed from H_2O_2 by $FeSO_4$ have been shown to produce depolymerization of nucleic acids in solution, as well as other effects produced by X-rays. To investigate this further, sections of frog liver were treated with the H_2O_2 - $FeSO_4$ mixture and changes in "polymerization" and hydrolyzability as in the irradiated sections were looked for. Preliminary results indicate that, as in the irradiated sections, there is no change in degree of polymerization as indicated by the methyl green stainability. (M.J. Moses, R. Applegit, A.H. Sparrow)

Effect of X-rays on Fibrinogen (6400)

The last progress report indicated that, by a study of the electrophoretic and ultracentrifuge patterns, it is possible to get a qualitative picture of the type of destruction taking place in solutions of fibrinogen subjected to radiation. Current experiments are concerned with the protective action of various compounds against the destructive effects of X-rays on fibrinogen. It has been found that thiourea, cysteine, methionine and glutathione are all fairly effective protective agents. One is tempted to generalize at the present time and say that sulfur-containing compounds have by far the greatest protective action of all classes of compounds so far investigated. (L.F. Nims; H.A. Scheraga, Cornell University)

Adrenal Cortical Requirements of Adrenalectomized, X-Irradiated Rats (6400)

Preliminary results were reported in BNL 82 (S-7) on the amount of adrenal cortical hormone required to maintain an X-irradiated, adrenalectomized rat in the same condition as the X-irradiated control rat. These results have been confirmed and extended. Rats were adrenalectomized and maintained by injection of minimal quantities of adrenal cortical extract. The animals were then exposed to 600 r of total body X-irradiation and the amount of extract administered was adjusted to counteract weight loss. Results indicate: 1) that more than 2-1/2 times the minimal amount of extract per animal is required to inhibit weight loss for 3 days post-irradiation. 2) After this period, the requirements fall off until pre-irradiation levels are approached. 3) Animals continued on minimal extract injections after irradiation exhibit severe weight loss and are moribund the 5th day post-irradiation. This shows that part of the normal reaction of an animal to radiation is a greatly increased adrenal cortical activity for about 3 days post-irradiation. (S. Katsh, A. Edelmann)

Effect of Glucose Injection on the Radiation Syndrome (6400)

It has been reported by Loiseleur and Velley (1950) that glucose injected

intraperitoneally 45 min before irradiation will have a significant protective action against the radiation. Their experiments have been repeated. The results indicate: 1) that all animals show severe weight loss subsequent to irradiation; 2) only one glucose-treated rat remains alive 25 days post-irradiation while two of the controls are alive at this time; 3) that glucose-treated animals died more rapidly after irradiation than did the controls. Thus, the results of Loiseleur and Velley are not confirmed. (S. Katsh)

Water Metabolism Following X-Irradiation (6400)

It has previously been reported that there is an increased urine output following X-irradiation in rats. This diuresis occurs in two stages, the first starting almost immediately after irradiation and lasting about 36 hr, and the second starting about 5 days after irradiation and lasting about 2 days. It was further shown than there is a decreased amount of circulating antidiuretic hormone following irradiation. In a further effort to analyze this effect, rats have been hypophysectomized and then subjected to irradiation in doses of either 200 r or 650 r. Present indications are that the initial diuresis is not present in these rats; however, the second peak may appear. This gives further indication that the posterior lobe of the pituitary is at least secondarily, and possibly primarily, responsible for the first period of diuresis; the second period remains unexplained.

In a further experiment, the adrenal glands have been shielded in rats and their water metabolism studied. These rats show a diuresis comparable in every respect to that shown by the normal following irradiation. Thus, it seems safe to say that the adrenal gland has been effectively eliminated as a possible cause of the diuresis.

As a continuation of this work, the effect of X-irradiation on the water and food intake, urine volume and urinary sodium, potassium, chloride, ascorbic acid and total nitrogen is being studied in guinea pigs. Preliminary results indicate that there is no change in water metabolism following irradiation in the guinea pig, as there is in the rat. (A. Edelmann, S. Katsh, C.S. Nagareda)

The Role of the Adrenal in the Irradiation Syndrome (6400)

It has previously been reported that when the adrenal glands of rats are shielded from X-rays, survival following X-irradiation is considerably increased. It was further shown that when rats were adrenalectomized and maintained on whole gland adrenal extract, the dose of extract after irradiation would have to be increased by at least a factor of 3 in order to prevent a severe weight loss and increased mortality. These experiments indicated strongly that the adrenal gland plays a major role in the reaction of the body to irradiation. They have now been extended and it is possible to show that there is an increased concentration in adrenocorticotrophic hormone concentration in the pituitary of rats 1 hr after 1,000 r whole body irradiation. This further substantiates the idea that the pituitary is activated immediately following irradiation. This activation in turn activates the adrenal gland to increase its output. If the adrenal gland itself has also been subjected to irradiation then it presumably cannot put out as much hormone as if it had been shielded.

As a further substantiation of these ideas, rats were adrenalectomized at various

periods of time after irradiation and their survival times were noted. When adrenalectomy is performed within 1/2 hr after irradiation there is a decrease in survival of about 75% from the non-irradiated adrenalectomized rat. Adrenalectomy performed within 3-4 days after irradiation results in significant reduction in survival time but the effects begin to be lost at 5 days. This gives added weight to the idea there is a greatly increased requirement for adrenal hormone for 3 days after X-irradiation. (A. Edelmann, S. Katsh, G. Mateyko)

Sucrose Storage in Corn Plants (6400)

In attempting to study the genetic control of sucrose storage in the stalks of maize, several complicating problems have arisen. Sucrose is an active metabolite in the plant and therefore sucrose levels in the stalk are continually changing. Before genetic studies could be attempted, it was first necessary to study sugar metabolism in the normal inbred strains. Four highly inbred strains have been studied. In half the plants, ear development was thwarted by preventing pollination. At various stages in the plant growth, stalks were cut and the stalk juice expressed. Percent total dissolved solids were estimated from readings on the index of refraction of the expressed juice. Some of the samples were subjected to chemical analysis for sucrose and reducing sugars in an attempt to correlate the index refraction readings with sugar concentration.

It was found that in a general way the index of refraction readings were proportional to the sugar content. The results of this study are presented in Figure 5, which shows the change in the percent dissolved solids as a function of time, both with and without ear formation. It will be seen that the pattern of change is similar for strain C103 and Ind. 38-11, but that the absolute concentration in these two is quite different. These two strains then would be suitable for genetic studies. The other two strains, Wf and Te, also show similar patterns, but the absolute concentrations in the two are so nearly the same as to make them unsuitable for genetic studies. This study is continuing in an analysis of grain yield and when the analysis is complete, it will be possible to map a future program. (R. Van Reen)

The Effect of Generation Time on Mutation Rate in Bacteria (6400)

A series of experiments have been in progress for some months to determine the relative sensitivity of bacteria to X-rays and beta-rays as a function of the time and number of cell divisions. In order to do this, it was first necessary to show that the irradiation itself had no appreciable effect on the growth rate. Accordingly, a radiation-resistant strain of bacteria, E. coli B/r, was studied. There was no detectable effect on growth rate during continuous irradiation at the rate of 5,000 r/hr This characteristic was subjected to extreme conditions of different types of media in a range of inoculum varying a million-fold. The results agree with previous findings in P^{32} experiments in which no modification of growth kinetics was observed with high concentrations of P^{32} in the media in this strain of bacteria. It is possible to control the rate of cell division during irradiation by varying the proportion of inoculum to fresh media. For example, if a completely grown culture is mixed with an equal amount of fresh medium, the bacteria may be expected to go through one division. If the ratio is changed to correspond to one part of culture to three parts of fresh medium, there would be two divisions, etc.

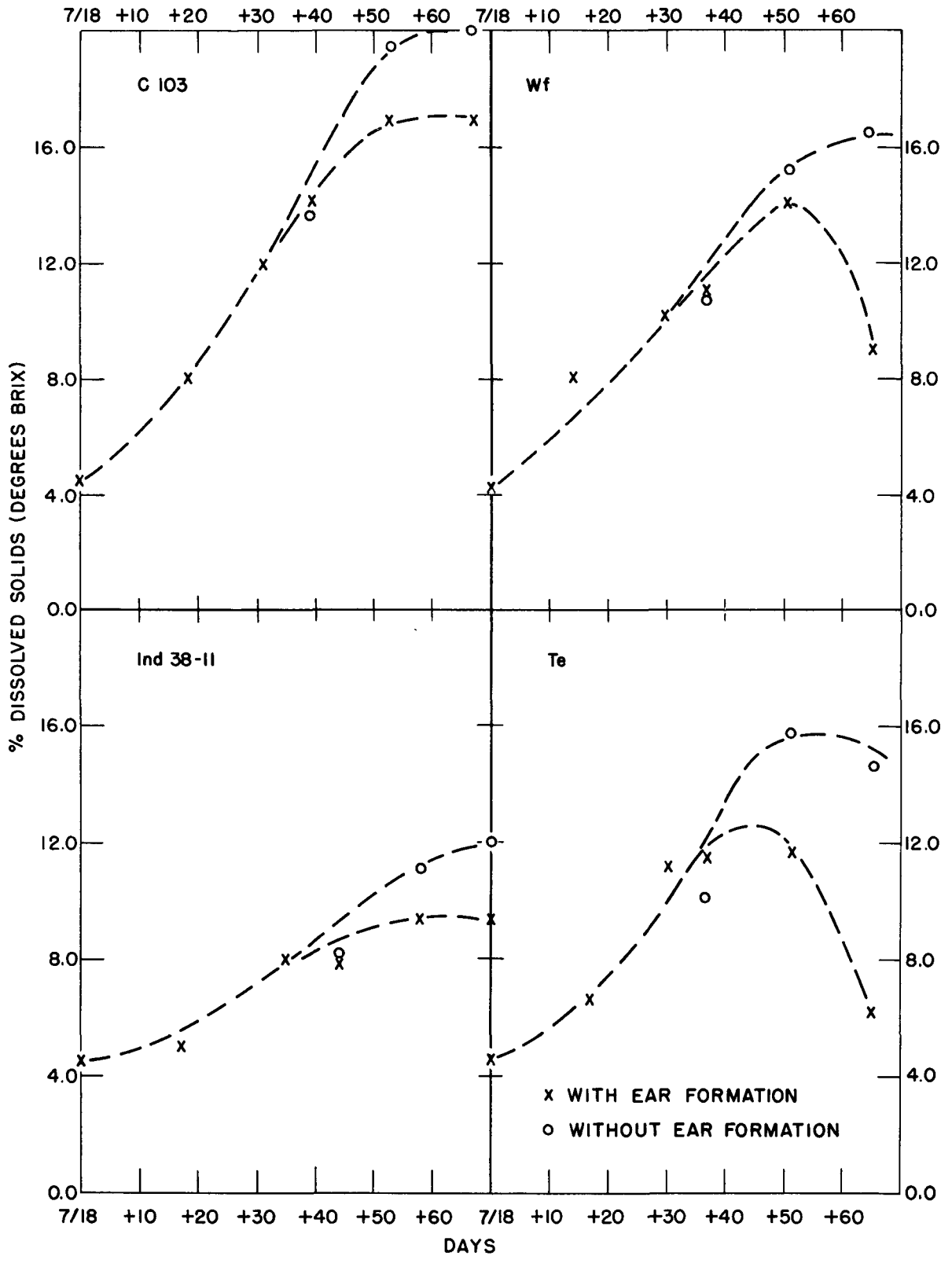
C 103
Wf
Ind 38-11
Te
7/18 +10 +20 +30 +40 +50 +60
16.0
12.0
8.0
4.0
0.0
% DISSOLVED SOLIDS (DEGREES BRIX)
DAYS
x WITH EAR FORMATION
o WITHOUT EAR FORMATION

Figure 5.

Cultures were irradiated at a rate of 5,000 r/hr and for constant times so that all cultures received the same total dose. Cultures were then chosen which could be expected to go through from 0 to 4 generations during the exposure time. Since it already has been established that the full expression of the mutants is delayed after irradiation, the mutant populations were followed for as many as 22 generations after irradiation.

Results are not yet complete, so only tentative conclusions can be drawn. It appears, however, that immediately after irradiation there was an increase in the number of mutants which varied directly with the number of generations through which the cultures had grown while being irradiated. However, when the cultures were followed through subsequent generations, it appeared that the cultures that had gone through 1, 2 or 3 generations during the irradiation showed no differences in the peak number of mutants or in the time of appearance of this peak. There seem to be some discrepancies in the 0 and 4 generation groups, but it appears probable that the general pattern will be followed in these groups also.

The inescapable conclusion to be reached at the moment is that bacterial cells differ from those of higher organisms in that the number of mutations produced seems to be independent of cell division.

This is a rather sweeping conclusion and experiments are now in progress to check it from every possible angle. (B.A. Rubin)

Effect of X-Irradiation on Blood Proteins (6400)

Preliminary experiments indicate that whole body X-irradiation in rats leads to a decrease in the level of the metal-binding protein in blood plasma. The apparent decrease occurs several days after irradiation, coinciding temporarily with other known changes in composition of blood plasma. (J.R. Klein)

Tracer Studies of Biological Problems

The Effect of Substrate on the Endogenous Respiration of a Mold (6400)

An investigation was undertaken to determine the effect of substrate on endogenous respiration. The mold, Streptomyces coelicolor, which has a high endogenous respiration, was allowed to grow in a medium containing C^{14}-glucose. The radioactive medium was washed out after there was a fair concentration of the C^{14} in the mold. The endogenous respiration in the mold was followed by collecting the $C^{14}O_2$ that it generated. When a non-radioactive respirable substrate, glucose or pyruvate, was added, it was found that the endogenous respiration did not change appreciably. One would infer from these experiments that endogenous CO_2 production proceeds via metabolic pathways completely separate from those involved in substrate oxidation. (M. Gibbs; V. Cochrane, Wesleyan University)

The Effect of Dinitrophenol on Phosphate Metabolism (6400)

A preliminary experiment has been carried out in collaboration with Dr. Sinex of the Medical Department on the effects of dinitrophenol on phosphate transfers in the rat diaphragm as the experimental object. It has been well established than dinitrophenol in suitable concentration markedly stimulates the respiration of tissues and even tissue minces. It has further been established that dinitrophenol will block the incorporation of amino acids into tissue slice proteins, and it has been postulated that this is due to the blocking of the phosphorylating mechanism of the cell. Preliminary results indicate that the turnover rate of the labile phosphorus of the adenosinetriphosphate in the presence of dinitrophenol was not markedly reduced below the value obtained in the controls. The oxygen consumption of the diaphragm, however, was increased by more than 50% above that of the controls. This result furnishes additional evidence that the phosphorylating mechanism is only one of the pathways of metabolism in the intact cell. (J. Sacks)

Disappearance from Mouse Tissues of Carbon from Assimilated Sucrose (6400)

Ten male mice, C57 blacks, 3 1/2 to 6 1/2 months old, were each fed a single dose of uniformly enriched C^{14} sucrose. Total sucrose fed was 5.0 to 8.3 mg per gram mouse body weight. Stock mouse pellet diet preceded and followed the dose. At various times, from 3 1/2 hr to 36 days, after C^{14} sucrose ingestion mice were killed by withdrawing heart blood under nembutal anaesthesia and dissected immediately. Dissected parts were powdered at liquid nitrogen temperature and portions subjected to combustion. The resulting CO_2 was counted as $BaCO_3$. Specific activity was expressed in mμc per mg tissue carbon for 1 μc C^{14} fed per gram mouse body weight. For the carbon of each of 31 organs or tissues, the logarithm of the specific activity was plotted against elapsed time. Each curve was resolved into as many straight line components as necessary for its description. Organs concerned with alimentation required four-component description, most other organs required three. The organic carbon of the solid portion of long bone has a component with a half-life of about 200 days. The 3 1/2 hr concentration of this component is about 0.05 mμc per mg carbon for 1 μc C^{14} sucrose fed per gram mouse body weight. Abdominal storage fat has a very low turnover rate as measured by this method. Throughout the 36 days, its C^{14} concentration remained around 0.12 mμc per mg carbon for 1 μc C^{14} sucrose fed per gram mouse body weight. (R. Steele)

Exchange Between Plasma Iron and Red Cells (640C)

To determine whether normally bound plasma iron (as opposed to iron added to blood in a flask) is taken up by red cells on incubation, a duck was injected intraperitoneally with Fe^{55} and bled after 30 min when the plasma/erythrocyte activity ratio was high. This blood was incubated and it was found that there was a transfer of Fe^{55} from plasma to cells comparable to that obtained if inorganic iron is added directly to blood. It is concluded that the incorporation of iron in hemoglobin, which has been observed to occur on incubation, takes place by the same mechanism as when the iron is in the form of naturally occurring plasma iron. (L.M. Sharpe, J.R. Klein)

Publications

1. J.L. Nickerson, M.I. Gregersen, W.S. Root, and L.M. Sharpe, The influence of blood incompatibilities on the measurement of blood volume by cell-tagging methods, Proc. Soc. Exptl. Biol. Med. 75, 61-2, October (1950)

2. M.J. Moses, R. Steele, and A.H. Sparrow, Quantitative determination of nucleic acids during meiosis in Trillium, J. Nat. Cancer Inst. 10, #6, 1345 (1950)

3. V.T. Bowen, Manganese metabolism of social vespidae, J. Exp. Zool. 115, 175-205, October (1950)

4. A.A. Bothner-By and M. Gibbs, The epimerization of glucose-1-C^{14}, J. Am. Chem. Soc. 72, 4805 (1950)

5. A.H. Sparrow and M. Maldawer, Differential rejoining as a factor in apparent sensitivity of chromosomes to X-ray breakage, Proc. Nat. Acad. Sci. 36, 636-43, November (1950)

6. B.A. Rubin, The nature of streptomycin requirement and its effect on the genetics of streptomycin resistance in E. coli, Rec. Gen. Soc. Am. 19, 121-2 (1950)

7. W.R. Singleton, Corn grass, a dominant monogenic spontaneous mutant and its possible significance as an ancestral type of corn, Rec. Gen. Soc. Am. 19, 125 (1950)

8. A.H. Sparrow and V. Pond, Supernumerary chromosomes in diploid and triploid Trillium erectum L., Genetics 35, #6, 694, November (1950)

9. J. Sacks and G.G. Culbreth, Absorption of phosphate from subarachnoid space, Am. J. Physiol. 163, #3, December (1950)

10. A. Edelmann and W.J. Eversole, Changes in antidiuretic activity of rat serum after X-irradiation, Am. J. Physiol. 163, 709 (1950)

11. W.R. Singleton, Some high lights of the first half century of genetics, Scientific Monthly 71, December (1950)

MEDICAL DEPARTMENT

Division of the Hospital

Biological Effects of Radiation: Cancer Control (6210)*

During the quarter ended December 31, 1950, the hospital continued to grow. Treatment of patients with metastatic thyroid carcinoma was continued with I-131. Patients with hyperthyroidism were also treated with I-131. Patients with ovarian carcinoma, agnogenic myeloid metaplasia, enchondroma, fibrosarcoma and glioblastoma multiforme have been admitted for care, treatment and study. Studies are also continuing on children with the nephrotic syndrome. (C.G. Foster, J.L. Gamble, Jr., J.S. Robertson, L.E. Farr)

Division of Bacteriology

Biological Effects of Radiation: Immunology (6300)

The new cobalt source is proving to be very satisfactory for studying the effects of radiation on infection. We have accurately determined the LD^{50} for mice and find that we can duplicate our results without difficulty. Work is continuing on the problems previously outlined. Collaborative work with Dr. Bacon Chow from Johns Hopkins University has been started this quarter using our cobalt radiation source for studying the effect of nutrition on susceptibility to radiation. There have been 105 bacteriological determinations done for the hospital. (W.M. Hale, R.D. Stoner, H.T. Gardner)

Effects of Radiation on Bacterial Metabolism (6300)

Work is continuing on the effects of radiation on the pneumococcus transforming substance. (R.M. Drew)

Division of Pathology

Influence of Mechanical Injury, Radiation Injury, and Disease States upon Body Protein Stores (6300)

Work is continuing on certain aspects of protein and amino acid metabolism during injury and disease states. (S.C. Madden, J.A. Fancher, Jr., L.V. Hankes)

*For explanation of these numbers, see Foreword.

Division of Biochemistry

Combined Determination of Total Carbon and C^{14} Activity (6300)

The methods for wet carbon combination outlined in the April-June progress report have been refined and extended. The procedure based on Van Slyke-Folch wet combustion and manometric measurement of the CO_2, followed by quantitative transfer of the CO_2 to the Bernstein-Ballantine gas counter, has been extended so that it has become practical to measure specific activities as little as 0.01 as great as those measurable by current procedures based on counting the C^{14} as $BaC^{14}O_3$. With the gas counter $Na_2C^{12}O_3$-$Na_2C^{14}O_3$ solutions can be standardized in millimicrocuries per mg of carbon to better than $\pm$ 1% accuracy, for use in standardizing $BaC^{14}O_3$ counters, whereas the standard $BaC^{14}O_3$ previously obtainable had a $\pm$ error of 10%. (D.D. Van Slyke and J. Plazin in collaboration with R. Steele, Biology Department).

Determination of C^{14} in the Carboxyl Groups of Free Amino Acids (6300)

The reaction of free amino acids with ninhydrin, by which the amino acids are decomposed according to the reaction, $R{\cdot}CH(NH_2){\cdot}COOH$ -- $RCHO + CO_2$, developed for quantitative micro determination of free amino acids by Van Slyke and Dillon, has been applied to determination of C^{14} in the carboxyl groups of free amino acids. The CO_2 evolved is measured and counted in the gas counter by the technique outlined above, and has been applied in studying the incorporation of amino acids into tissue proteins. (F.M. Sinex)

Factors Affecting Incorporation of Amino Acids into Tissue Proteins (6300)

Surviving rat diaphragms were incubated in solutions containing alanine labeled with C^{14} in the carboxyl group. The incorporated alanine was measured by hydrolizing the isolated muscle proteins, and determining the carboxyl C^{14} of the amino acids in the hydrolysate by the method outlined in the preceding paragraph. Addition of insulin to the incubated mixture accelerated the incorporation of the C^{14} into the proteins. Cortisone, on the other hand, was found to decrease the amount of carbon-14 found in the protein. Work now in progress is directed toward understanding the mechanism by which amino acids are concentrated within tissue prior to their incorporation into protein. (F.M. Sinex)

Division of Physiology

This division was activated on October 1, 1950.

Chemical Anatomy of the Body Fluids and Membrane Permeability (6300)

Work previously begun in the Division of Biochemistry is continuing on the distribution of body fluids and membrane permeability. Na-24 studies were carried out on 11 patients during the period, together with renal function tests, estimation of total

red cell mass, and observations of extracellular fluid volume with sucrose, together with total body water estimation using antipyrine and deuterium. Methods are presently being revised to increase accuracy of analyses. (J.L. Gamble, Jr., J.S. Robertson, C.G. Foster, L.E. Farr)

Effects of Internally Administered Isotopes on Renal Function (6210)

At the meeting of the American Association for the Advancement of Science in Cleveland, December 30, 1950, a paper was presented from the Division giving a report on studies to date of effects of I-131 administration on renal function of patients with metastatic carcinoma of the thyroid:

> Twelve patients with thyroid carcinoma have received total doses of I-131 ranging from 4 to 360 mc. Included in this series are 4 patients who have received very large single doses of the isotope ranging from 200 to 300 mc. Renal function tests carried out on these patients at varying time intervals after isotope administration up to over 2 years have failed thus far to disclose any renal abnormalities caused by radioactive isotope administration.
>
> From these preliminary studies which are being extended and enlarged, it would appear that doses of I-131 which have in the past been administered with hematological safety to patients with malignancies are unlikely to produce significant adverse effects on renal function. (J.L. Gamble, Jr., J.S. Robertson, C.G. Foster, L.E. Farr)